Energetic Particle Transport/Confinement Studies Due to Low Frequency MHD Activity in JET and the Non-axisymmetric RFP

P. J. Bonofiglo

Princeton Plasma Physics Laboratory, Princeton, NJ 08540 USA

NSTX-U/Magnetic Fusion Science Seminar

September 20, 2021

PPPL - Remote

Outline

- Fast Ion Transport in the Non-axisymmetric RFP
  - Energetic Particle Instabilities
  - Neoclassical Enhancement
  - Tearing Mode Effects
- Integrated Modeling on JET
  - JET's Fast Ion Loss Detector
  - Synthetic Loss Model
  - Experimental Validation
- Future Work

The RFP is Dominated by a Large Tearing Mode Spectrum

- Comparable poloidal and toroidal fields
- RFP q-profile < 1 and monotonically decreases towards edge
- Many m=1 rational surfaces result in overlapping tearing mode islands

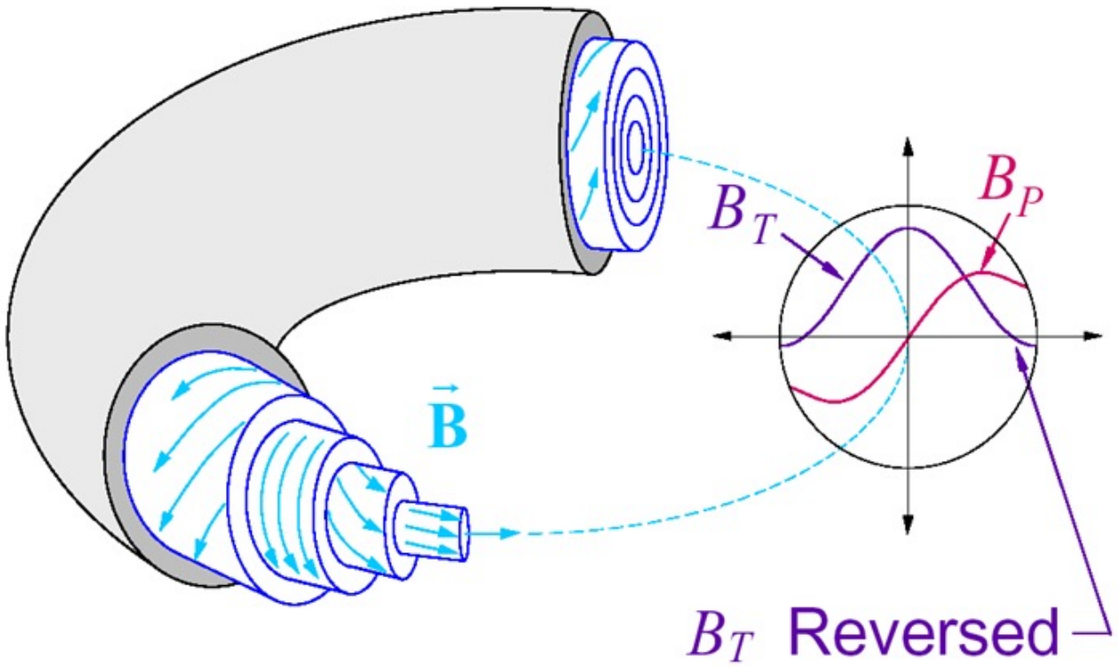

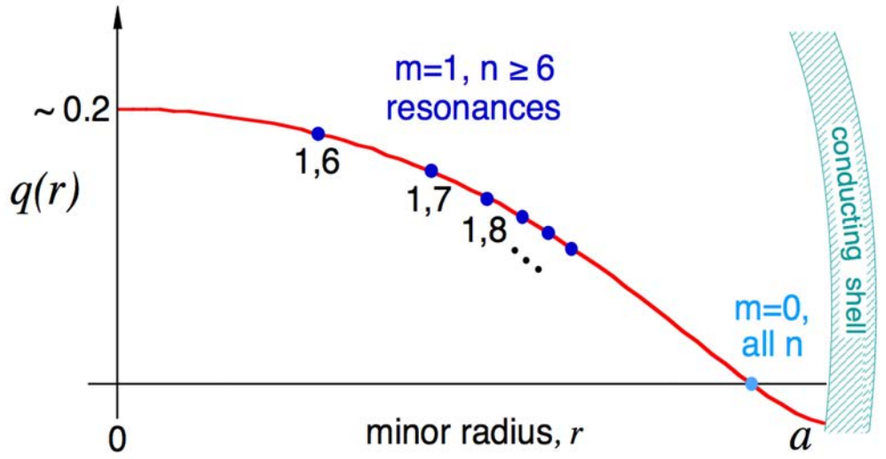

Madison Symmetric Torus

R_0=1.5 m; a=0.52 m

I_p ~ 200 – 600 kA; |B| ~ 0.2 – 0.5 T

$T_e(0)$ ~ 200 – 1000 eV; $n_e \sim n_i \sim 10^{13}$ cm^{-3}

25 keV tangential H- or D-NBI

1 MW heating; super-alfvenic; $\beta_{fi} \sim 5-8\%$

Fast Ions are Well Confined in the Standard RFP

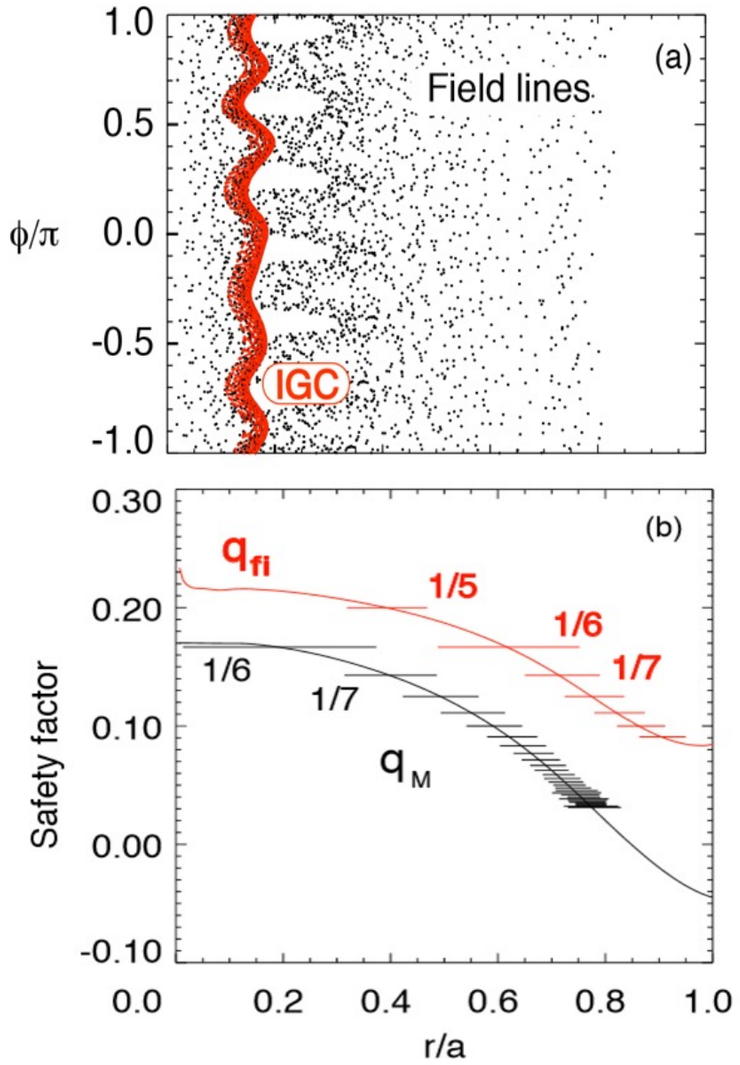

(a) Field line and fast ion orbit traces
(b) Magnetic and fast ion q-profiles

- Grad-B and curvature drifts are <u>along</u> flux surfaces in the RFP:

$$\vec{v}_{\nabla B} = \frac{w_\perp}{qB}\left[\frac{\hat{B}\times\vec{\nabla}B}{B}\right] \qquad q_{\mathrm{mag}} = \frac{rB_\phi}{RB_\theta}$$

$$\vec{v}_{R_c} = \frac{2w_\parallel}{qB}\left[\frac{\hat{B}\times\hat{R}_c}{R_c}\right] \qquad q_{\mathrm{fi}} = \frac{rv_\phi}{Rv_\theta} \approx q_{\mathrm{mag}} + \text{Drift Terms}$$

- Fast ions ignore stochasticity due to GC-drifts
  - Well measured and modeled[a]
  - Minimal fast ion losses[b]
- Electrons follow field lines = poor thermal confinement

[a] *Fiksel (PRL 2005)*
[b] *Bonofiglo (RSI 2016)*

Helical RFP is Defined by a Collapse of the Tearing Mode Spectrum

- MST plasmas self-organize into a 3D-helical equilibrium at high Lundquist number

$$S = \frac{L v_A}{\eta} \sim \frac{I_p T_e^{3/2}}{\sqrt{n_e}}$$

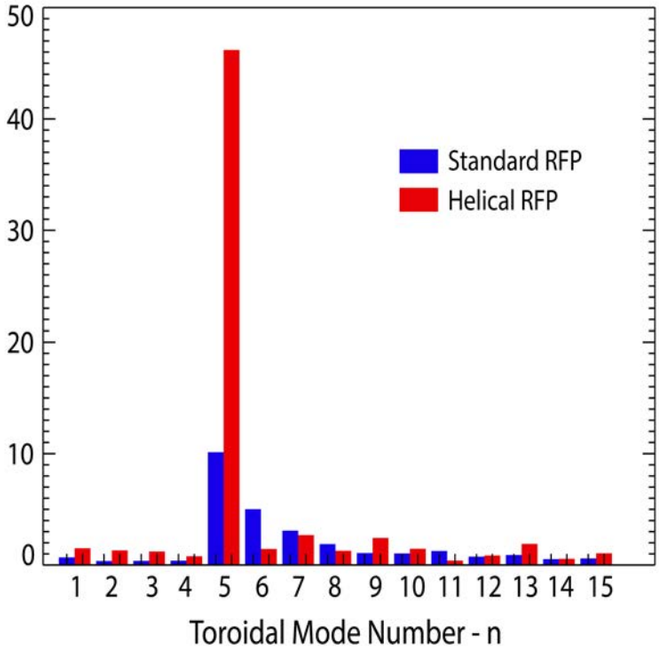

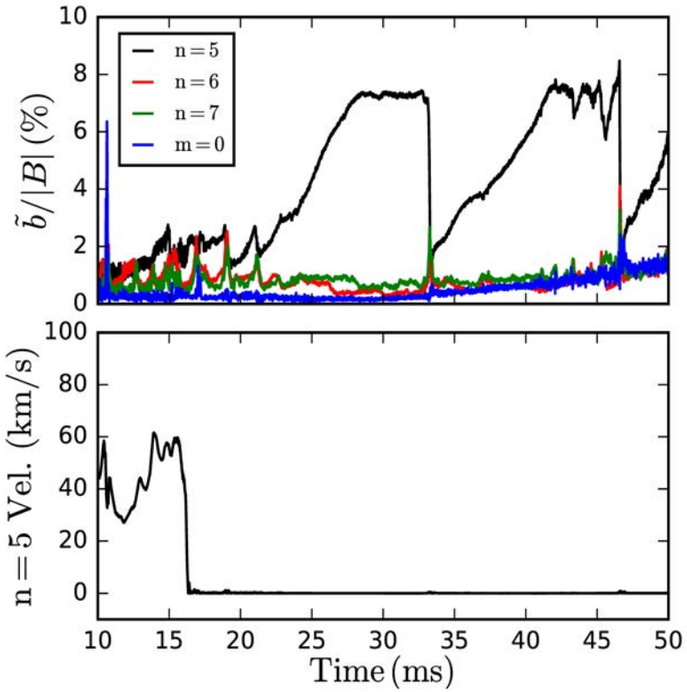

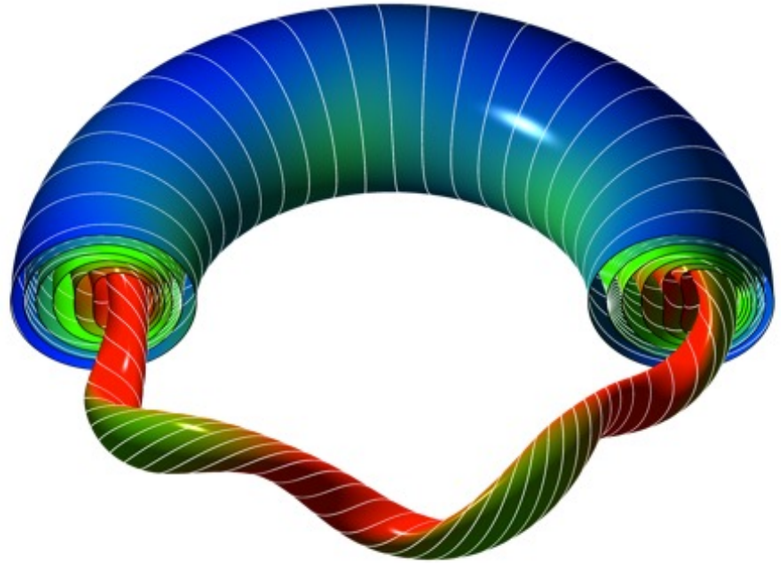

MH = Multiple Helicity = Standard RFP

QSH = Quasi-Single Helicity = Helical RFP

m=1,n=5 core-resonant tearing mode

Phase controlled with RMPs

$$\frac{\tilde{b}_5}{|B|} \sim 5 - 8\% \quad \frac{\tilde{b}_{6-16}}{|B|} \sim 0.5 - 2\%$$

3D-RFP Possesses a Helical Core Surrounded by Typical RFP Stochasticity

- The core-most resonant tearing mode grows and envelops the magnetic axis forming a well-ordered helical core
- Helical RFP exhibits good thermal confinement

Standard RFP

Helical RFP

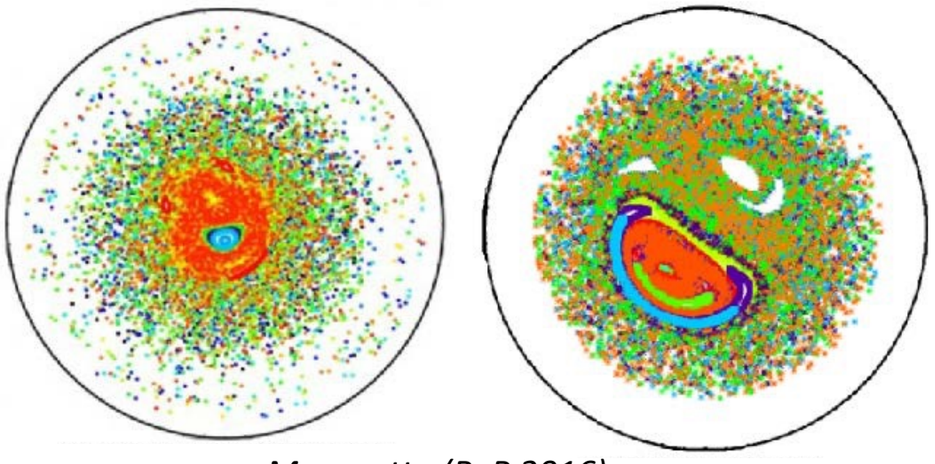

Munaretto (PoP 2016)

Temperature Increase

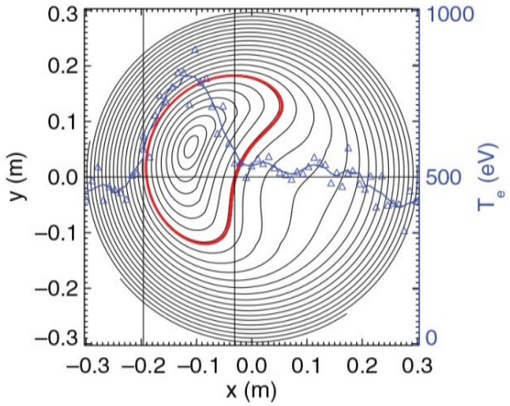

Lorenzini (PRL 2016)

Density Increase

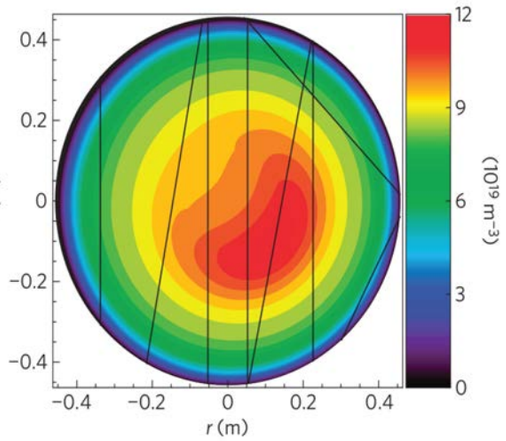

Lorenzini (Nature 2009)

SXR Emissivity Increase

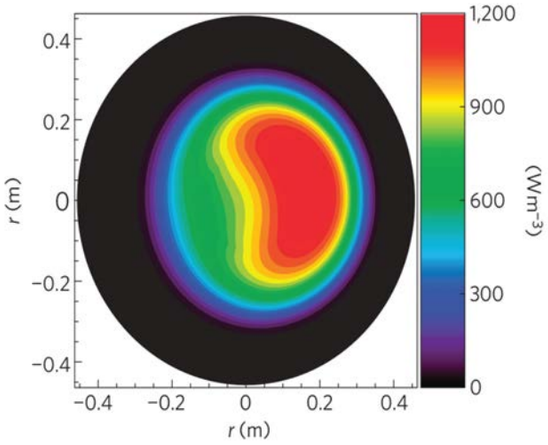

Lorenzini (Nature 2009)

Problem: Fast Ion Confinement Worsens in the Helical State – Why?

- Fast ion confinement time measured from decaying neutron rate with beam-blip technique

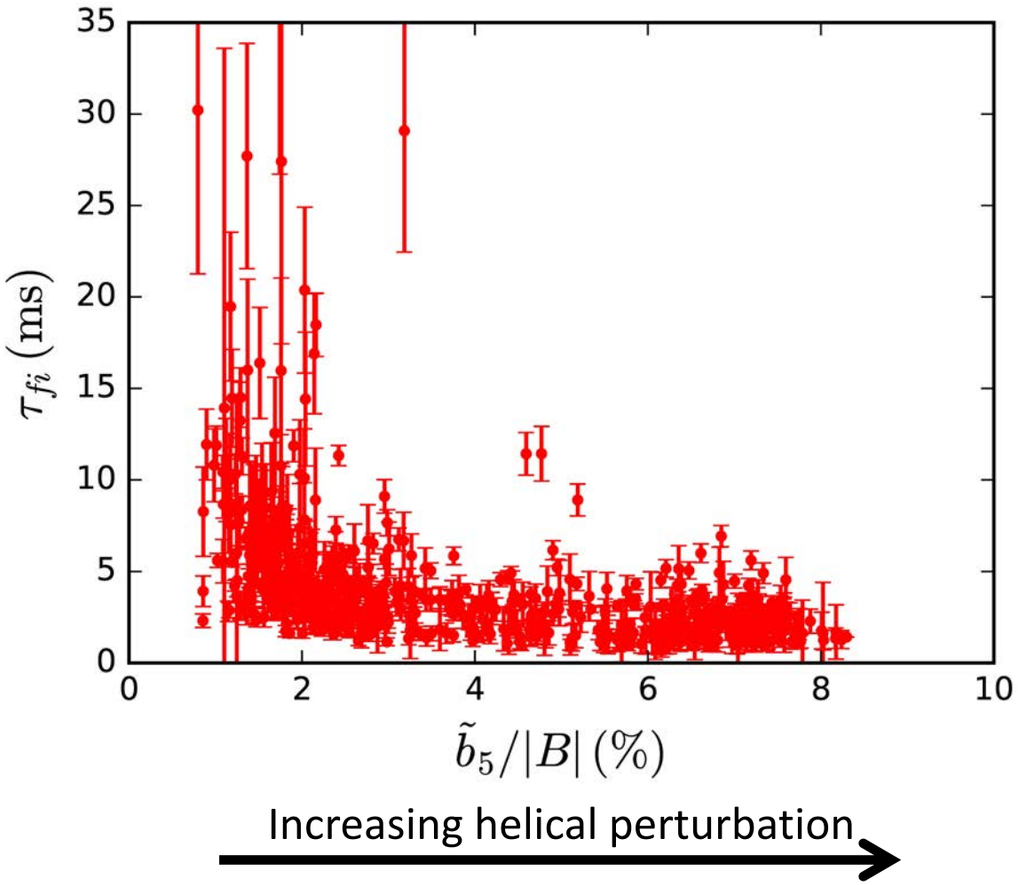

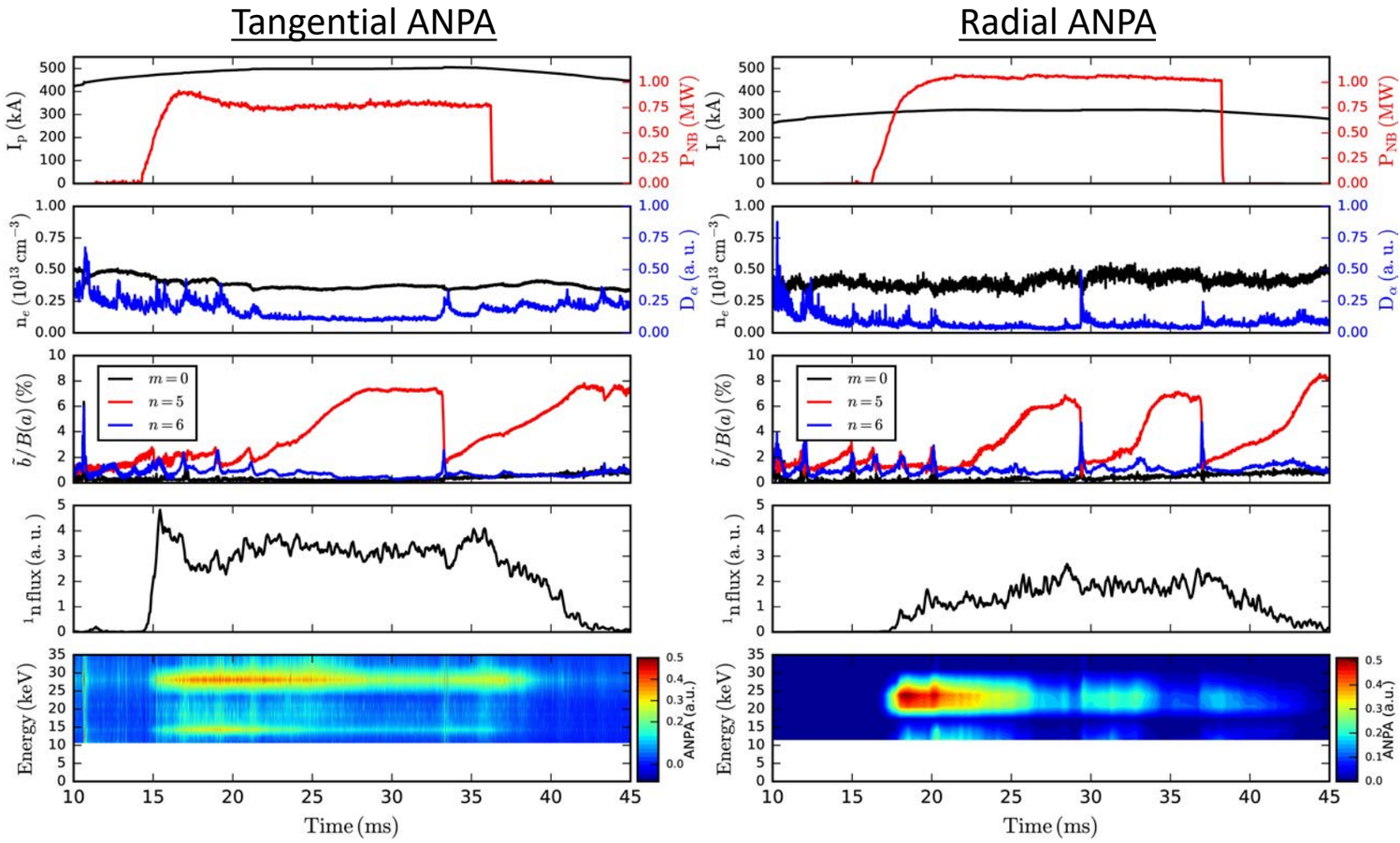

Energetic Particle Bursts React Strongly to the Changing Equilibrium

- Bursts up-shift in frequency with growth in the n=5 perturbation and then disappear

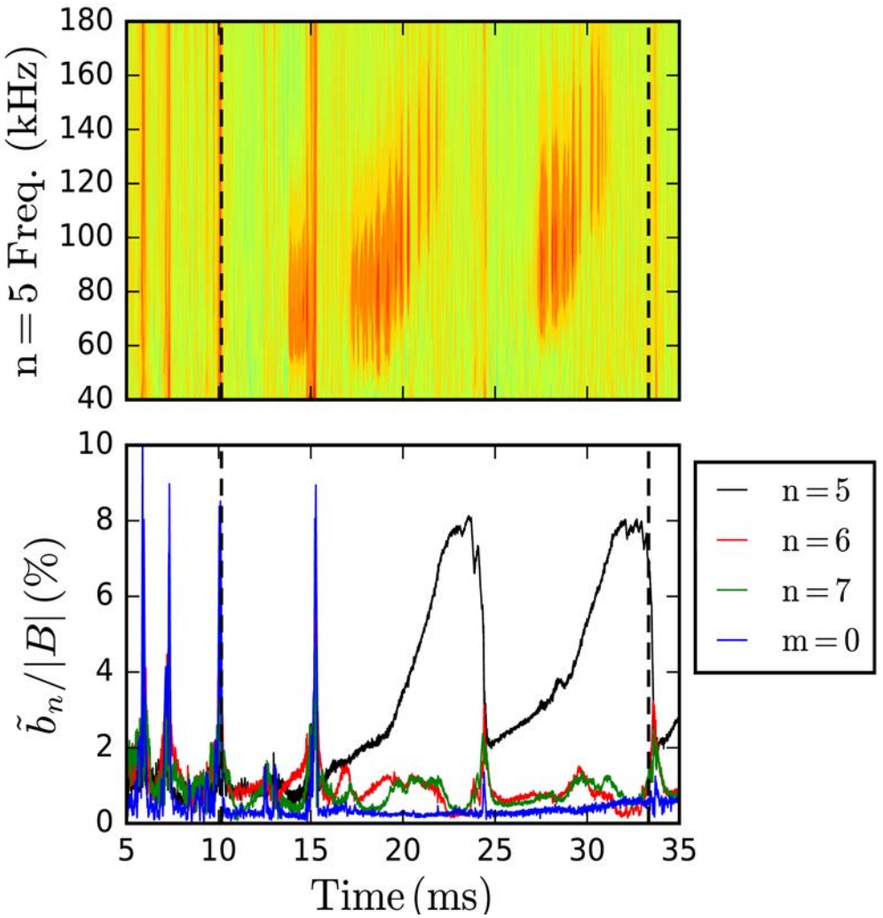

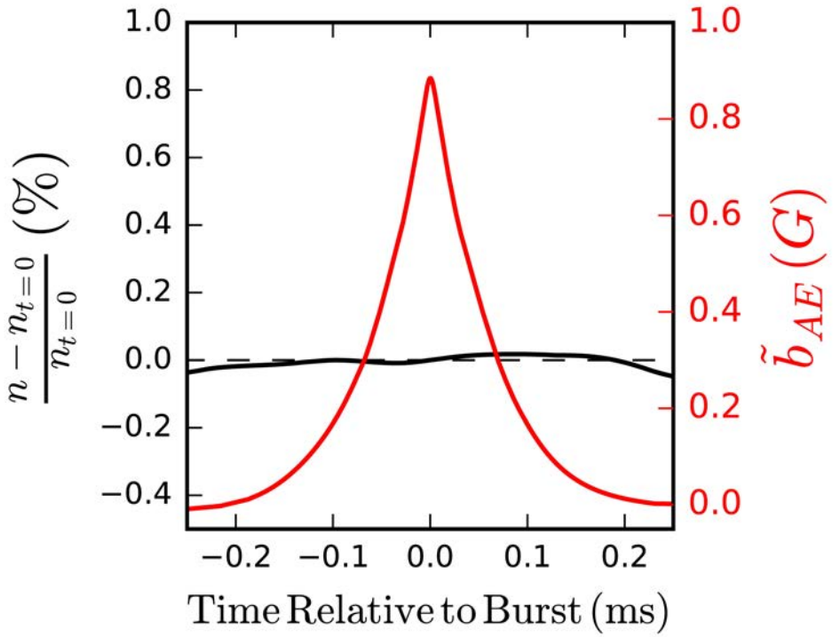

- Global neutron flux is nearly constant throughout burst
- Overall volume integration of the particle content is conserved
- Well observed in the standard RFP and shown to cause local redistribution of fast ions but not global losses

Lin (PoP 2013,2014); Koliner (PRL 2012); Cook (PoP 2015); Capecchi (NuclFus 2019)

Helical RFP Promotes the Possibility for Toroidally Trapped Ions

- Standard RFP: Fast ions possess $\rho_L > w_B \rightarrow$ larger diffusive step size (right)
- Toroidal variations in the magnetic field allow for superbanana orbits (bottom left) → Notable in stellarators[a]
- Superbanana orbits can lead to enhanced transport (bottom right)

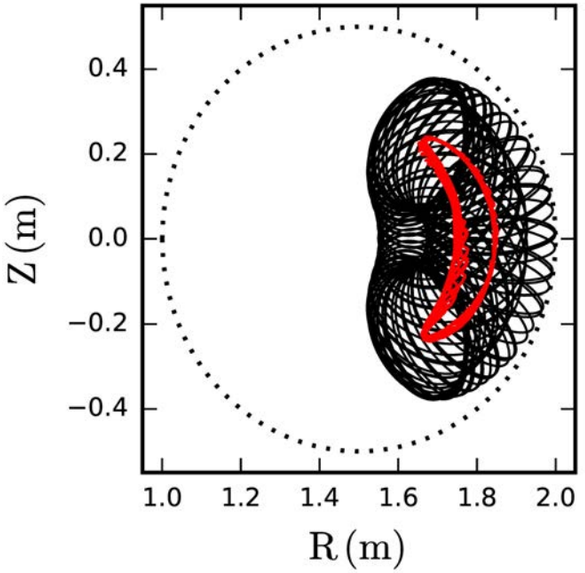

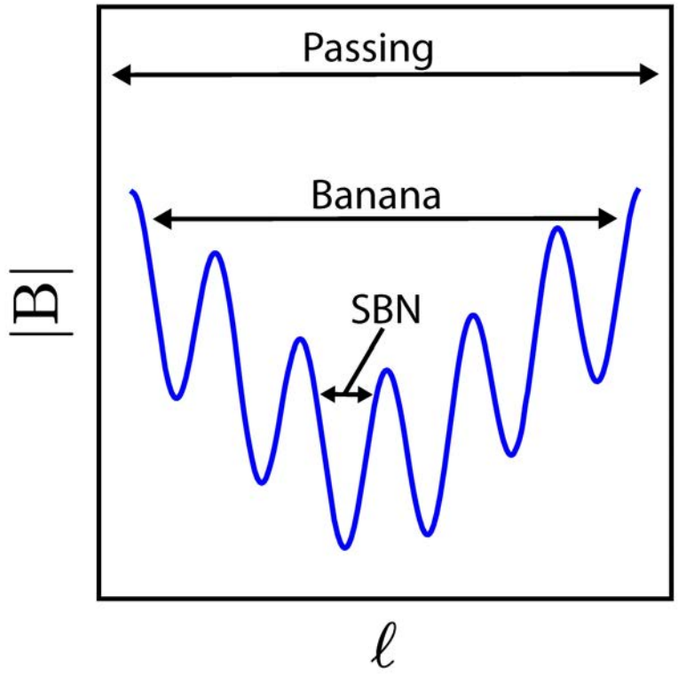

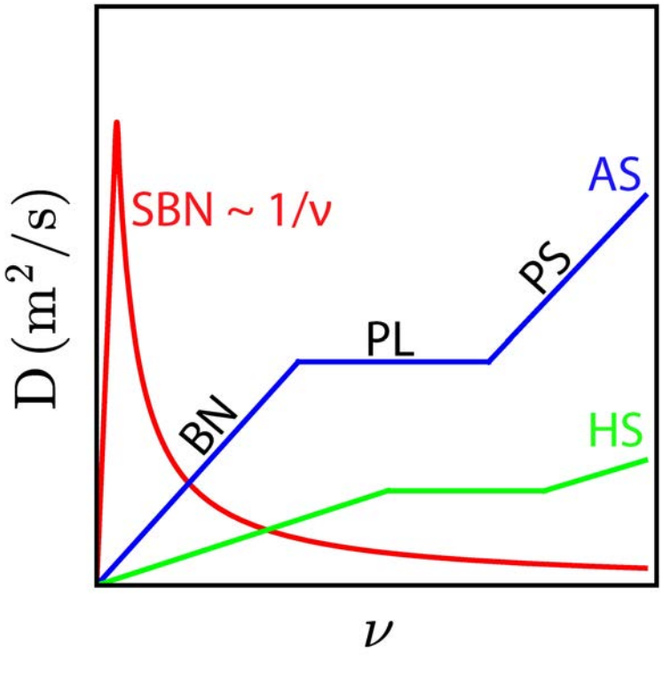

[a]*Mynick (PoP 2006)*

Toroidal Symmetry Breaking Leads to Helical Magnetic Wells

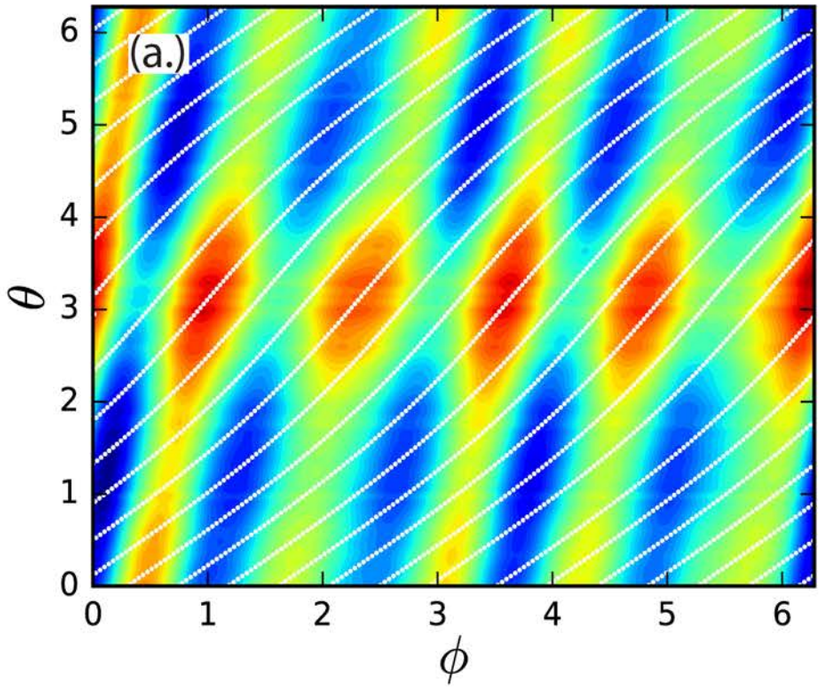

- Toroidal wells exist for helical trapping of low-pitch fast ions and the presence of superbanana orbits

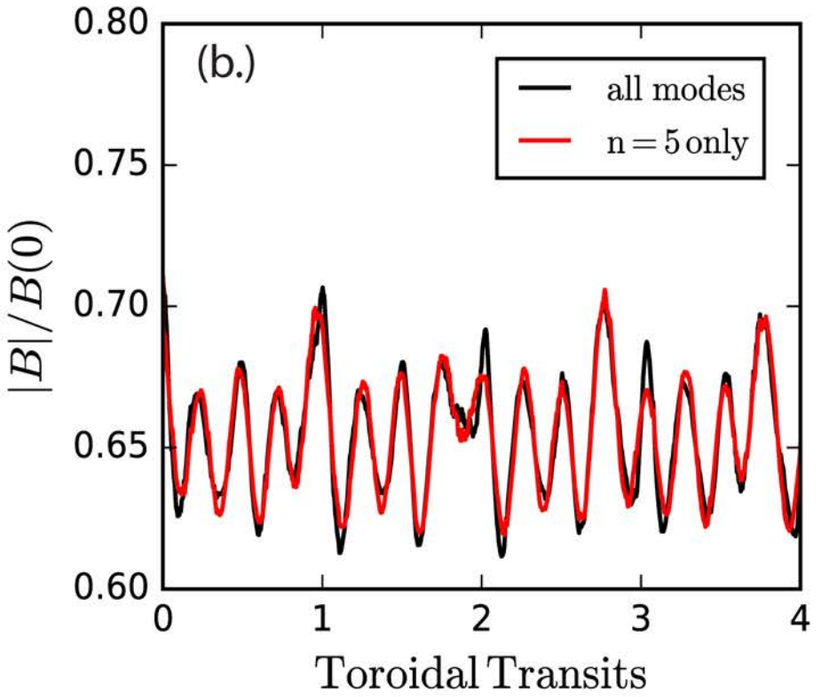

- Fast ion GC's observe different magnetic topology due to drifts

(a.) QSH magnetic contours with field line trace (white lines)

(b.) Magnetic field strength per toroidal transits

Helical RFP Lacks Strong Neoclassical Behavior

$$\Gamma = D\nabla n \longrightarrow D = \frac{\Gamma}{dn/dr}$$

- ORBIT: only (1,5) mode active; no slowing
- No 1/v or superbanana observed
- Consistent with prior work on thermals[a]
- Confirmed with full orbit code where toroidally trapped fast ions are confined
- Helical RFP like omnigenous stellarator[b]:

$$< \vec{v}_d \cdot \vec{\nabla}\psi >\sim 0$$

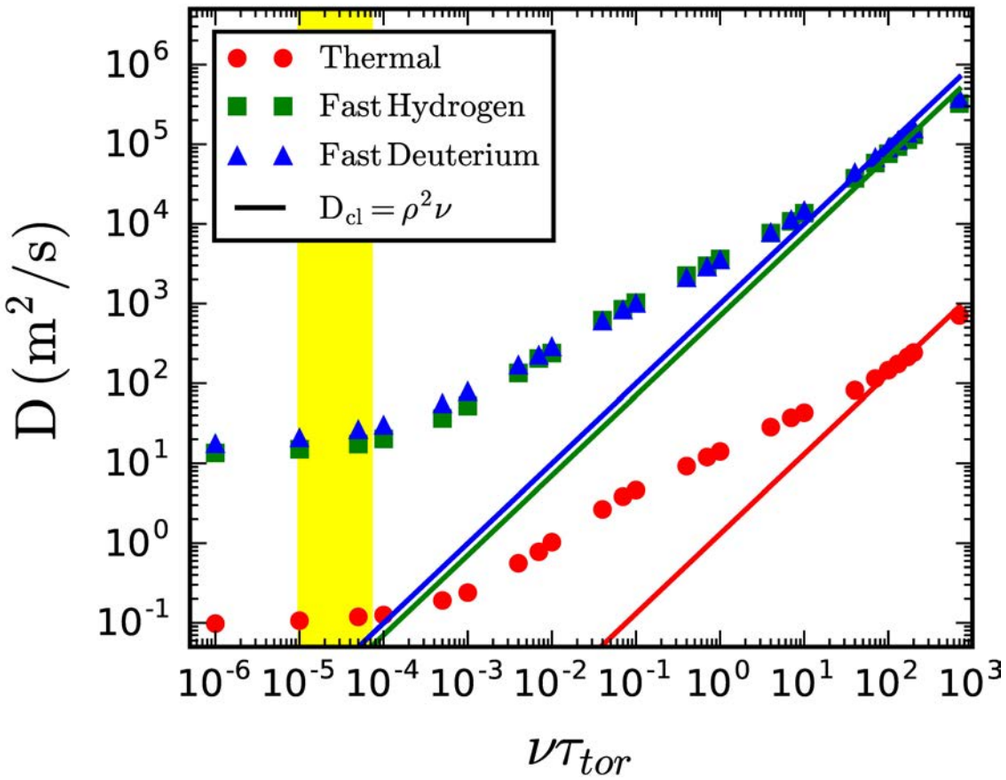

= Experimental Fast Ion Regime

[a] *Gobbin and Spizzo (PRL 2010)*
[b] *Cary and Shasharina (PRL 1997, PoP 1997)*
[c] *Eigenfunctions: Zanca and Terranova (PPCF 2004)*

Fast Ion Confinement Reduces with Growing Helical Perturbation Strength

1.

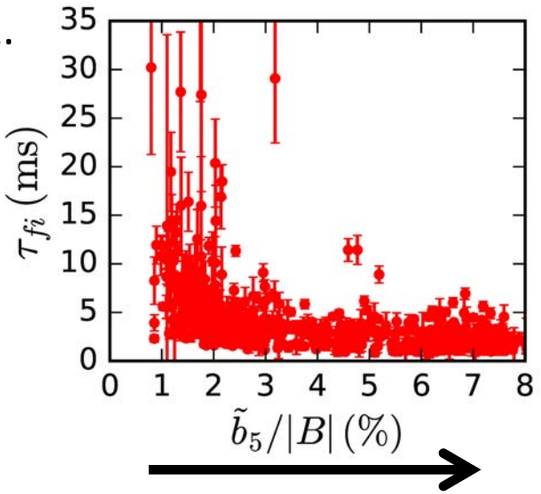

1. Experimental measurements

→ = Increasing helical perturbation

ORBIT Simulations Replicate Experimental Loss Times

1.

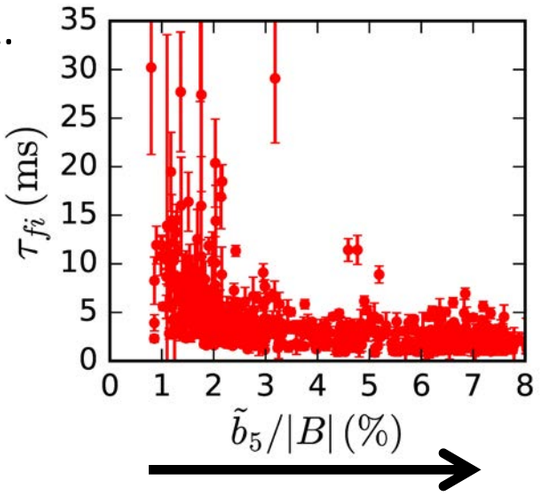

2.

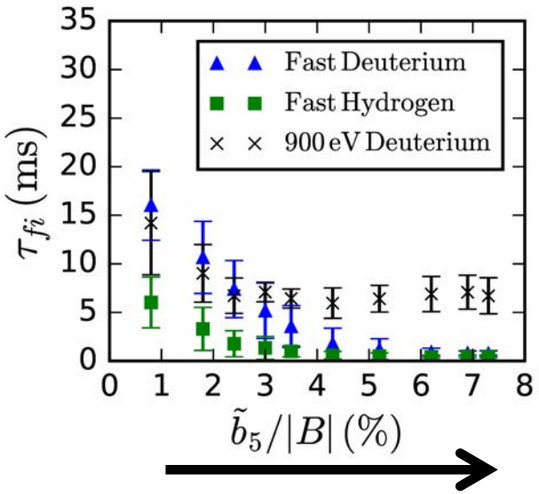

1. Experimental measurements
2. ORBIT simulations mimicking experiment

→ = Increasing helical perturbation

Fast Ion Loss Times Show Strong Dependence with Subdominant Tearing Modes

1.

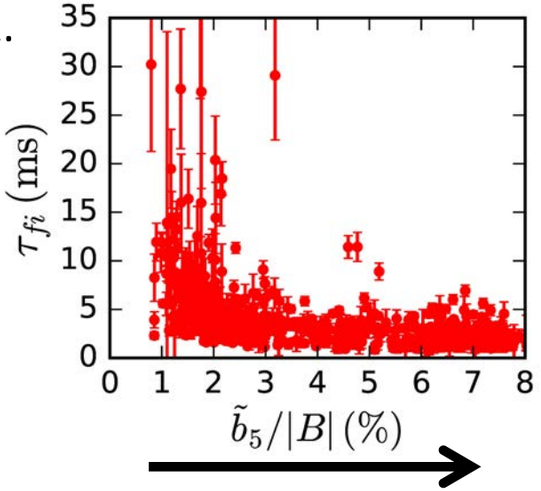

2.

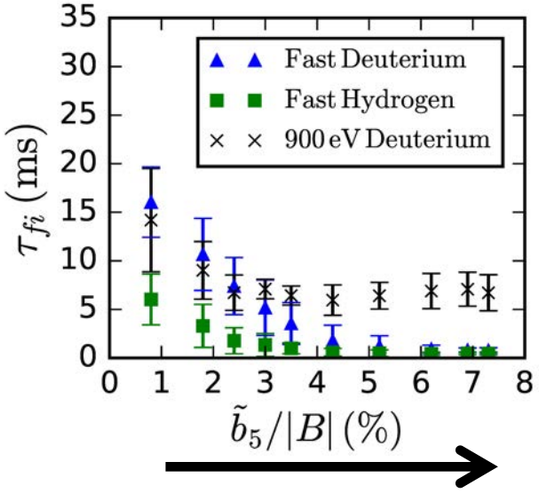

3.

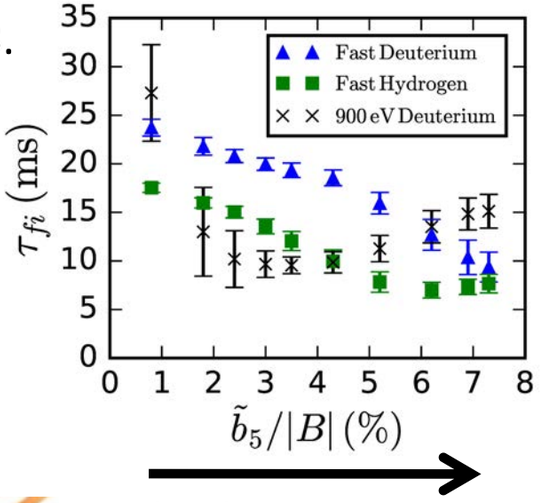

1. Experimental measurements
2. ORBIT simulations mimicking experiment
3. ORBIT simulations (1,5) only

→ = Increasing helical perturbation

Subdominant Modes in Helical State Cause Drastic Reduction in Confinement

1.

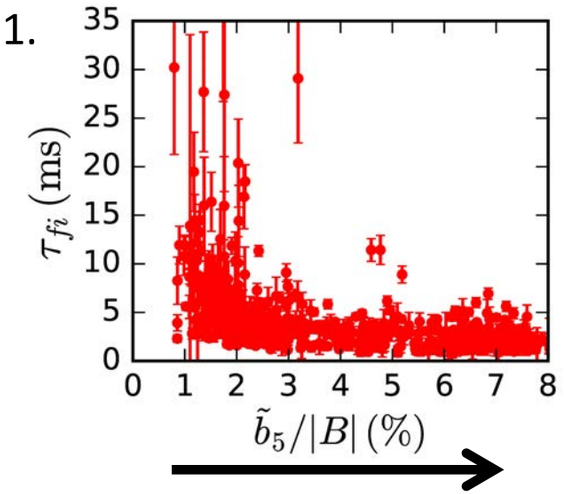

2.

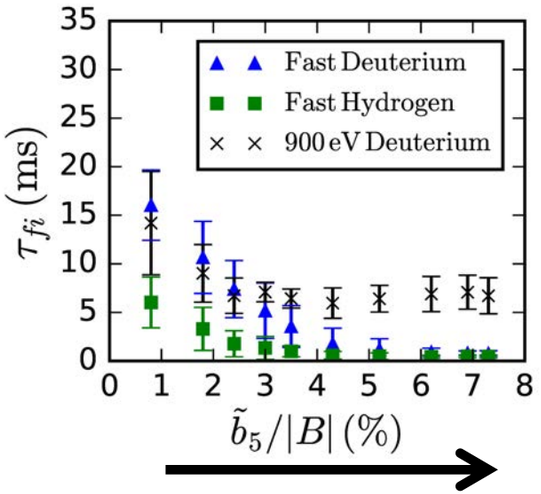

3.

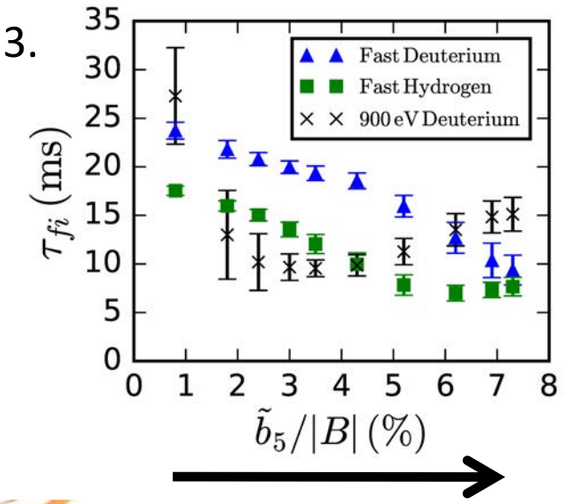

4.

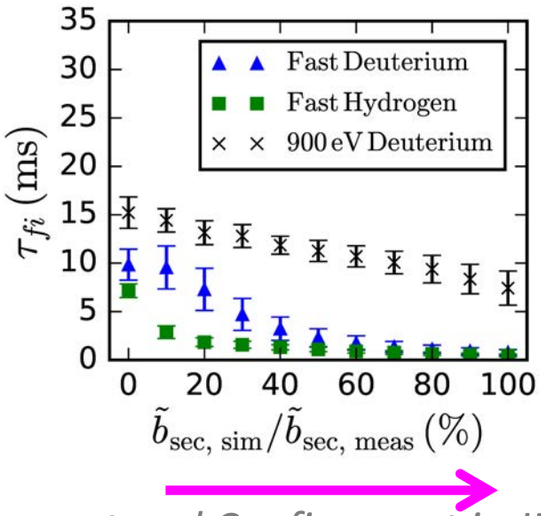

1. Experimental measurements
2. ORBIT simulations mimicking experiment
3. ORBIT simulations (1,5) only
4. ORBIT QSH simulations scaling secondary modes

→ = Increasing helical perturbation

→ = Increasing subdominant amps

Fast Ion Phase-Space Shows Increased Stochasticity in Transition to 3D-RFP

- Poincaré plots from ORBIT
- FAST ION PHASE-SPACE

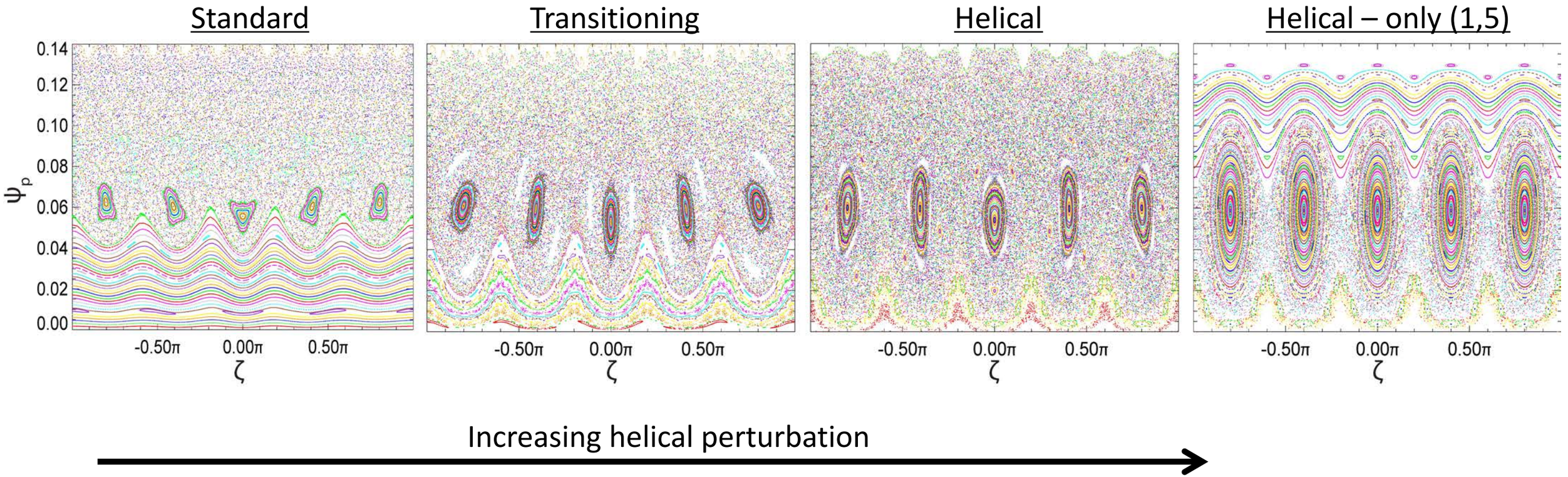

Fast Ion Phase-Space Stochasticity is Dependent on Subdominant Modes

- Poincaré plots from ORBIT: all plots have core-resonant strength of 7.5%
- FAST ION PHASE-SPACE

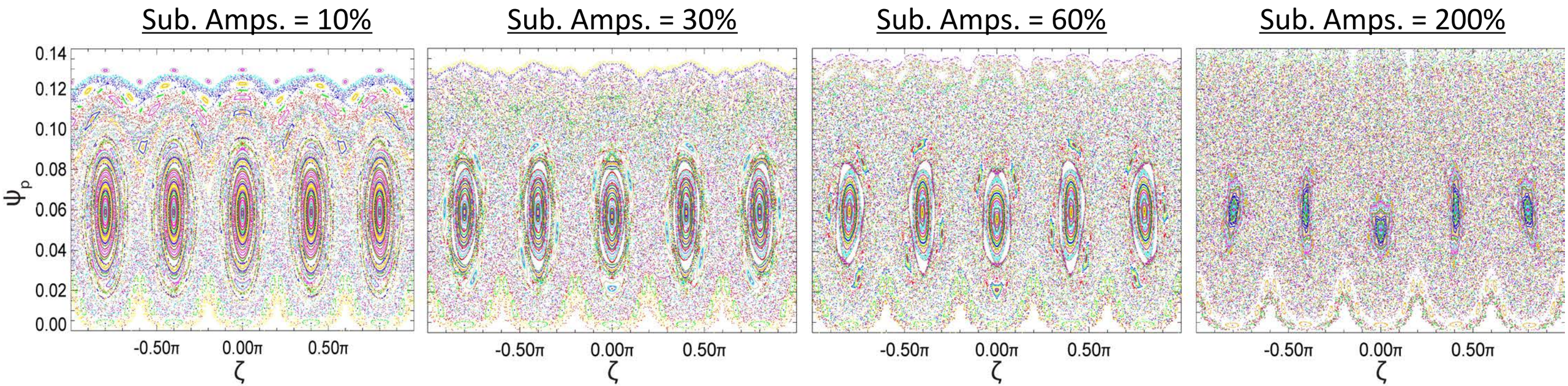

Increasing subdominant amplitudes

Fast Ion Transport Scales with Rechester-Rosenbluth like Diffusion

Stochasticity Parameter

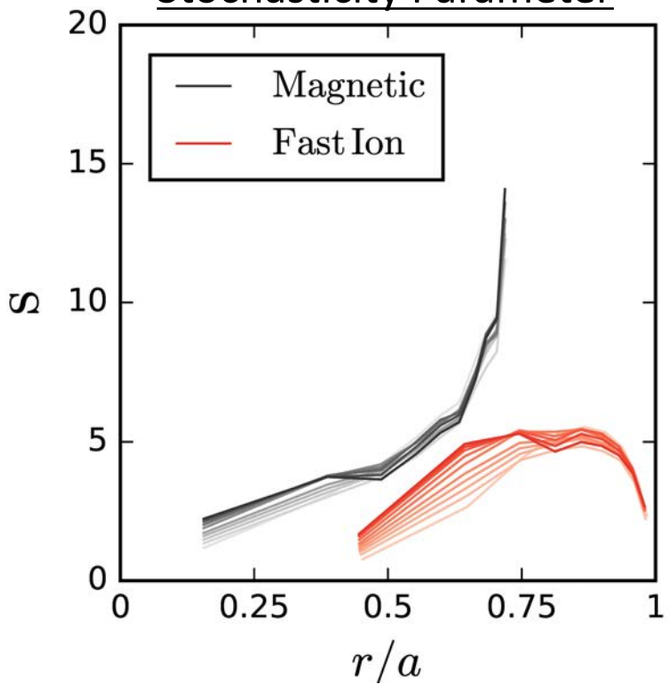

$$s = \frac{1}{2}\frac{w_{m,n} + w_{m',n'}}{|r_{m,n} - r_{m',n'}|}$$

Rechester & Rosenbluth (PRL 1977)

RR-Diffusion Scaling

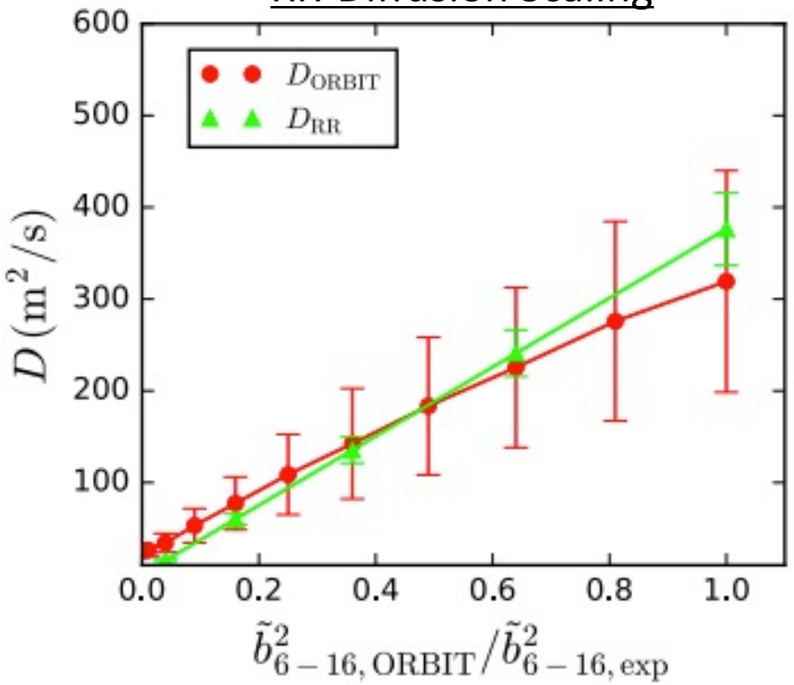

Light line = Standard RFP
Dark line = Helical RFP

$$D_{\mathrm{RR}} = \pi R v_{fi} \sum_{m,n} \frac{\tilde{b}_r^2}{B_\phi^2}\delta(m - nq)$$

$$D_{\mathrm{ORBIT}} = v_{fi}\frac{< \Delta r^2 >}{2L}$$

- Fast ion phase-space stochasticity approaches magnetic stochasticity
- RR transport is a function of the subdominant mode amplitudes
- Observed transport is consistent based on large n=5 island coupled with overlapping subdominant resonances

Conclusions/Future Work

- Fast ion transport in the helical RFP is dominated by tearing mode induced fast ion phase-space stochasticity with negligible neoclassical and wave-particle instability effects (*Bonofiglo 2019 PoP & 2020 PRL*)

- Scaling relations between MST and RFX-Mod show that subdominant tearing modes reduce further in amplitude with increase in Lundquist number:
    - Go bigger…
    - Further computational modeling seems most reasonable path forward

Outline

- Fast Ion Transport in the Non-axisymmetric RFP
  - Energetic Particle Instabilities
  - Neoclassical Enhancement
  - Tearing Mode Effects
- Integrated Modeling on JET
  - JET's Fast Ion Loss Detector
  - Synthetic Loss Model
  - Experimental Validation
- Future Work

Motivation

- Discrepancies between EP modeling and experiment still exist -> Still much to learn!
- Wish to better quantify effects of EP transport on local EP quantities of interest (ideally those that are measurable)
- Increasing complexity with multi-ion species plasmas, 3D-fields, heating scenarios, multi-modal interactions, etc.
- JET DT-ops are now! ITER is approaching and fusion pilot plants are being designed

Experimental FILD Signal on JET[a]

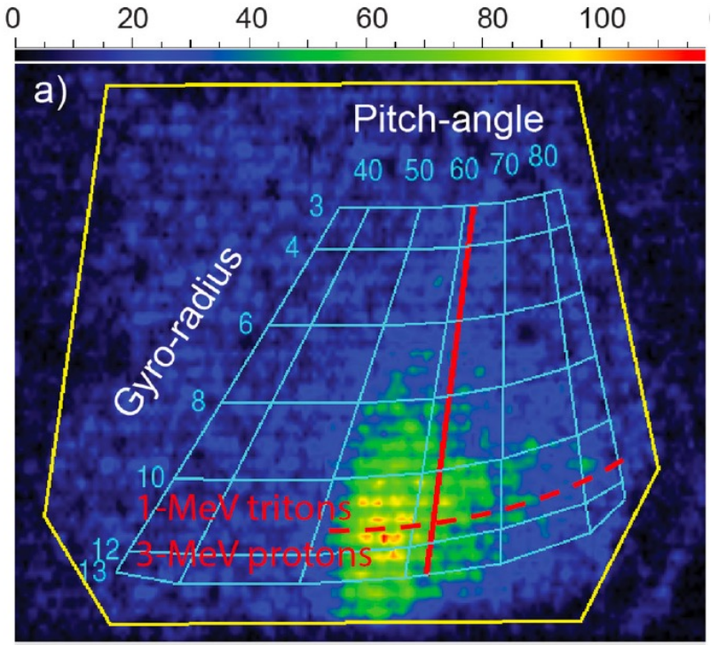

Synthetic FILD Signal for ITER[b]

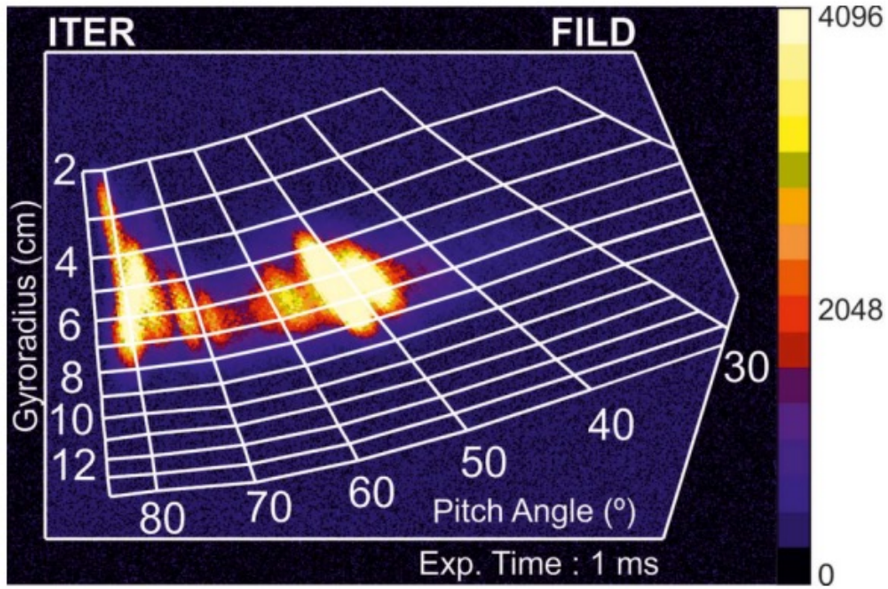

[a]*Kiptily (NuclFus 2018)* [b]*Garcia-Munoz (RSI 2016)*

Direct Comparison & Interpretation between Experiment and Numerical Modeling is Strongly Desired

- Need to develop and validate integrated modeling/predictive tools to study transport phenomena
  - How do these phenomena impact EP confinement (i.e. losses)?
  - Can we replicate experimental measurements with a numerical model?
  - Can we synergistically combine experiment and model to garner more information/physics?

- Experimental measurements (neutons, FIDA, NPA, FILD) lack detail while modeling needs verification and validation

Synthetic FILD Signals can be Used to Validate/Constrain EP Transport Models

- Need to develop and validate integrated modeling/predictive tools to study transport phenomena
  - How do these phenomena impact EP confinement (i.e. losses)?
  - Can we replicate experimental measurements with a numerical model?
  - Can we synergistically combine experiment and model to garner more information/physics?

- Experimental measurements (neutons, FIDA, NPA, FILD) lack detail while modeling needs verification and validation

- JET's FILDs well suited for the problem at hand:

  Synthetic Faraday Cup FILD:

  - Signal is a result of direct capture of lost ions
  - Measurements strongly correlate with loss mechanisms
  - Numerical interpretation is "straightforward" by strictly tracking particle motion
  - Poor statistics = many particles and long run time

JET Maintains an Array of 5 Faraday Cup Fast Ion Loss Detectors[a]

General

- Foil stacks are alternating layers of Ni and mica
- Ion energy determines deposition depth → Can't identify ion species
- Only way to differentiate ions is through modeling

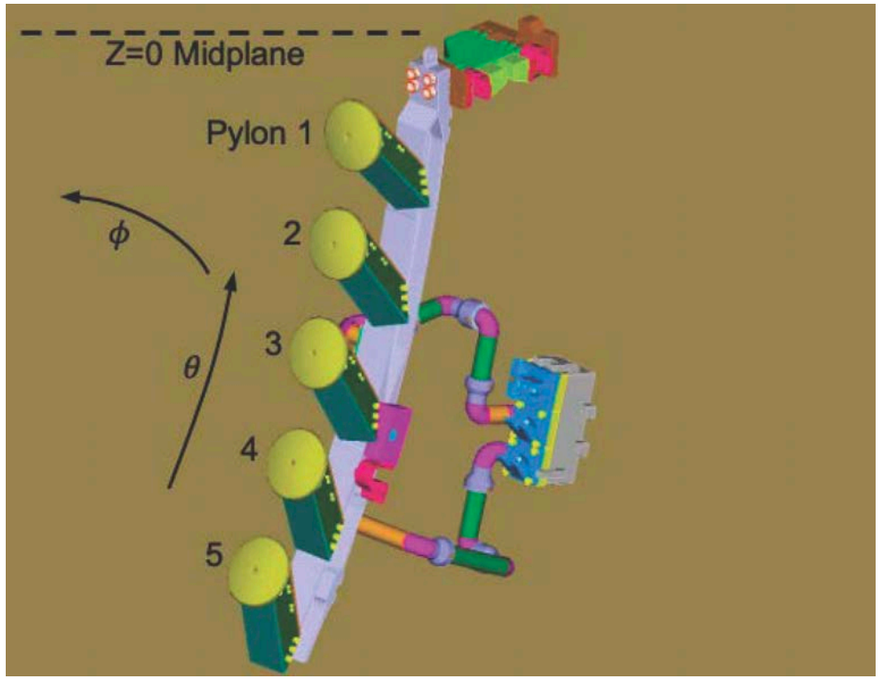

Faraday Cup Assembly (Old 8-stack Design)

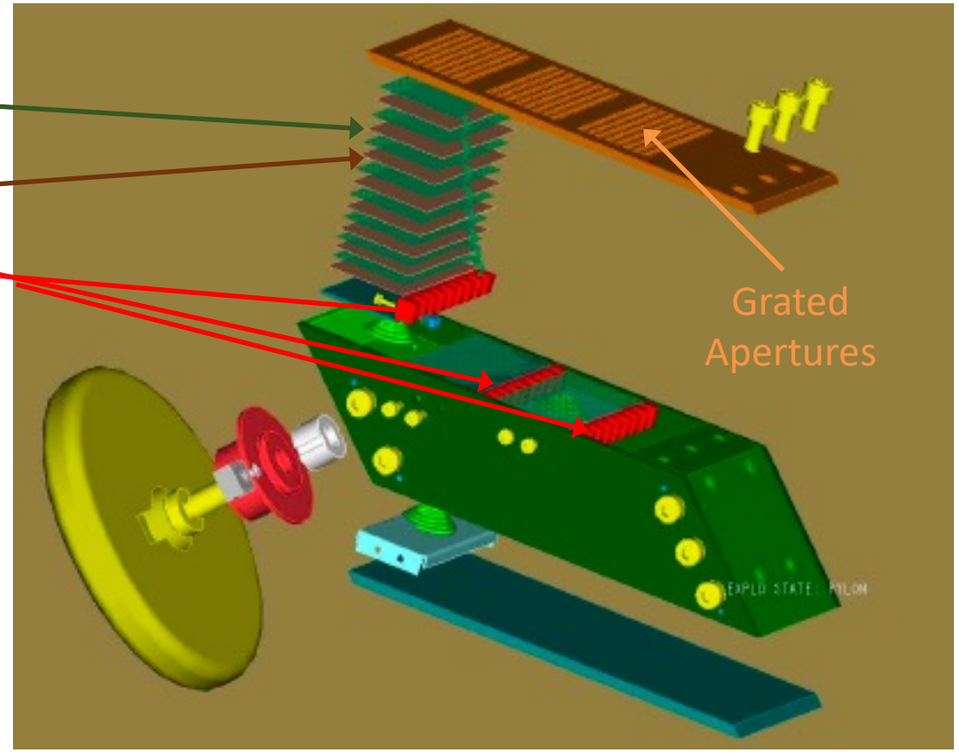

[a]*Darrow (RSI 2004, 2006, 2010)*

JET Maintains an Array of 5 Faraday Cup Fast Ion Loss Detectors[a]

General

- Foil stacks are alternating layers of Ni and mica
- Ion energy determines deposition depth → Can't identify ion species
- Only way to differentiate ions is through modeling

Faraday Cup Assembly (Old 8-stack Design)

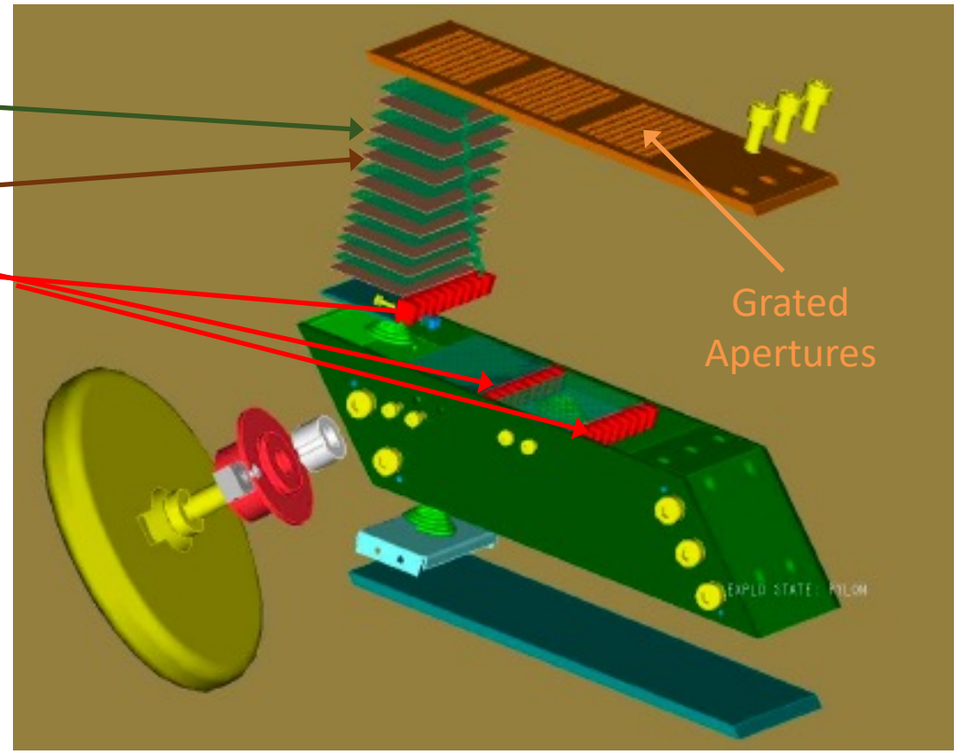

Energy Deposition Range per Foil[†]

Depth (μm)	Proton Energy Range (Mev)	Deuteron Energy Range (Mev)	Triton Energy Range (Mev)	He3 Energy Range (Mev)	Alpha Energy Range (Mev)
0.0 – 2.5	0.0 – 0.49	0.0 – 0.49	0.0 – 0.50	0.0 – 1.55	0.0 – 1.54
5.0 – 7.5	0.68 – 0.96	0.79 – 1.10	0.84 – 1.20	2.30 – 3.35	2.48 – 3.55
10.0 – 12.5	1.10 – 1.32	1.35 – 1.60	1.48 – 1.76	3.90 – 4.70	4.17 – 5.09
15.0 – 17.5	1.45 – 1.65	1.78 – 2.00	2.00 – 2.25	5.20 – 5.80	5.60 – 6.35

[†]*Found via SRIM code*

[a]*Darrow (RSI 2004, 2006, 2010)*

Losses due to a Variety of MHD Activity have been Observed in JET Deuterium Plasmas[a]

Kink Modes

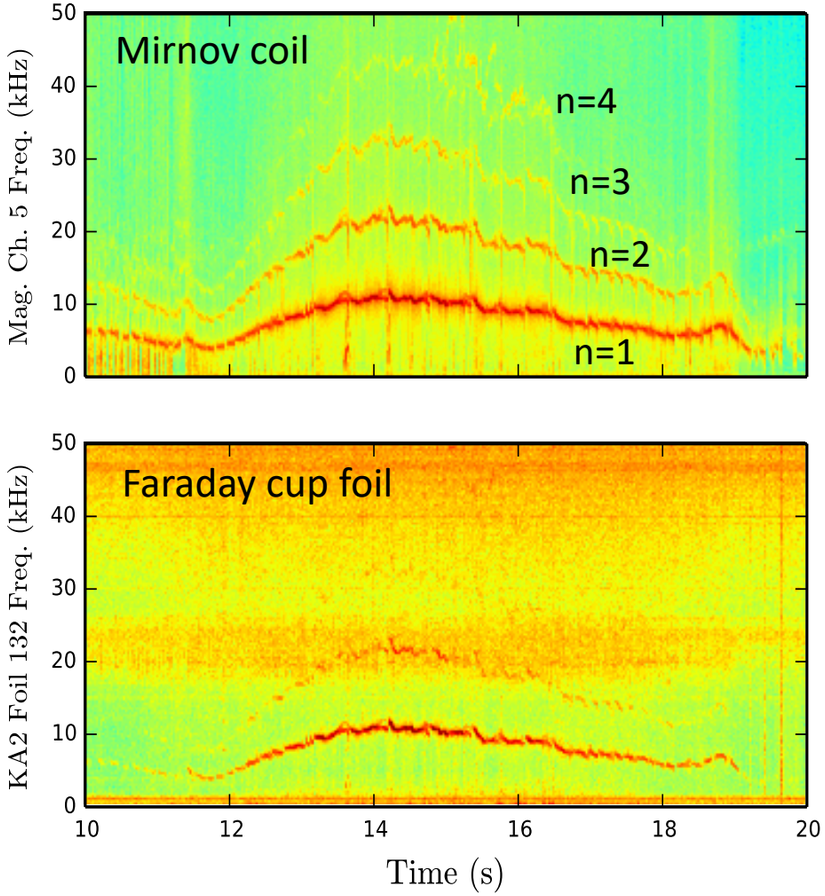

Fishbone Modes

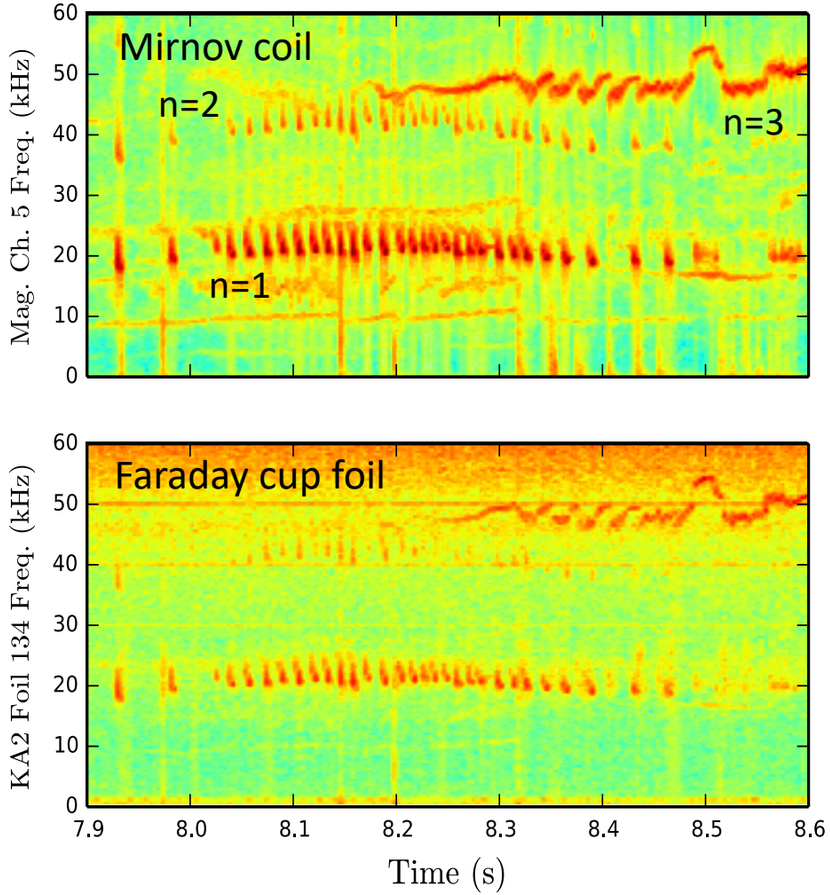

ELMs

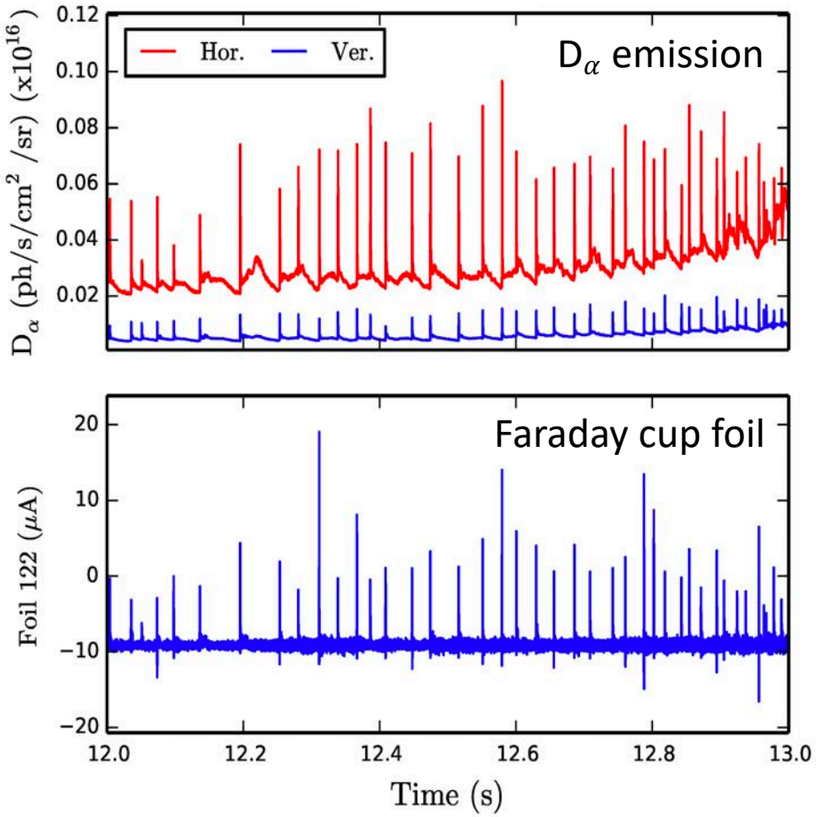

[a]*Bonofiglo (RSI 2020)*

Reference Case: D-Plasma with D-NBI+ICRH Low Freq. MHD

- Heating: 25 MW NBI, 6 MW ICRH
- Fast ions: deuterons, DD-tritons, DD-protons, (minority fraction <1% and ignored)
- Long-lived, low freq. modes observed in magnetics, scintillator probe, and Faraday cup

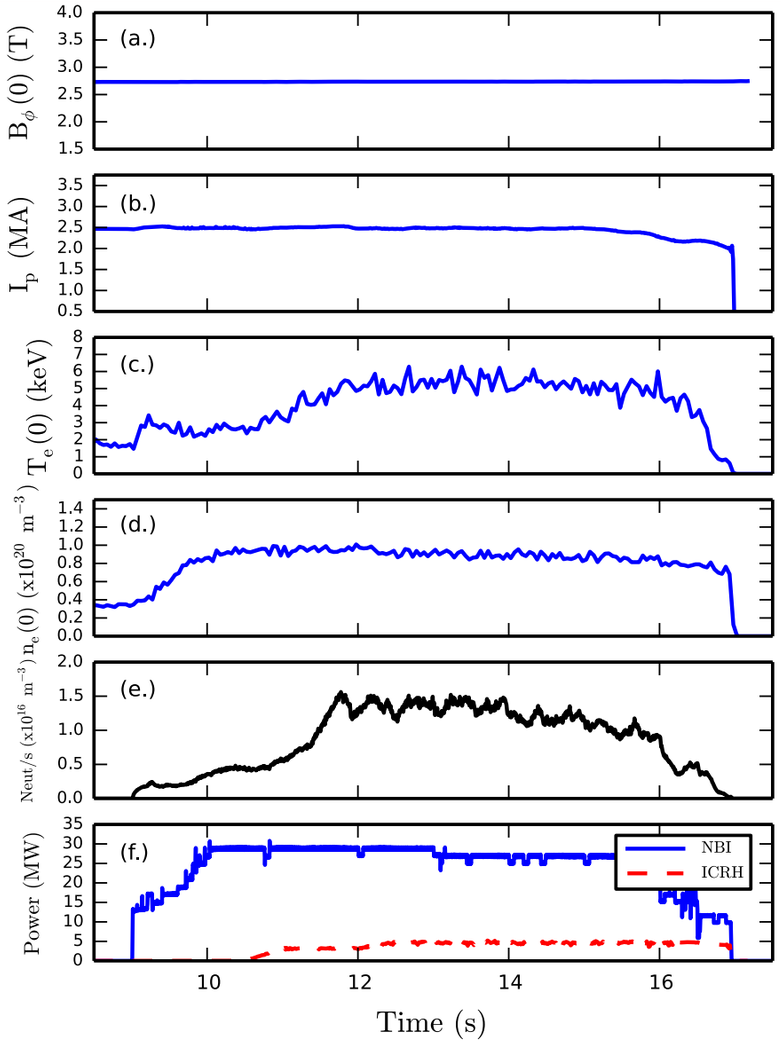

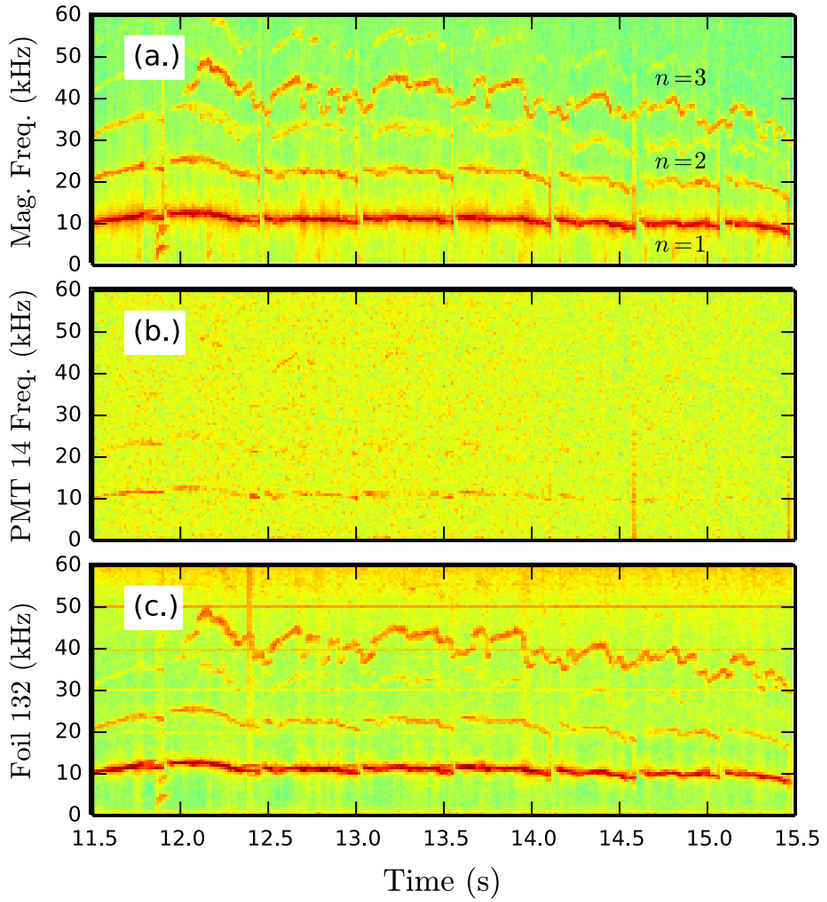

(a.) Magnetic Coil (b.) Scintillator FILD
(c.) Faraday Cup Foil

ORBIT Code Handles Main Particle Pushing in the Numerical Model with "Kick" Features

- ORBIT[a]: Particle pushing code that calculates fast ion motion using Hamiltonian guiding-center mechanics
- "Kick"-model[b]: Calculates EP transport due to a supplied perturbation in the form of changes in the constants of motion[c] (energy - E, canonical angular momentum - P_ϕ)

Example ORBIT "Kick"

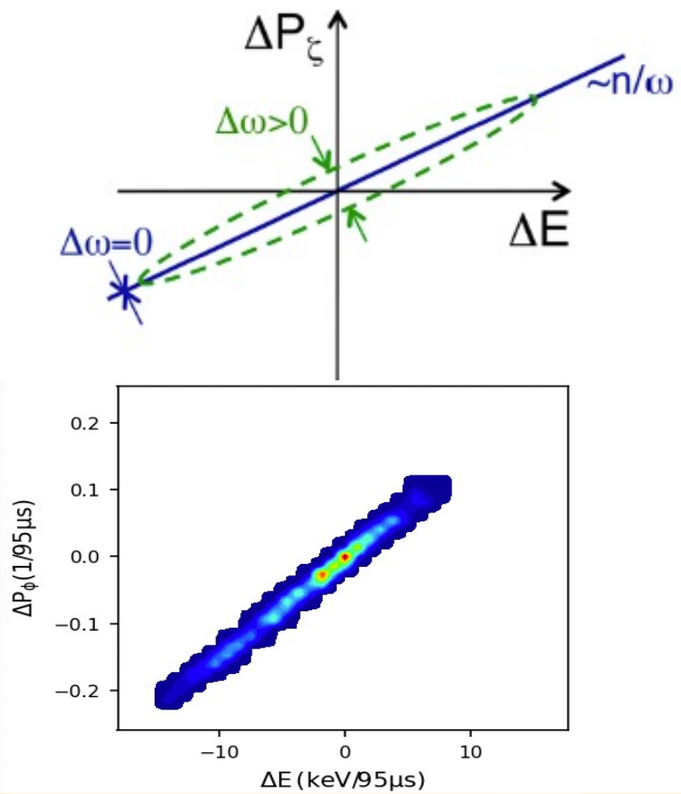

Example ORBIT Phase-Space Topology

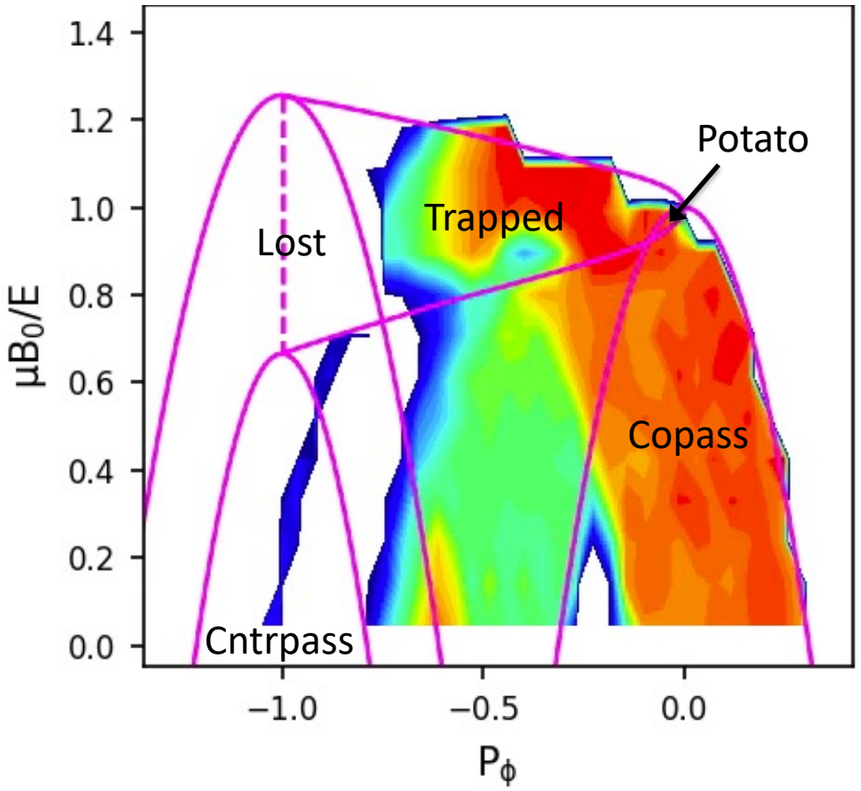

[a] *White (PhysFluids 1984)*
[b] *Podesta (PPCF 2014)*
[c] *Heidbrink (PoP 2008)*

Code Sets can be Combined to Form a Fully Integrated Model to Produce Synthetic Losses

- A classical/neoclassical transport model (TRANSP[a] EP dist.) is combined with resonant wave-particle interactions via the fast ions' constants of motion (ORBIT-kick[b]) which maps lost orbits to a synthetic detector
- TRANSP[a] provides a time-dependent simulation of the equilibrium and fast ion distribution within a large physics frame (evolving profiles, atomic physics, transport+heating, etc.)

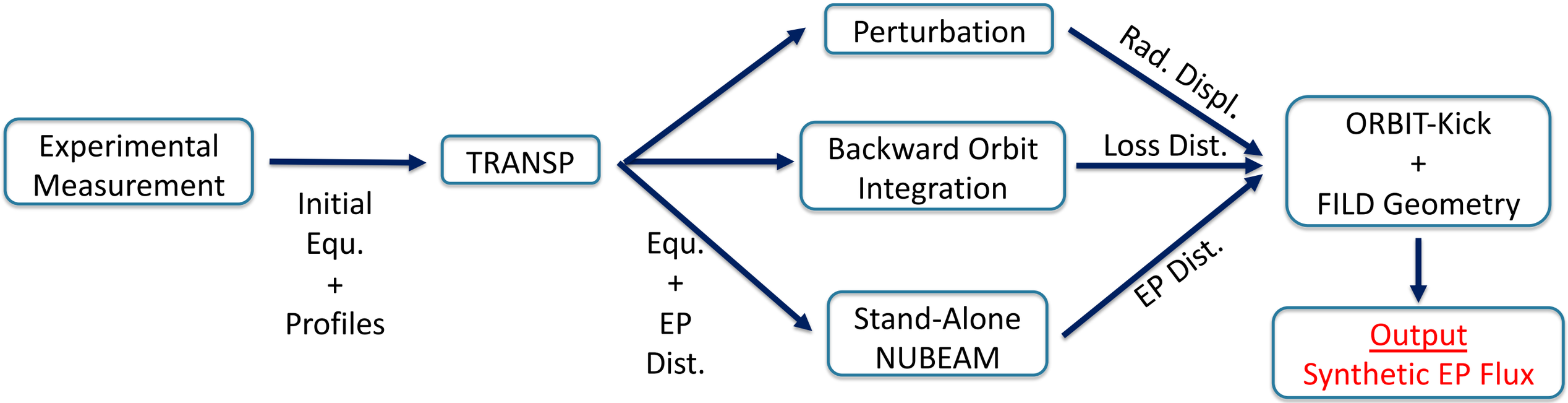

[a]*doi:10.11578/dc.20180627.4* [b]*Podesta (PPCF 2017)*

Stand-Alone NUBEAM Runs Add Statistics to the RF Tail at the Detector Resolveable Energies

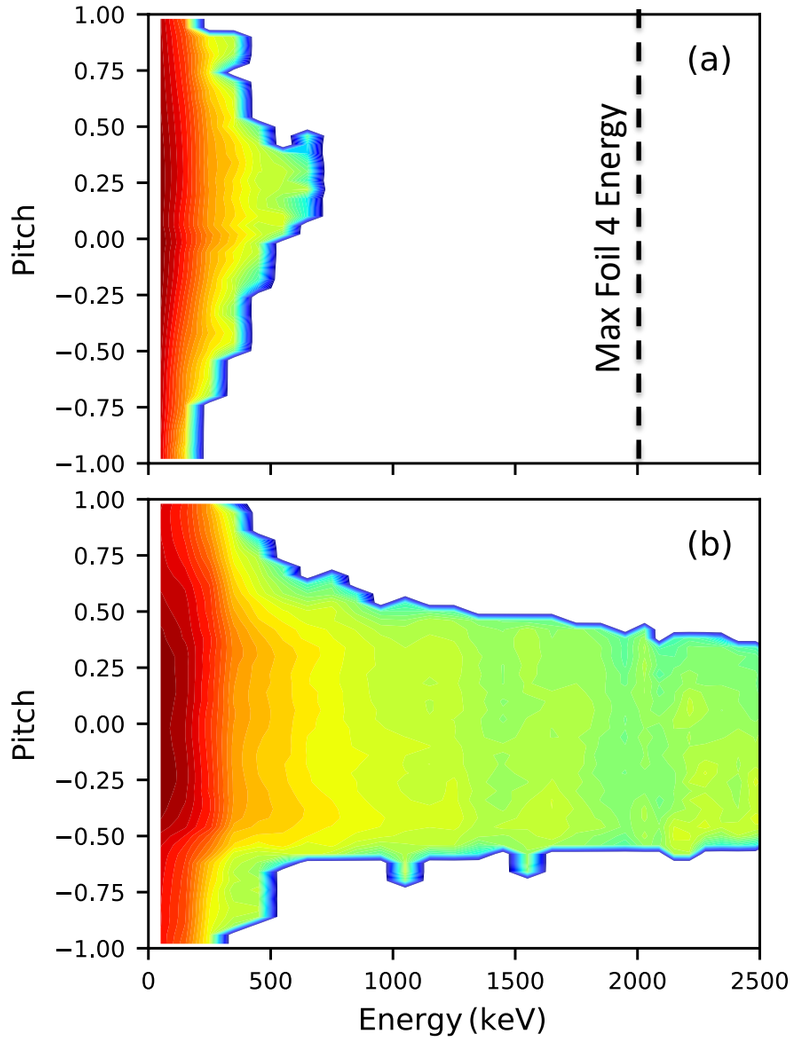

- Faraday cup FILD can measure up to 2 MeV deuterons → far on the RF-tail
- Typical TRANSP run uses 3e4-2.5e5 NBI markers which cannot fully resolve the RF-heated tail up to the needed energies
- Use plasma state files from TRANSP run as input for the NUBEAM submodule only
- Ensemble the individual runs together to better fill in the fast ion distribution

(a) Original deuteron distribution
(b) Ensembled deuteron distribution after 30 stand-alone NUBEAM runs

Detector Measurements are Connected to the Model by Integrating Loss Orbits Backward[a]

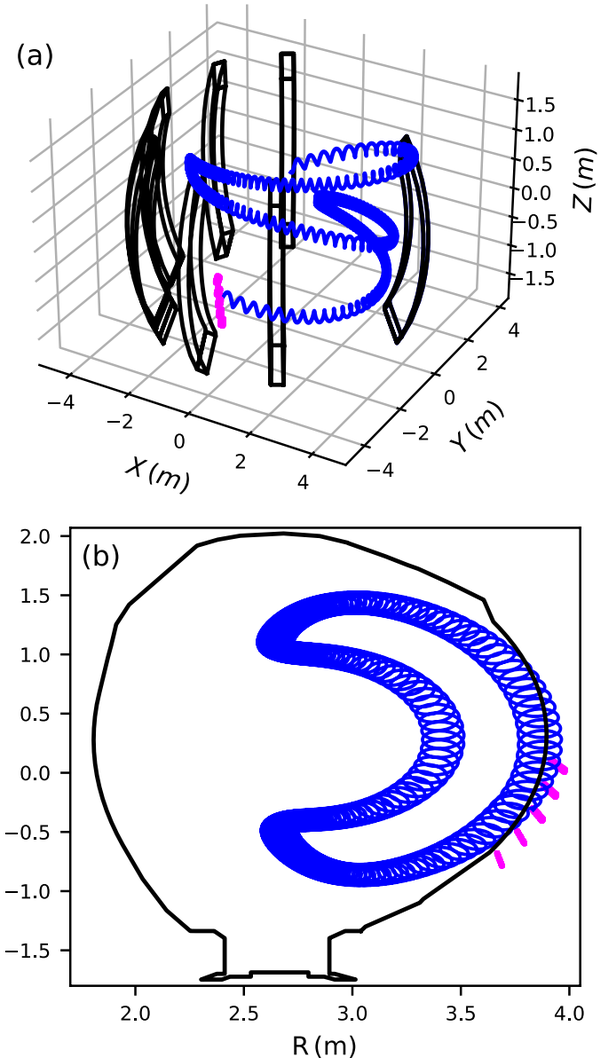

- Encompasses previous efforts on JET[b-c]
- Backwards integration performed with an ad-hoc full-orbit code without perturbation
- Initial conditions: equilibrium, Faraday cup apertures, energy, mass, charge, launch angle (pitch)
- Produce an exact loss distribution to compare/bias against the TRANSP computed distribution

(a) 1.5 MeV deuteron orbit in 3D (blue); limiters (black); FILD apertures (pink)
(b) Poloidal projection of orbit

[a]Code courtesy of V. Goloborodko
[b]Perez von Thun NuclFus 2011
[c]Fitzgerald NuclFus 2019

A Full Loss Distribution is Formed from Reverse Integrated Particles

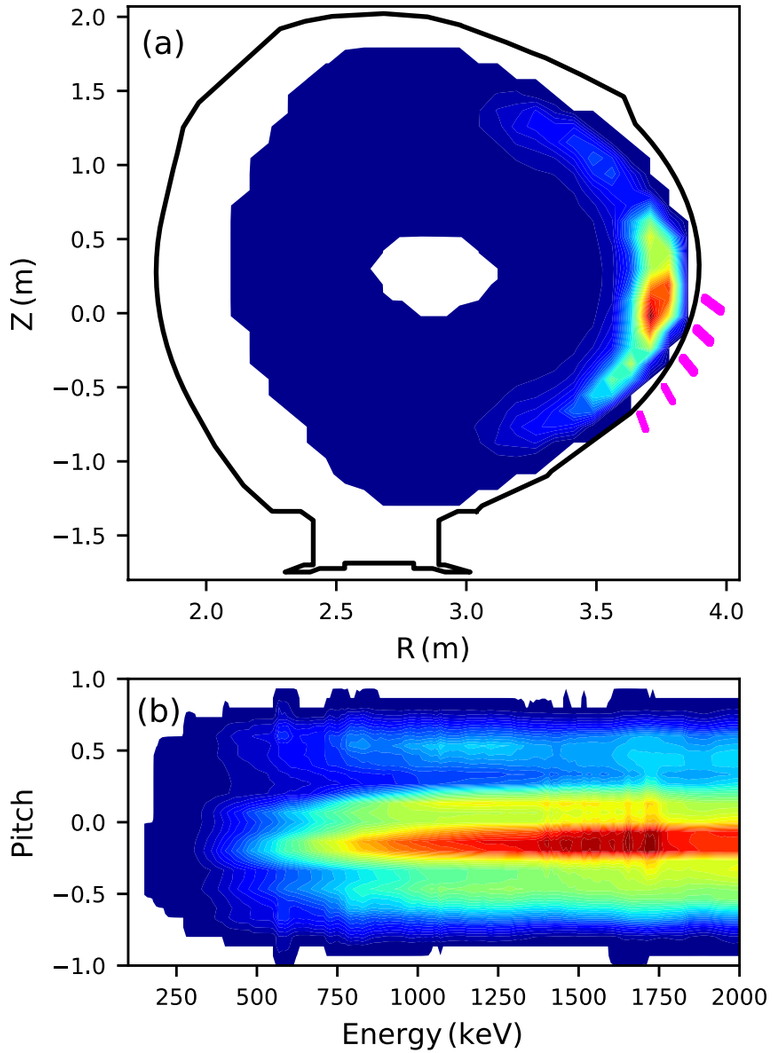

- Vary initial pitch and energy within the diagnostic's constraints and launch many particles of a given species to form an exact loss distribution
- Preferentially sensitive to particles near edge, low-pitch, and counter-passing
- Use this distribution to skew our initial particle sampling from the NUBEAM distribution → Only want to consider particles that are likely to be synthetically detected

(a) Relative intensity of deuteron loss distribution orbit in (R,Z) with FILD apertures (pink)
(b) Loss distribution in (energy,pitch)

The TRANSP Fast Ion Dist. is Biased Against the Reverse Integrated Dist. to Give Marker Weights

- Why? → To minimize wasted computational effort on particles that never reach the FILD
- Treat the reverse integrated dist. in a binary fashion (existence vs. nonexistence of a lost orbit)
- "Smear" the TRANSP dist. → connects physical EP density to loss dist. and breaks the GC vs. full orbit codes

Example Smear From TRANSP Dist. to Lost Dist.

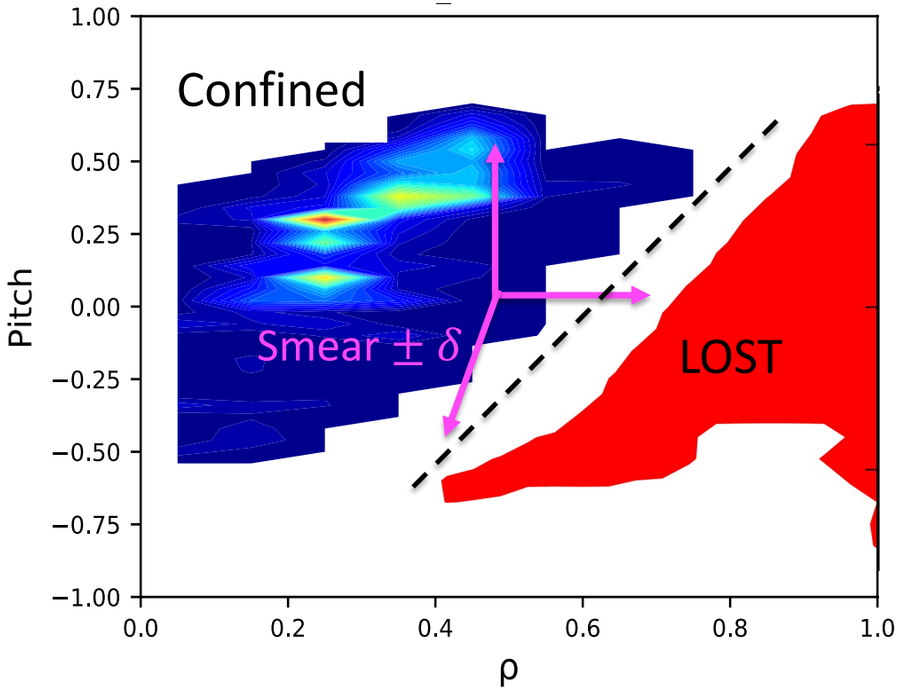

Magnitude of the smearing displacements are found from ORBIT "kicks"[a]:

Smears

$$R = R \pm \delta R$$
$$Z = Z \pm \delta Z$$
$$E = E \pm \delta E$$
$$\Lambda = \Lambda \pm \delta \Lambda$$

ORBIT "kicks"

$$\Delta P_\phi \rightarrow (\delta R, \delta Z)$$
$$\Delta E \rightarrow \delta E$$
$$\Delta \Lambda = 0.2 \rightarrow \delta \Lambda$$

where $\Lambda = v_{||}/v$

Example ORBIT "kick"

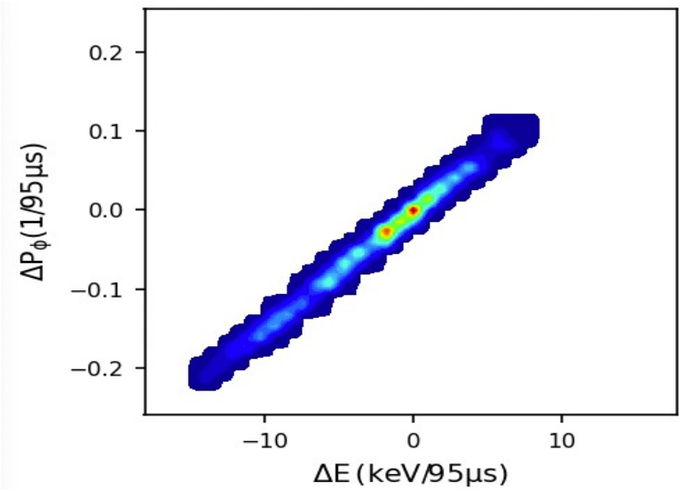

[a] *Podesta PPCF 2014 & 2017*

The TRANSP Fast Ion Dist. is Biased Against the Reverse Integrated Dist. to Give Marker Weights

- Take the TRANSP EP density as markers that can be translated to a particle flux on the detector
  - Translate TRANSP EP density [#/cm^3/eV/d$\omega/4\pi$] to relative particle flux on detector [#]
- Biasing and smearing skews initial sampling toward detector (shown below)

Example Smear From TRANSP Dist. to Lost Dist.

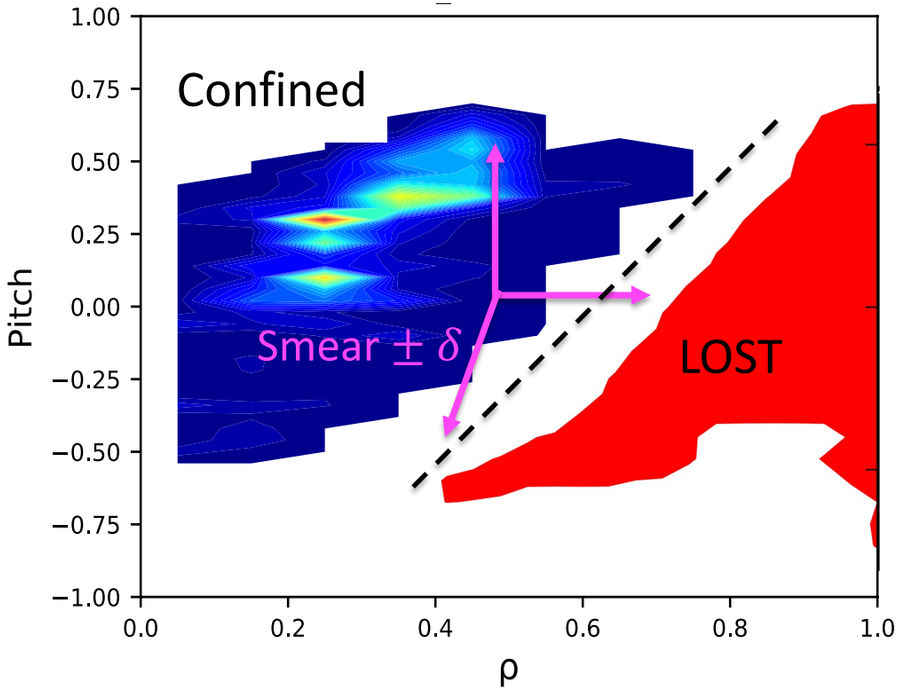

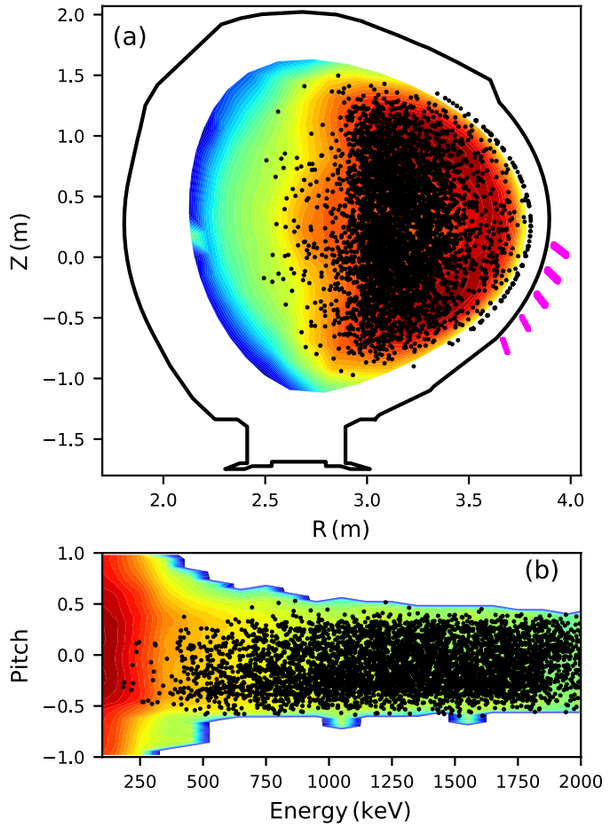

(a) Initial sampling of deuterons (black) overplotted on TRANSP Dist.

(b) Initial sampling in (energy,pitch)

Particles are Tracked to the FILD Geometry Using an Effective Full Orbit Position

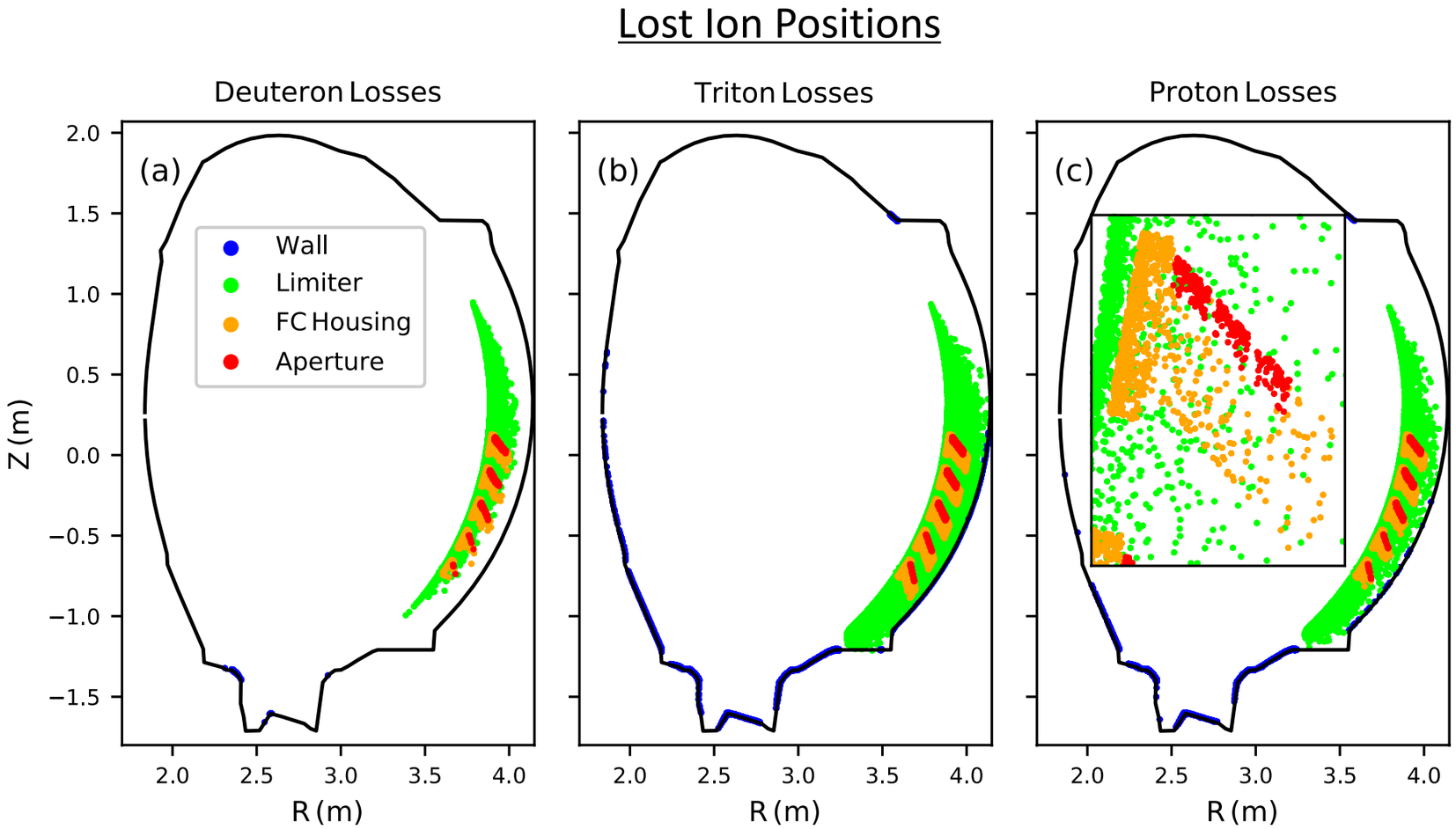

$$R_{FLR} = R_{GC} + \rho_L \cos(\phi_{gyro})$$
$$Z_{FLR} = Z_{GC} + \rho_L \sin(\phi_{gyro})$$

- Observe diagnostic structure well
- Only red markers are counted

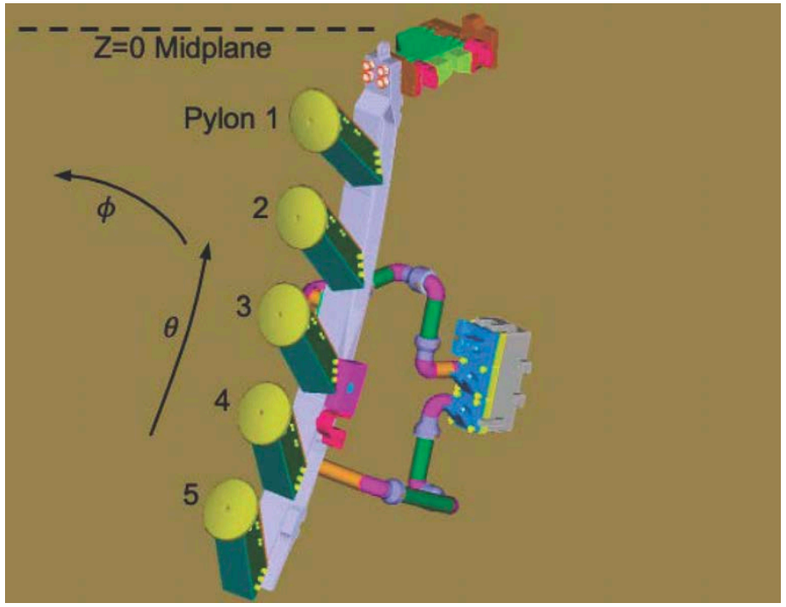

Final Synthetic Flux is Found by Tracking Particles in ORBIT to the FILD Aperture Geometry

1. Randomly sample from the TRANSP dist. & bias against the reverse loss dist.
2. Take the TRANSP fast ion density as a marker weight & track motion in ORBIT
3. Stop particles within a Larmor radius of the wall (may travel beyond LCFS) → track gyrophase to establish an effective "full orbit" position
4. Check if the particles reach the detector apertures and discriminate on accepted pitch
5. Sum over particles within foil energies for every ion species of interest

$$\Gamma_{ORB} = \sum_i \int w_i(R, Z, \Lambda, E)\Gamma_{NUB,i} dR dZ d\Lambda dE$$

Translate TRANSP flux to relative synthetic lost flux by summing over EP dist. with weighting function *w* for every ion species *i*

where

$$w_i(R, Z, \Lambda, E) = f_{bias,i}(R, Z, \Lambda, E) \cdot f_{ap}(\Lambda) \cdot \delta(E - E_{dep,i})$$

Bias in binary — Pitch Acceptance — Foil Deposition

$$\Lambda = v_{\parallel}/v$$

$$f_{bias,i} = \begin{cases} 1, & f_{rev,i}(R, Z, \Lambda, E) \neq 0 \\ 0, & \text{otherwise} \end{cases}$$

Biasing Artificially Inflates Loss Counts to Weaker Mode Amplitudes

- Weaker modes = smaller ORBIT-kicks = smaller smearing factors
- Particles with weaker mode amplitudes will be initialized closer to the loss boundary and inflate loss counts
- Solution: Scale loss flux w.r.t. to the kick-subdistribution relative to the entire EP distribution

Unscaled Loss Counts

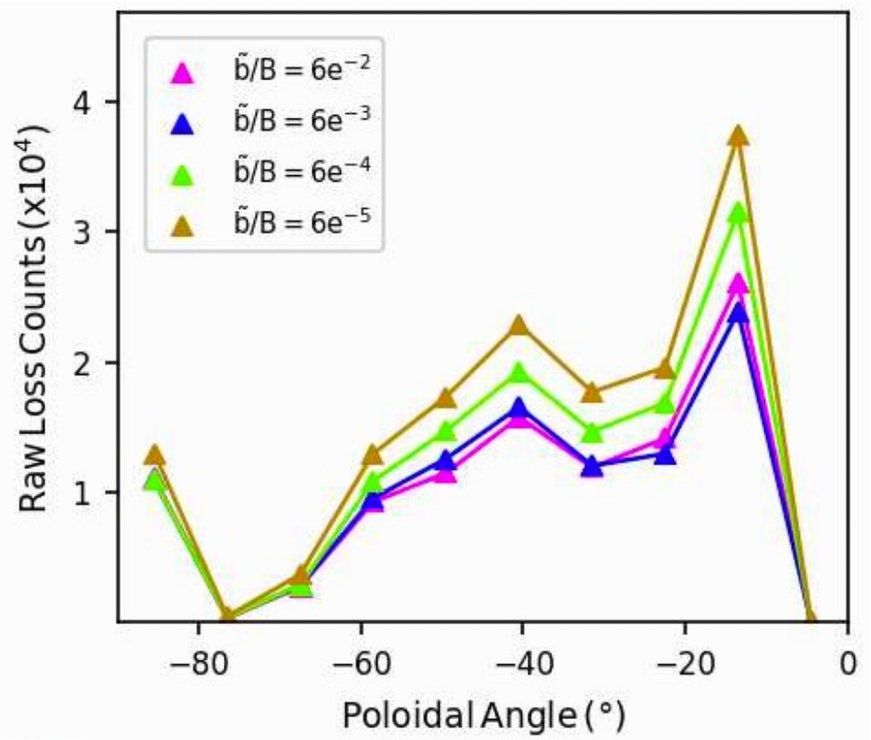

Scaled Loss Counts

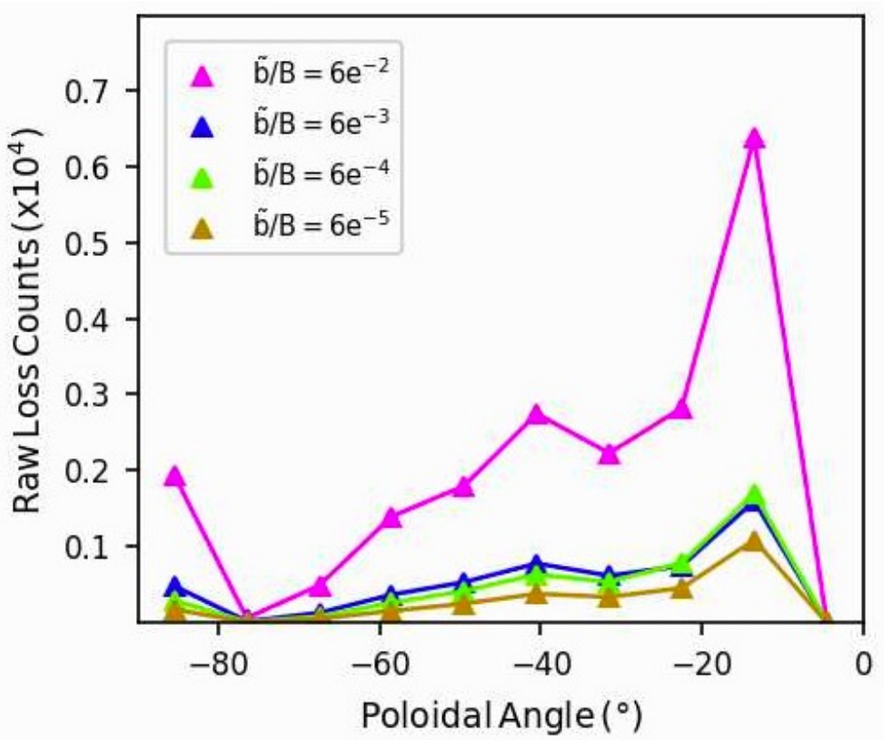

$$\Gamma_{ORB} \rightarrow \Gamma_{ORB} \frac{\int f_{NUB} dV_{kick}}{\int f_{NUB} dV_{NUB}}$$

- Limit $dV_{kick} \rightarrow 0$: losses ignored
- Limit $dV_{kick} \rightarrow dV_{NUB}$: recover uniform sampling

Representative Kink Mode Structure was Found with the NOVA[a] Code

- Mode was identified as a kink mode via EXE and SXR phase inversion, low mode numbers, & sawtooth precursors
- Only the n=1 mode and losses are considered: dominant m=1 with subdominant m=2-3 poloidal harmonics

ECE and SXR Phase at n=1 Mode Frequency

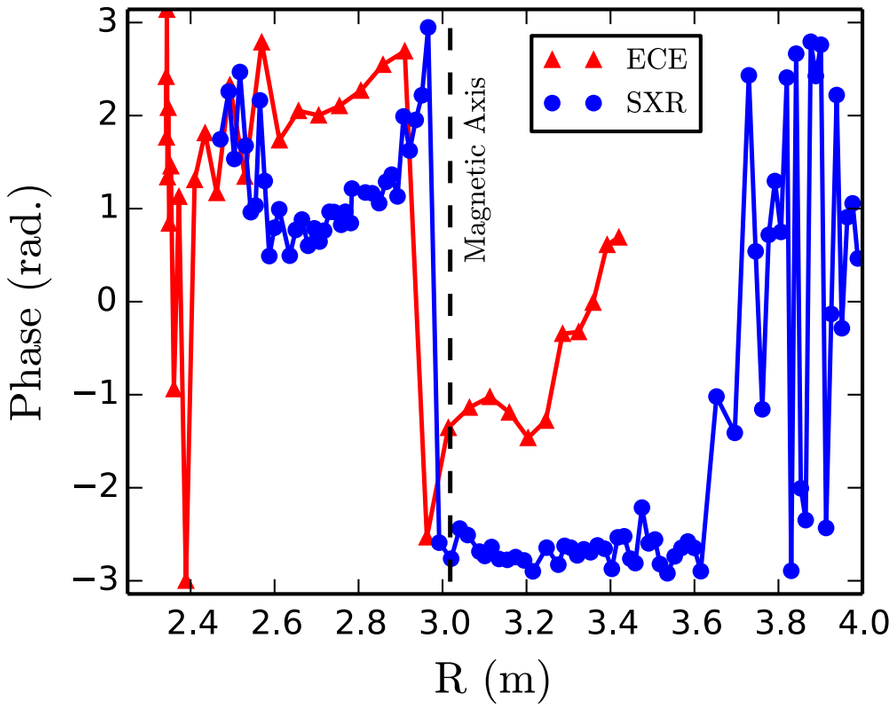

Normalized Radial Displacement Vector

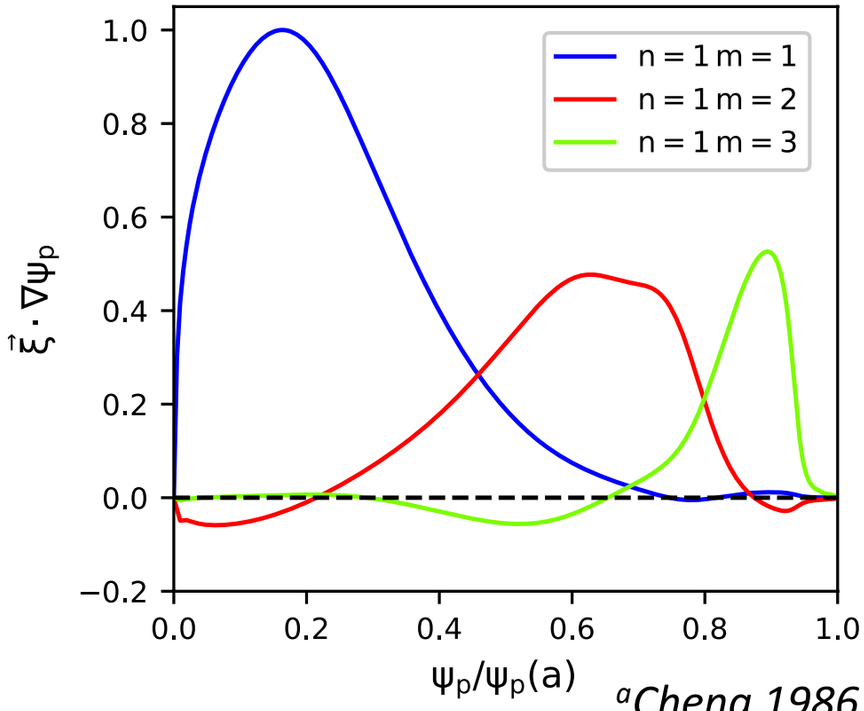

[a] *Cheng 1986 Phys. Fluids*

Mode Amplitude is Constrained by Converging Loss Model with Experimental Measurement

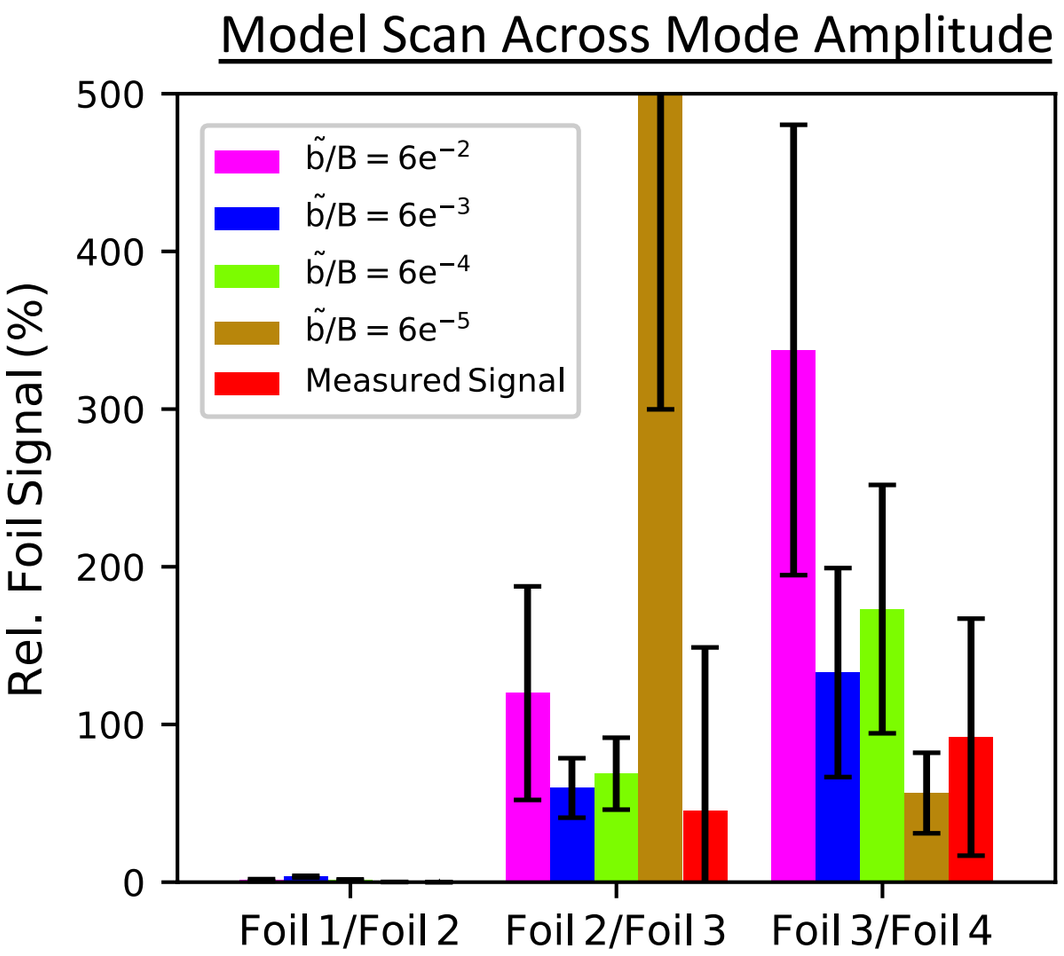

- $3x10^5$ particles used as input for each species; 0.5 ms integration time
- Convergence to $\frac{\tilde{b}}{B} \sim 6e^{-3} - 6e^{-4}$ between model and experiment
- Model error bars stem from count statistics
- Experimental signals are frequency filtered to the n=1 mode frequency
- Faraday cup detector array has not been absolutely calibrated so only relative measurements are of use
- Foil 1 measurement is discarded/corrected in the other foils due to capacitive plasma pickup[a]

[a] *Bonofiglo (RSI 2020)*

Relative Signal by Ion Species Can be Resolved with the Synthetic Diagnostic

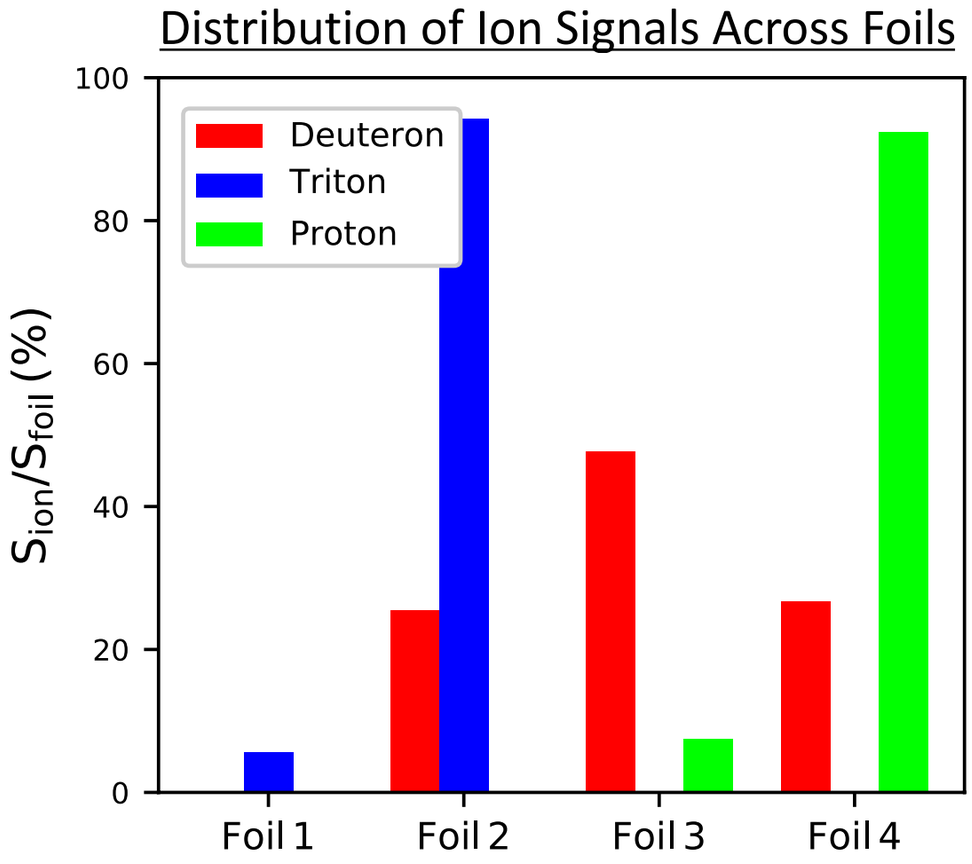

- DD-triton birth energy lies in Foil 2
- DD-proton birth energy >> Foil 4

- Impossible to know from Faraday cup measurements alone
- Scintillator-probe PMT losses indicate strong deuteron and triton losses which is in good agreement with the model
- NOTE: Deuteron component of the signal dominates each respective foil measurement because $n_{NBI} \gg n_{fus}$ (marker weights)
- Very useful information for multi-ion species plasmas such as DT-ops

Agreement Between Model and Experiment Exists within Errors

- $3x10^5$ particles for each species and total computational time is ~ 7500 computer hours (3 ion species and 4 mode amplitudes)[a-b]
- Improvements: Minor scaling factors to account for (E,pitch) sampling dependence, particle reinjection, toroidal deposition

Raw Loss Counts to Pylon 1 Faraday Cup 3

Ion Species	Foil 1	Foil 2	Foil 3	Foil 4
Deuts.	0	10	20	6
Triton	50	386	0	0
Proton	0	0	36	180

Relative Foil Signals for $\tilde{b}/B \sim 6e^{-4}$

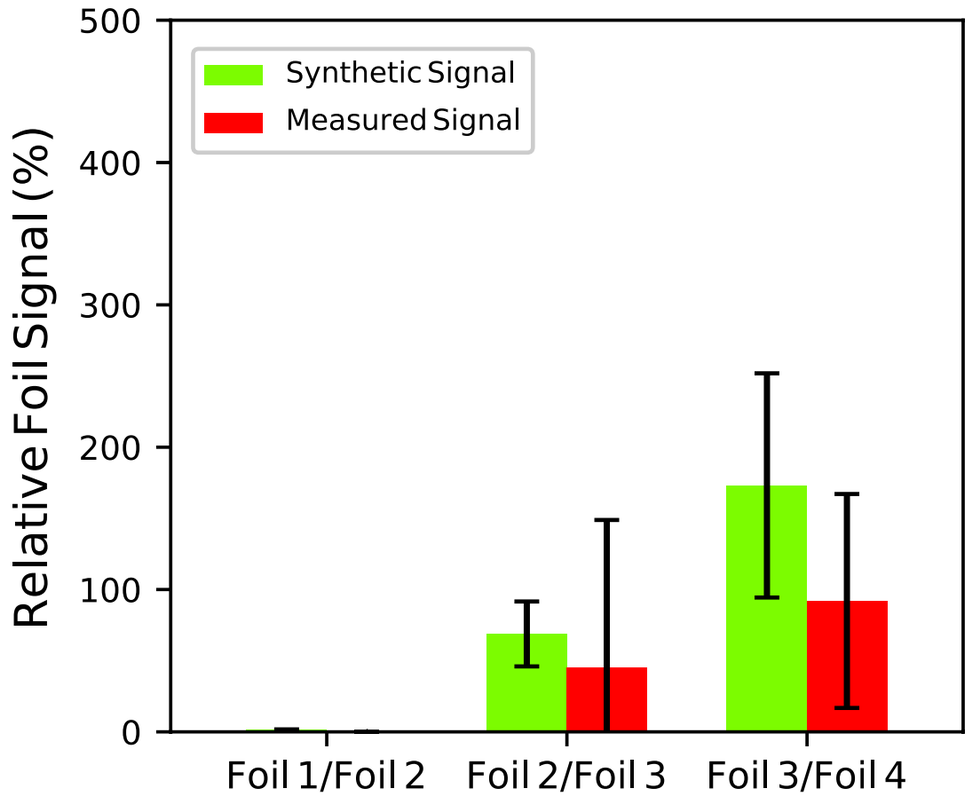

[a]Sipila (NuclFus 2021). [b]Garcia-Munoz (RSI 2016)

Conclusions

- An integrated model for fast ion transport and losses has been constructed to mimic measurements from JET's Faraday cup FILD array with the TRANSP and ORBIT codes *(Bonofiglo NuclFus 2021 Submitted Soon)*

    - Increased computational efficiency due to a reverse integration biasing scheme which skews sampled particles toward an increased likelihood of detection

    - Vetted against an experimentally observed kink mode induced losses with high NBI and ICRF heating

    - Relative lost EP fluxes are in good agreement between model and experiment

Future Work

- Examine other loss mechanisms (NTM, fishbone, sawteeeth, AE, etc.) in more plasma scenarios on JET:
  - Use full poloidal distribution of Faraday cups
  - Use scintillator probe FILD geometry
  - DT-alpha losses due to EP instabilities are occurring today!

- Further improvements to the reduced model:
  - Use purely reverse particle integration
  - Use reverse Monte-Carlo schemes[a-b]

- Extend model to other devices (NSTX-U, MAST-U, DIII-D)

- Form a time-dependent, self-consistent, model for fast ion losses:
  - Incorporate my reduced EP loss model into TRANSP to supplement the NUBEAM submodule
  - Ongoing work to incorporate ORBIT-kick with multi-EP species into TRANSP

[a]Zonta (EPS 2021) [b]Hirvijoki arXiv:1905.04952

BACK UP SLIDES

Energetic Particles Can Destabilize Shear-Alfvén Waves

- Continuum (energetic particle mode) and gap mode (Alfvén eigenmode) instabilities require[a]:
  1. Free energy source to drive instability – spatial gradient in fast ion distribution
  2. Resonance between wave and fast ions

$$\omega = k_{\|} v_A \text{ where } k_{\|} = \frac{m - nq}{r}\frac{B_\theta}{B} \text{ and } v_A = \frac{B}{\sqrt{\mu_0 \rho_i}}$$

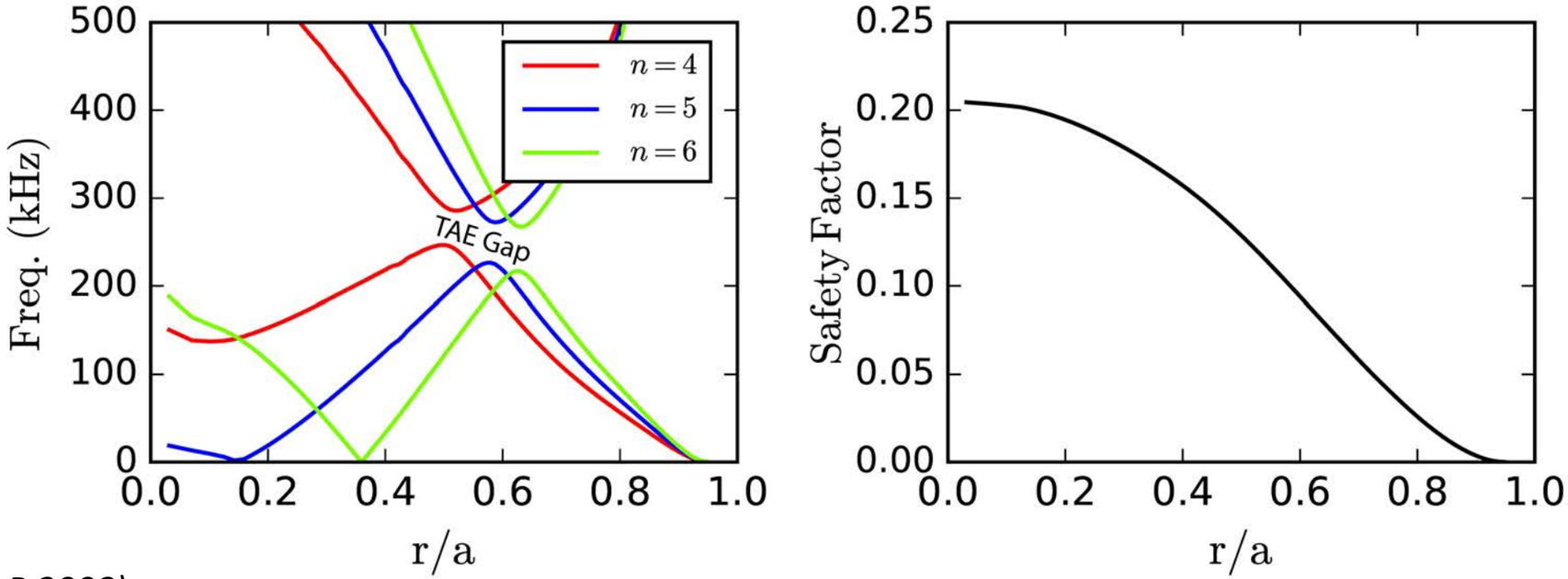

[a]*Heidbrink (PoP 2008)*

Energetic Particle Bursts React Strongly to the Changing Equilibrium

- Bursts up-shift in frequency with growth in the n=5 perturbation and then disappear

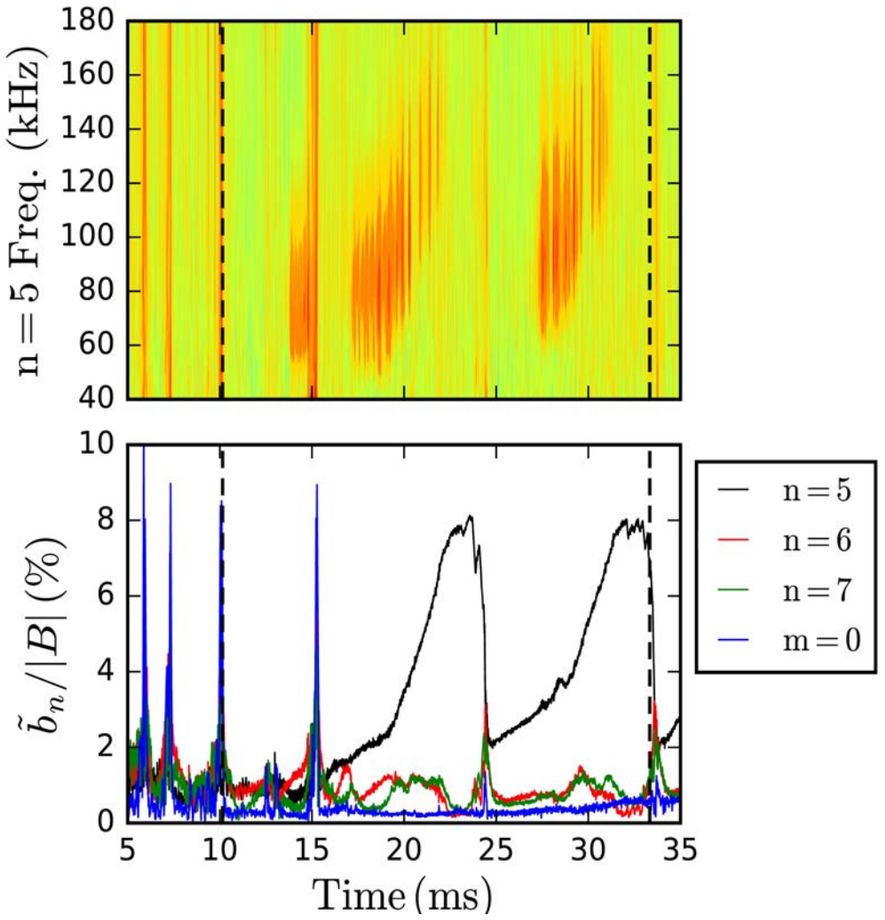

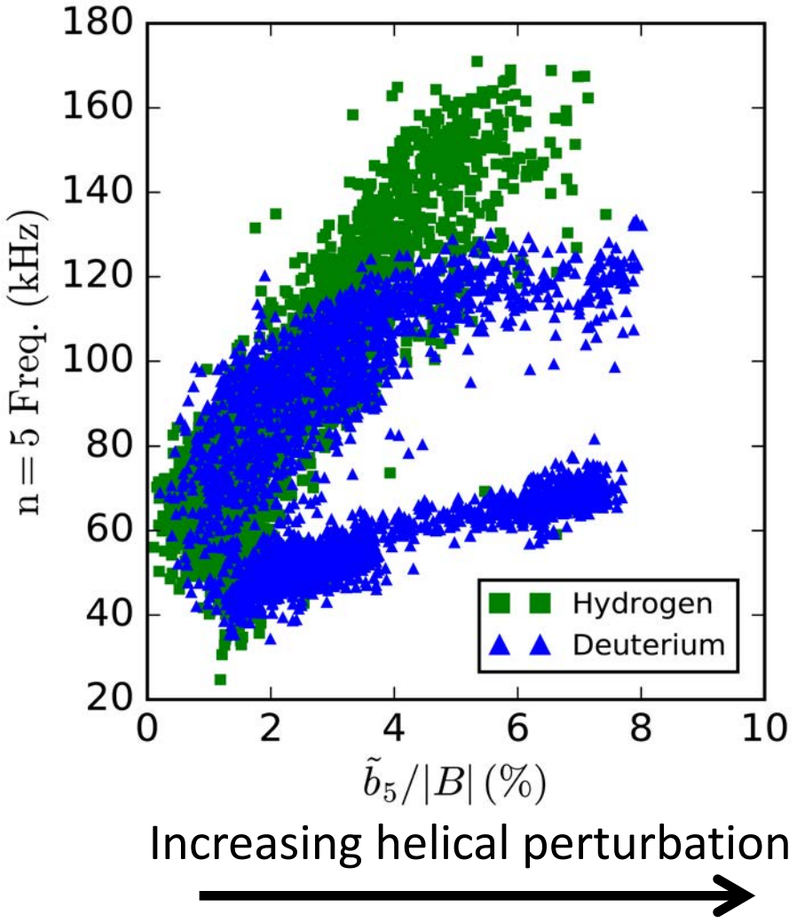

Increasing helical perturbation

Electron Density Perturbations Resolve Spatial Structure of Alfvénic Modes

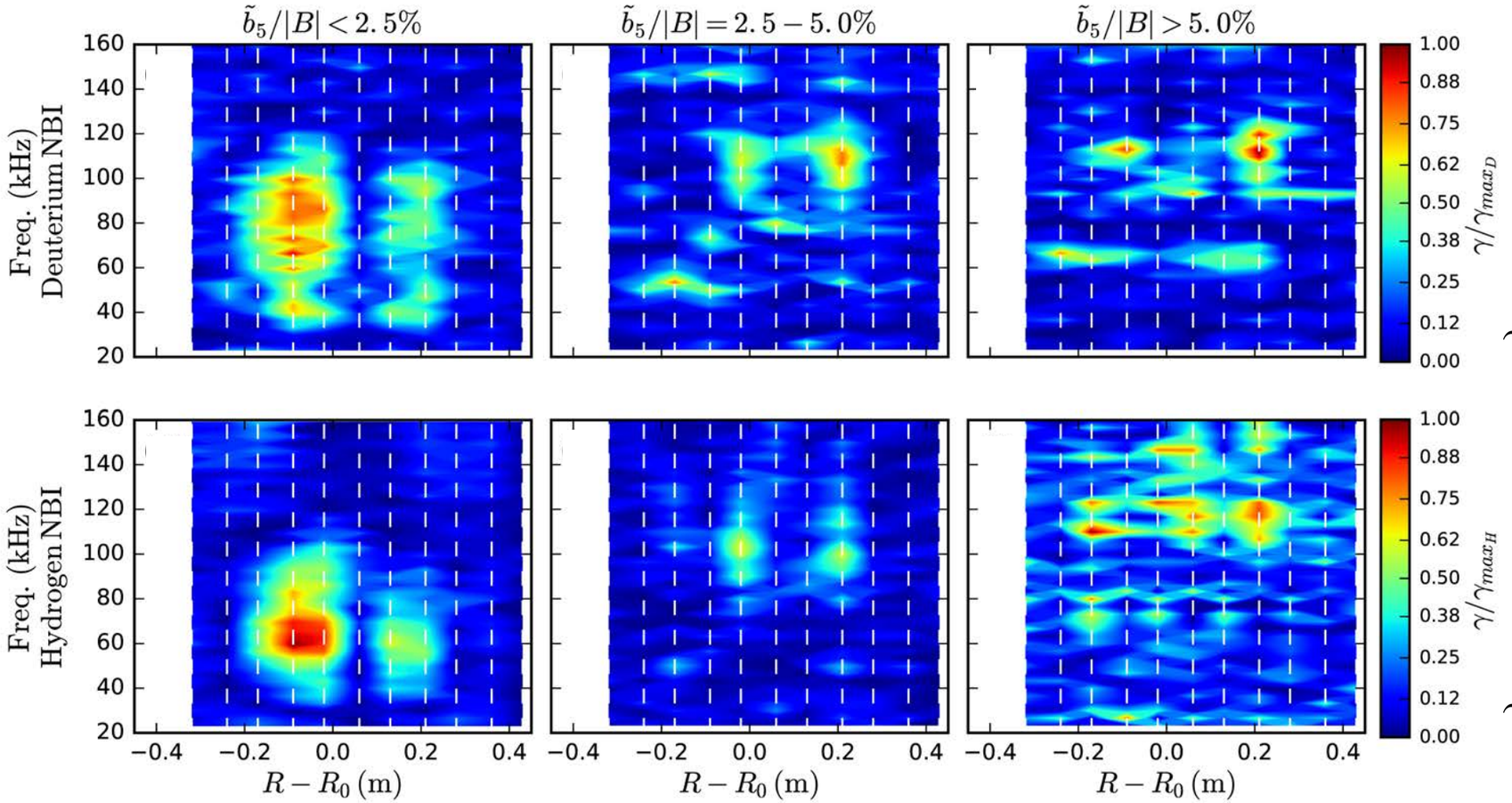

Increasing helical perturbation

Spectral Coherence

$$\gamma^2 = \frac{| < \mathcal{F}_{\tilde{b}} \mathcal{F}_{\tilde{n}} > |^2}{< |\mathcal{F}_{\tilde{b}}|^2 >< |\mathcal{F}_{\tilde{n}}|^2 >}$$

$\gamma_{\max_D} = 0.25$

$\gamma_{\max_H} = 0.32$

STELLGAP Solved Alfvén Continua Describe Mode Frequency Response

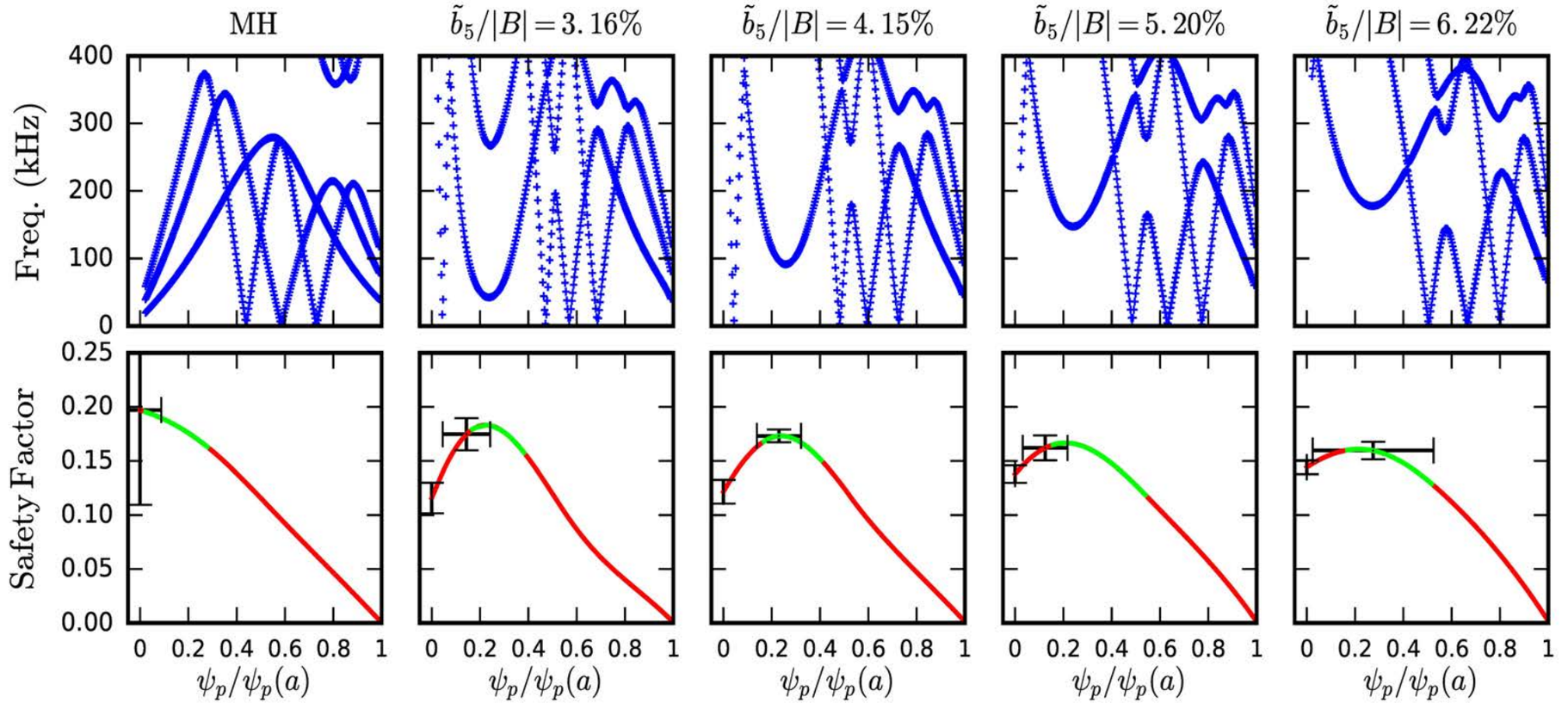

STELLGAP Calculated AC

$$\omega = k_{\|} v_A$$

Mapped FIR Measurements

VMEC/V3Fit q-profile

Increasing helical perturbation

STELLGAP
Spong (PoP 2003)

V3Fit
Hanson (NuclFus 2009)

EP Instability Tracks Well with AC Minima

- Localized density perturbations track extrema in the AC
- AC minima suggest extrema modes (RSAE, GAE, BAE, etc.) → Make no attempt to ID mode

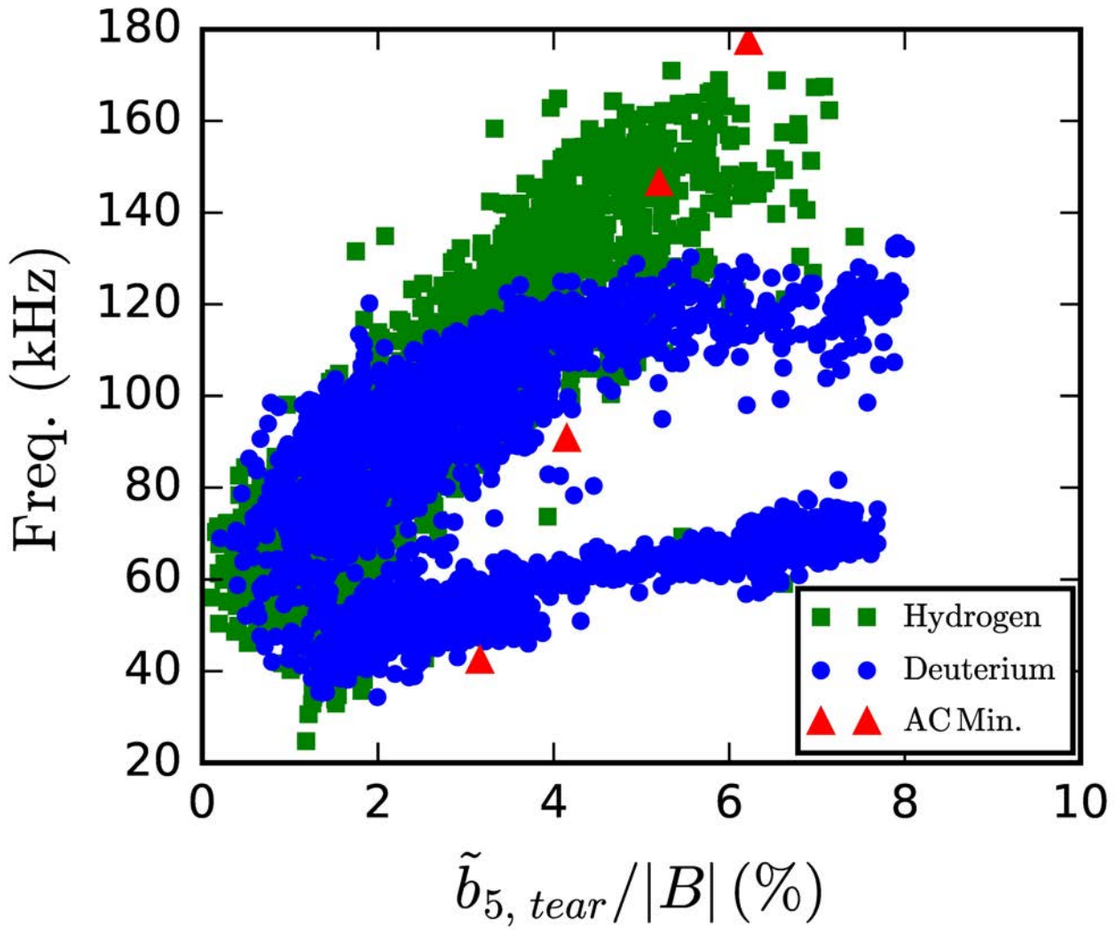

Rate of Change of Neutron Flux Exposes Tearing Effects on Fast Ions

$$D + D \rightarrow {}^{3}He(0.82\,\mathrm{MeV}) + n(2.45\mathrm{MeV}) \;\; 50\%$$

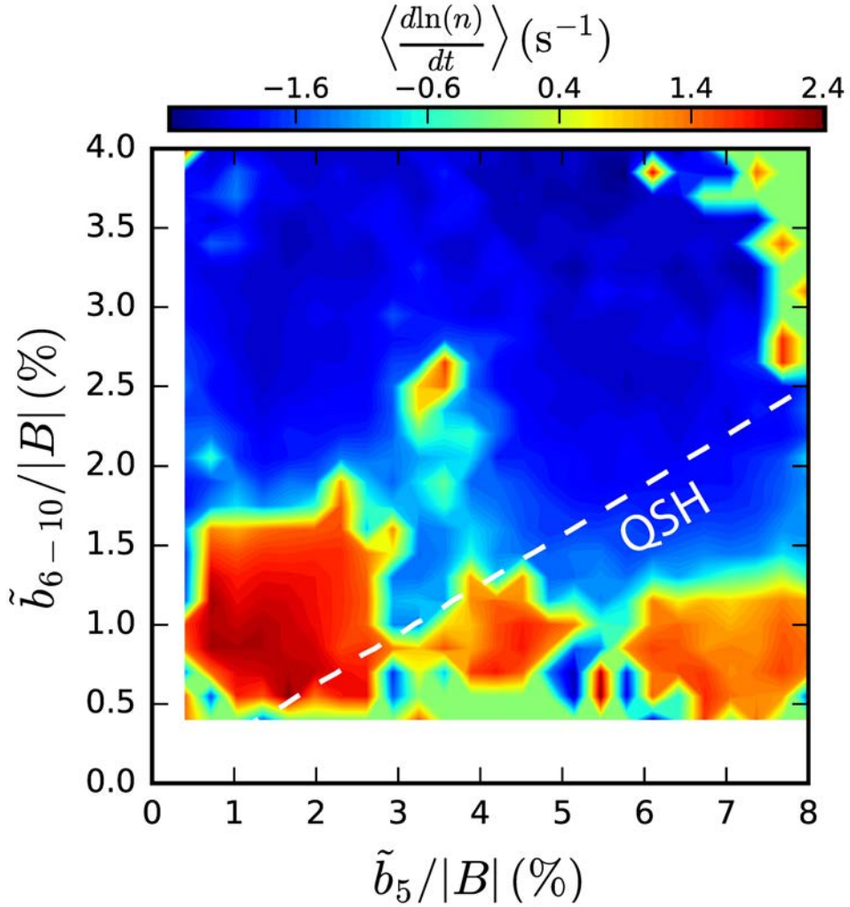

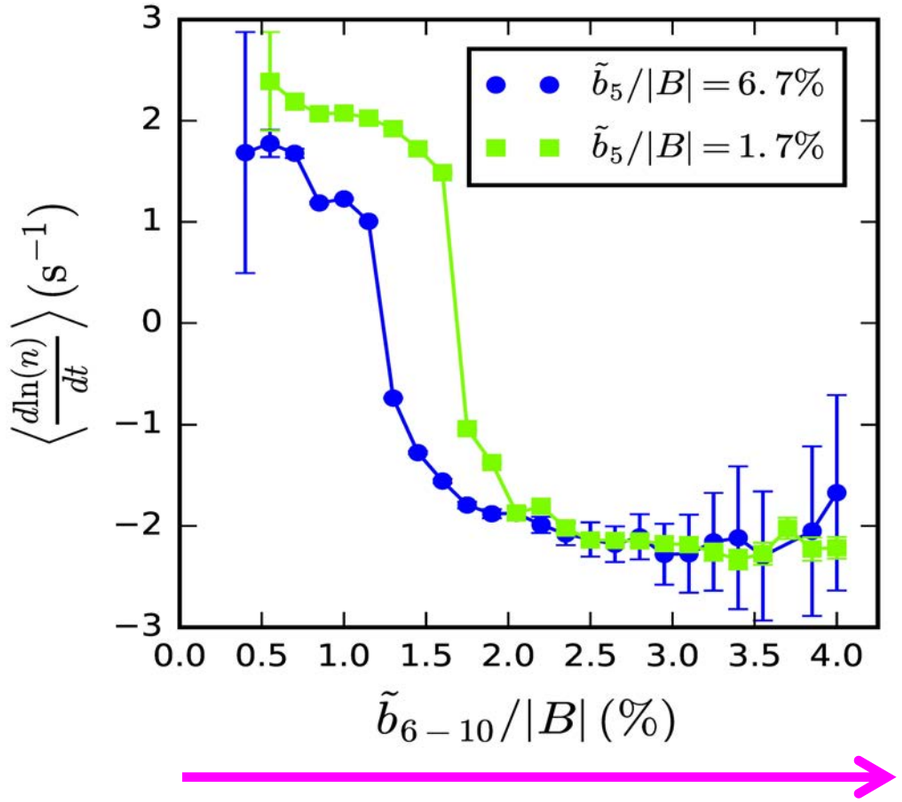

- Neutron signals decrease with rise in core tearing mode amplitude
- Secondary modes in QSH tend to destroy fast ion confinement more quickly

RFP Superbanana Orbits Remain Confined

- Below made with full orbit code
- RFP benefits: favorable GC drifts; high rotational transform
- Helical RFP like omnigenous stellarator[a]: $< \vec{v}_d \cdot \vec{\nabla}\psi > \sim 0$

Toroidal View

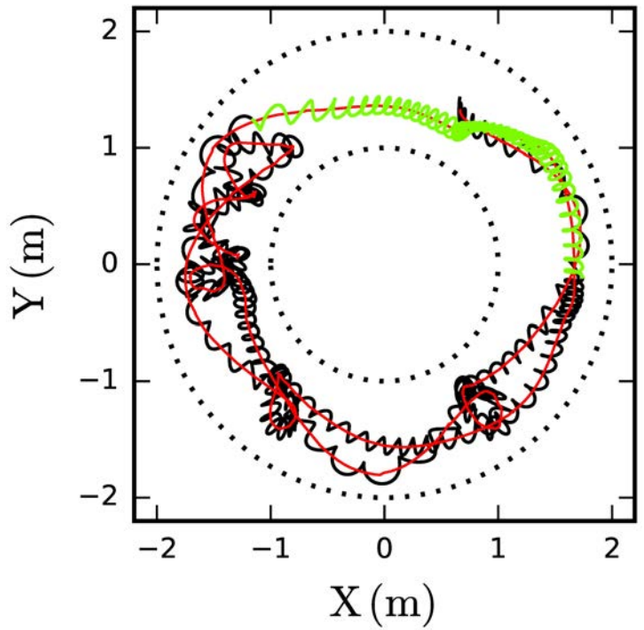

Poloidal View - Full

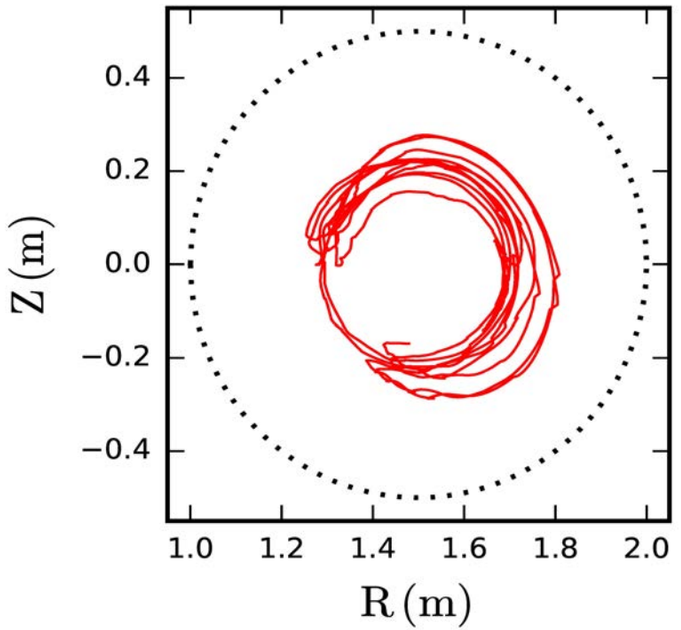

Poloidal View - SBN

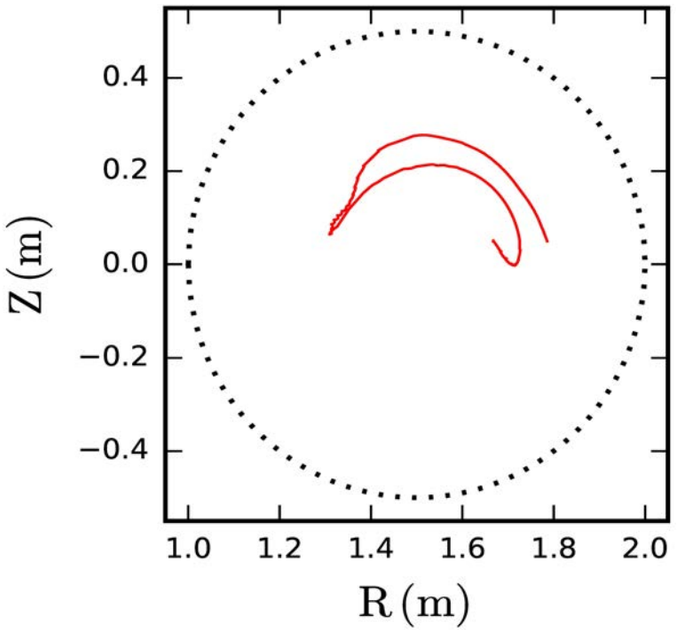

— Guiding Center — Particle Path — SBN

[a] *Cary and Shasharina (PRL 1997)*

Fast Ion Island Overlap Increases with QSH Transition

$$q_{\mathrm{mag}} = \frac{rB_\phi}{RB_\theta} \qquad w_{\mathrm{mag}} = 4\sqrt{\left.\frac{r\tilde{b}_r}{nB_\theta\left|\frac{dq}{dr}\right|}\right|_{rs}} \qquad q_{\mathrm{fi}} = \frac{rv_\theta}{Rv_\phi} \approx q_{\mathrm{mag}} + \text{Drift Terms} \qquad w_{\mathrm{fi}} = 4\sqrt{\left.\frac{r\tilde{b}_r}{nB_\theta\left|\frac{dq_{fi}}{dr}\right|}\right|_{rsfi}}$$

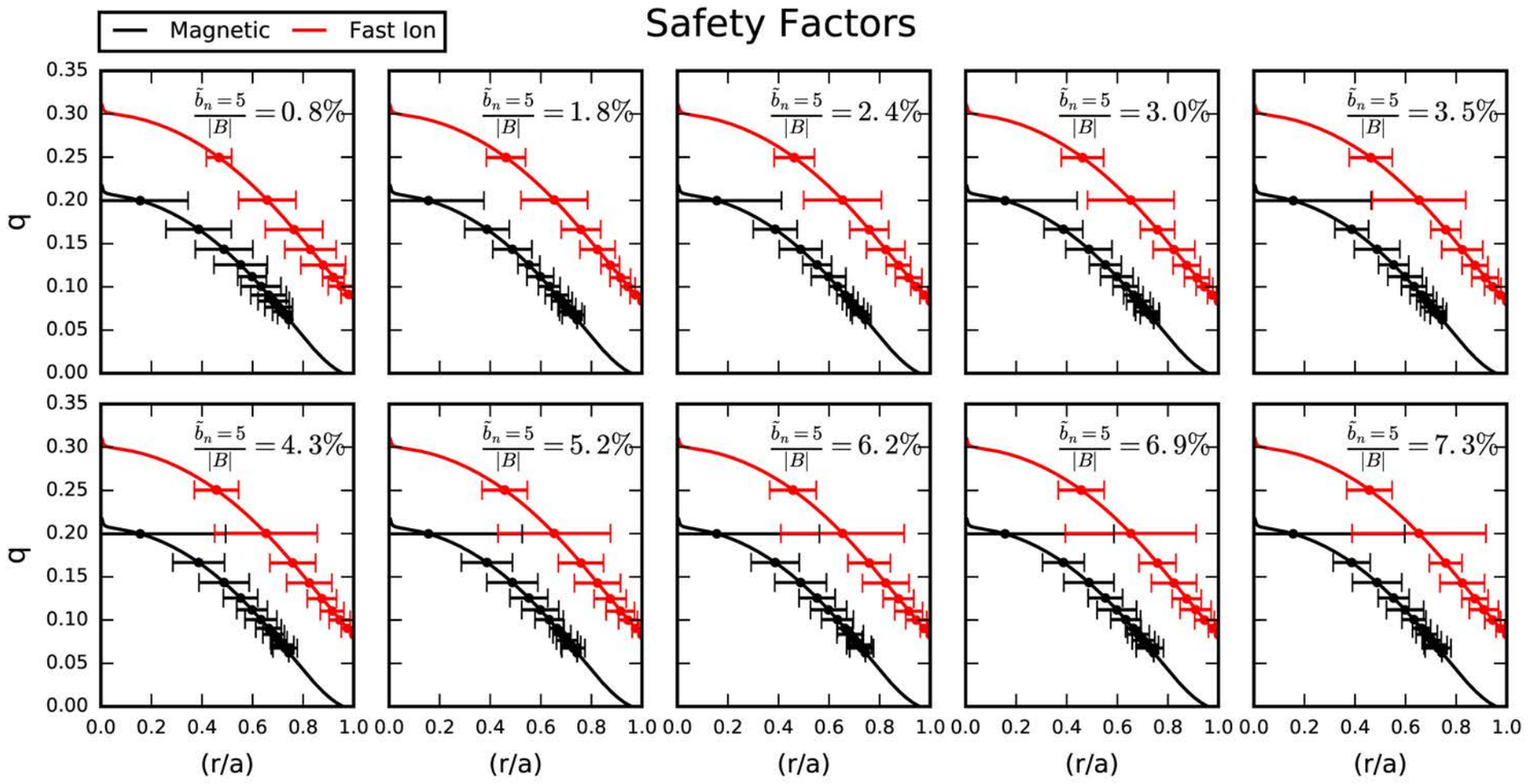

Fast Ion Stochasticity Approaches Magnetic Stochasticity in QSH

Rechester & Rosenbluth (PRL 1977)

$$s = \frac{1}{2}\frac{w_{m,n} + w_{m',n'}}{|r_{m,n} - r_{m',n'}|}$$

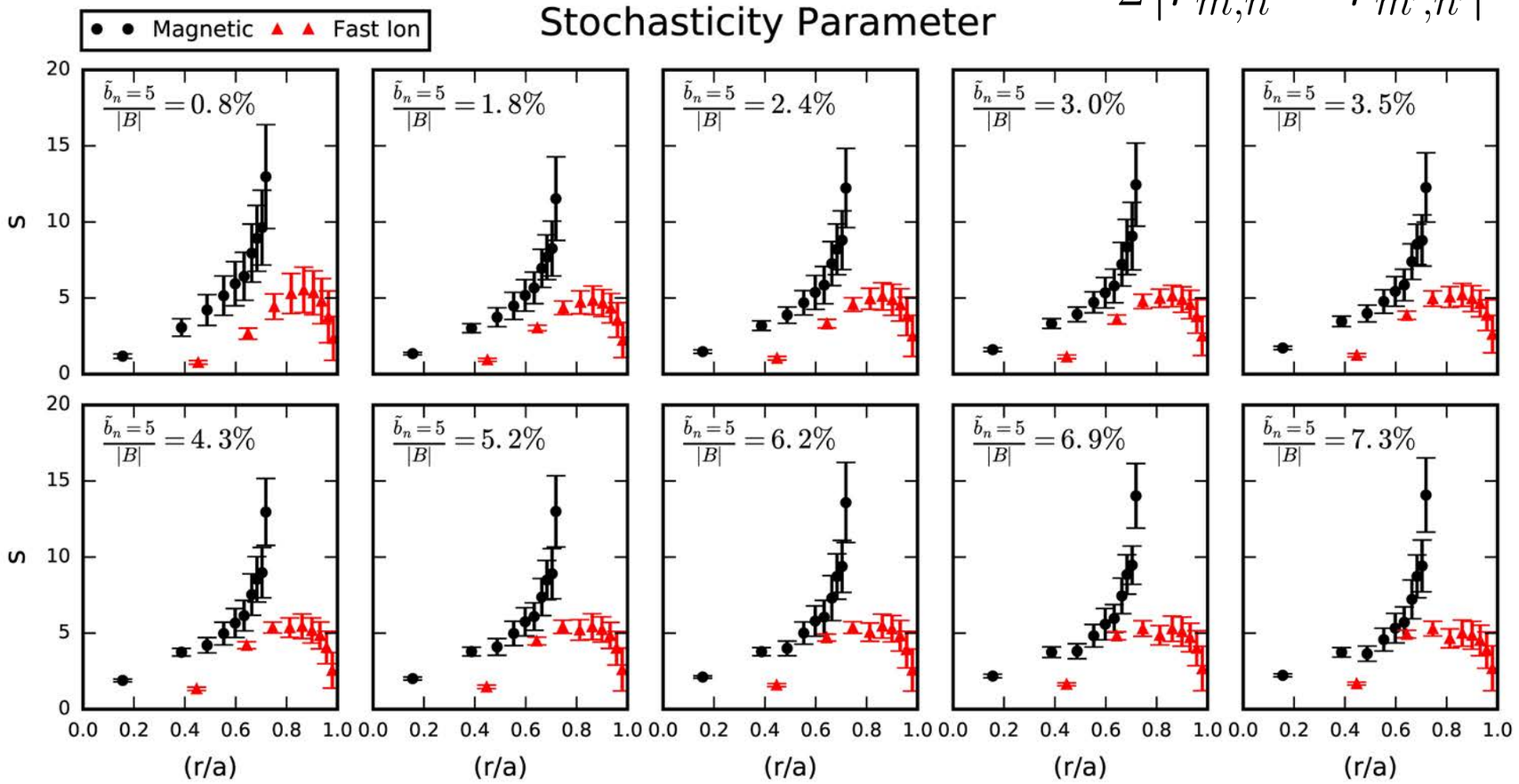

Fast Ion Diffusivity Consistent with RR-Like Transport

Dominant Mode Dependence

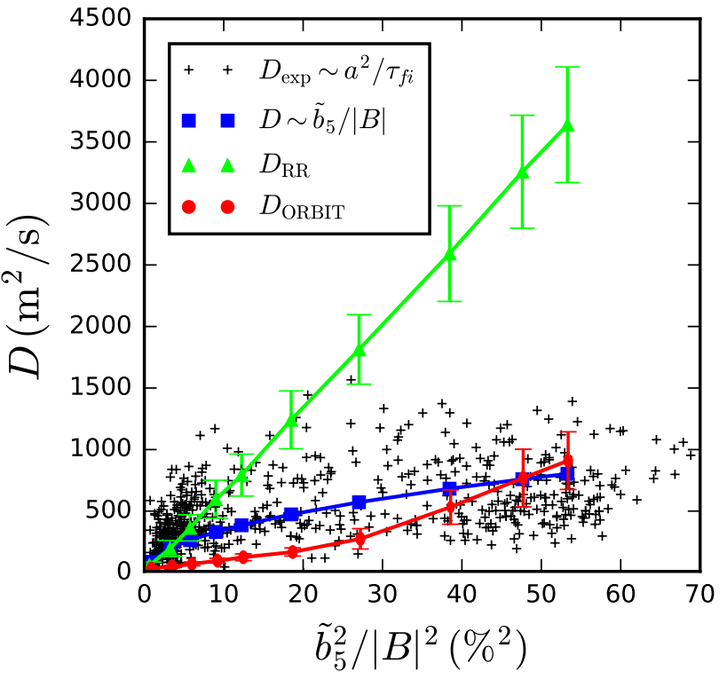

Rechester & Rosenbluth (PRL 1977)
Biewer (PRL 2003)

Subdominant Mode Dependence

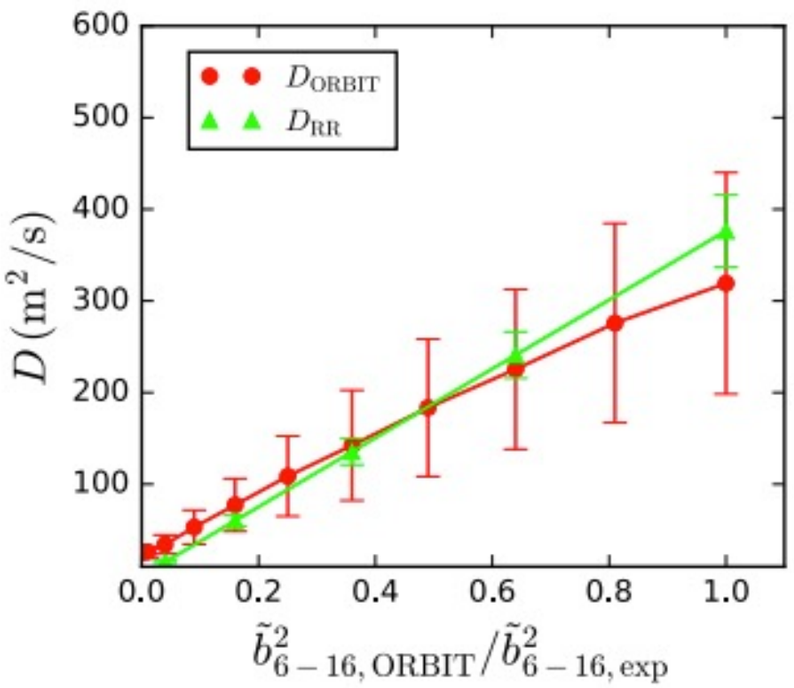

$$D_{\rm RR} = \pi R v_{fi} \sum_{m,n} \frac{\tilde{b}_r^2}{B_\phi^2} \delta(m - nq)$$

$$D_{\rm ORBIT} = v_{fi} \frac{< \Delta r^2 >}{2L}$$

- Diffusive step-size on order of the n=5 fast ion GC island width
- RR transport is a function of the subdominant mode amplitudes
- Observed transport is consistent based on large n=5 island coupled with overlapping subdominant resonances

A Faraday Cup Fast Ion Loss Detector was Designed for the RFP

- Compact probe design: wall to LCFS ~ 1 cm
- Faraday cup style sensitive to high pitch ions
- Background signal removed from ion collection via a differential amplifier
- Sensitive to edge-field alignment
- Noise sources: plasma electrons, UV, secondary electrons

Probe Design

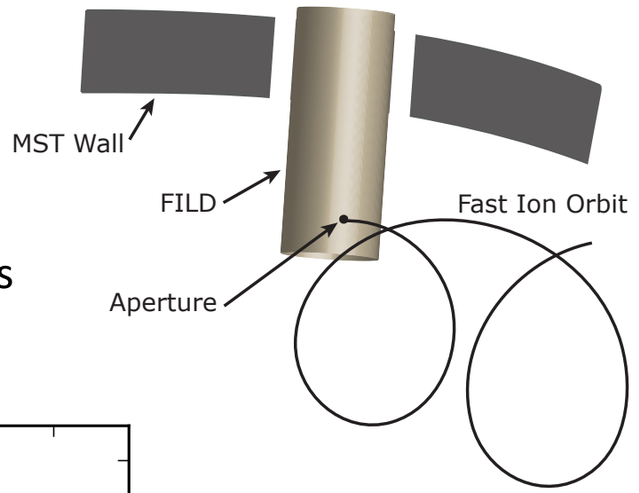

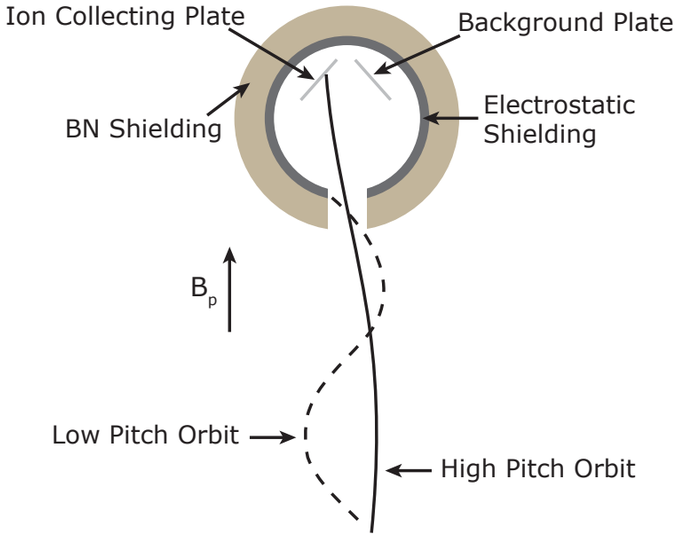

Background Scan (no NBI)

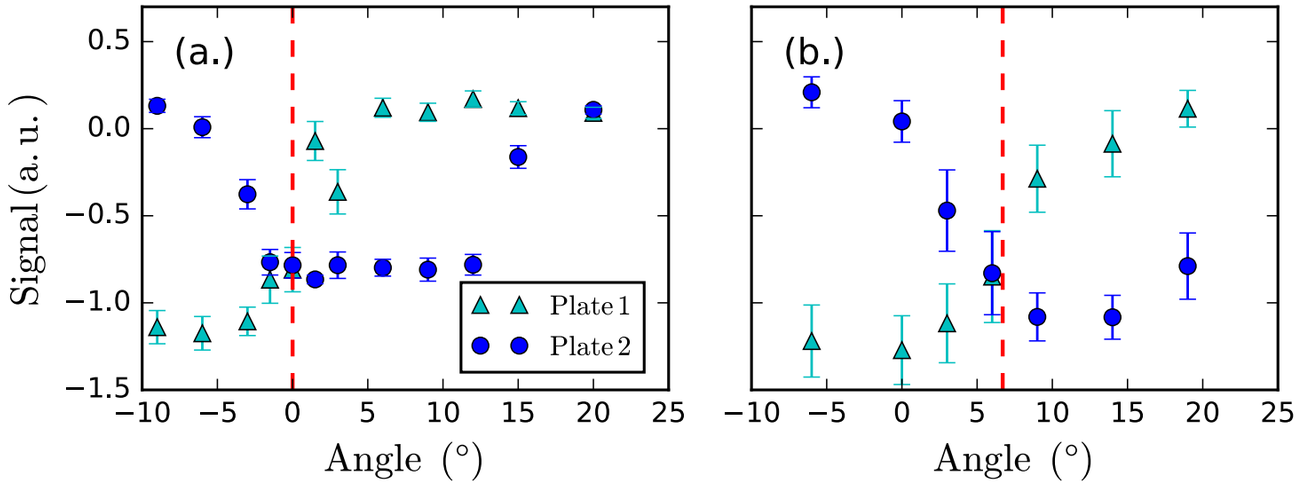

(a) Non-reversed plasmas
(b) Reversed plasmas

Bonofiglo (RSI 2016)

Lost Ion Signal is Observed During NBI Heated Plasmas

- Negative signal implies strong electron noise
- Minimal losses and extension beyond beam turn off is indicative of well-confined nature of fast ions
- Improvements: mitigate electron noise, better geometrical cup design, increase amplifier gain
- FILD is not suitable in 3D-RFP plasmas due to probe outgassing and the need for density control

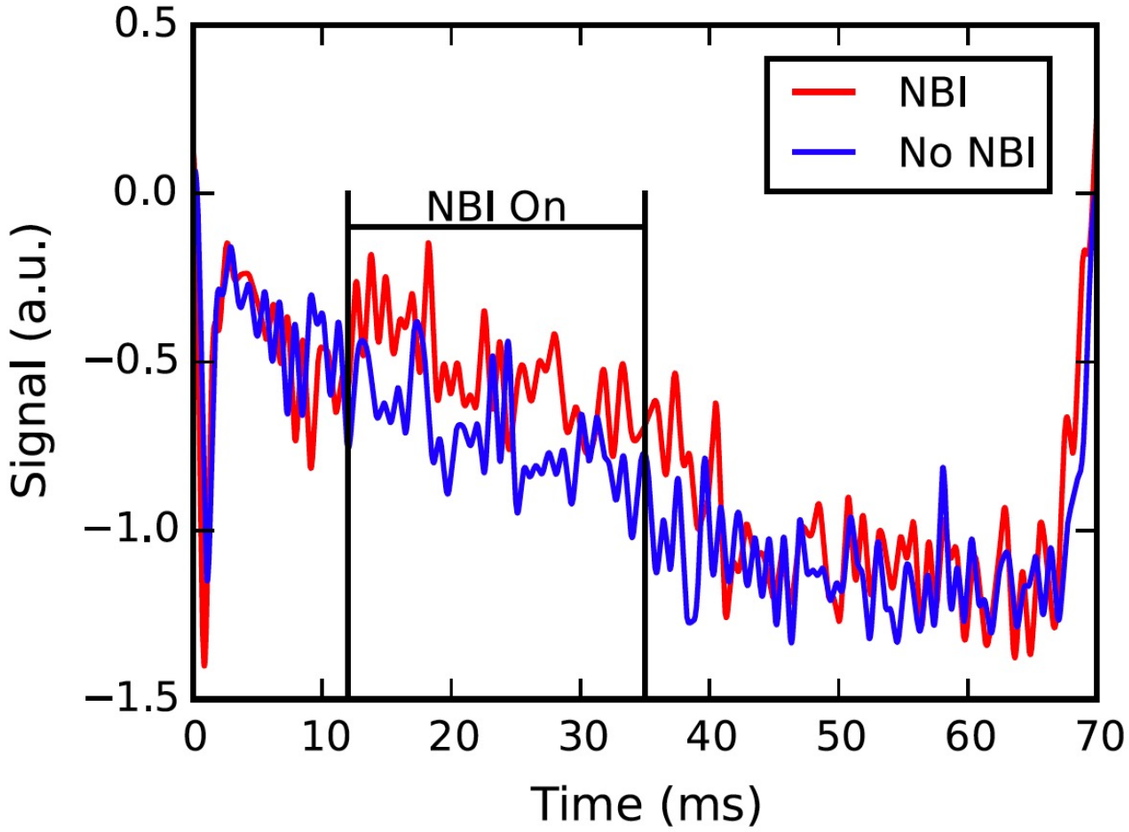

Bonofiglo (RSI 2016)

JET Features Two Fast Ion Loss Detectors

Scintillator Fast Ion Loss Detector[a]

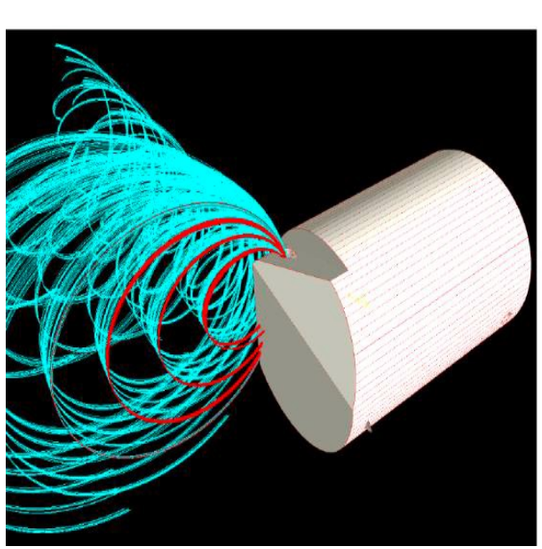

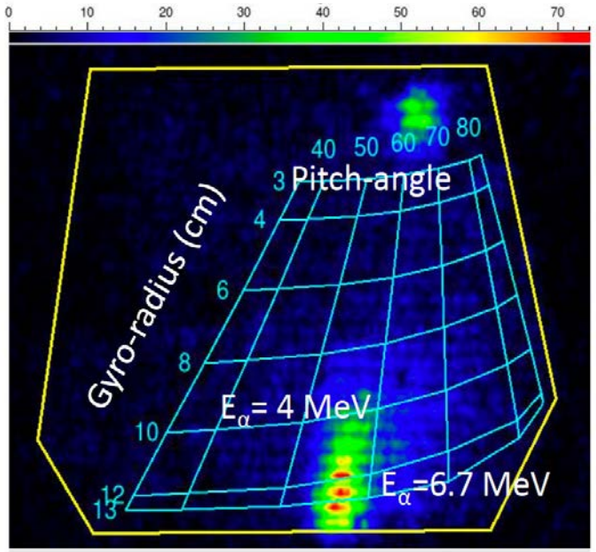

- Functions like a mass spectrometer
- More sensitive to fusion products
- Good energy and pitch resolution
- Single spatial position

Faraday Cup Fast Ion Loss Detector Array[b]

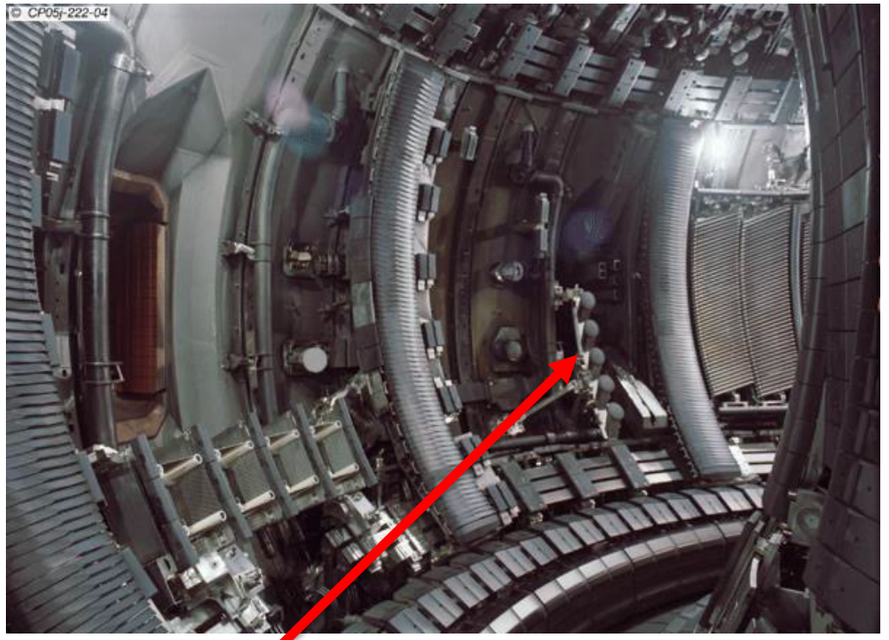

Faraday Cups

- Sensitive to “lower energy” (RF-tail) fast ions
- Decent energy resolution and limited pitch resolution
- Wide spatial resolution poloidally and radially

[a]*Baeumel (RSI 2004)*
[b]*Darrow (RSI 2004, 2006, 2010)*

Additional Model Information: Poloidal Dependence & Orbit Topologies

- Only 7 FCs were fitted with appropriate data acquisition hardware for this discharge
- Spatial sensitivity of losses can be examined from the model and compared to experiment
- Most losses occur from counter-passing and trapped orbits

Poloidal Dependence

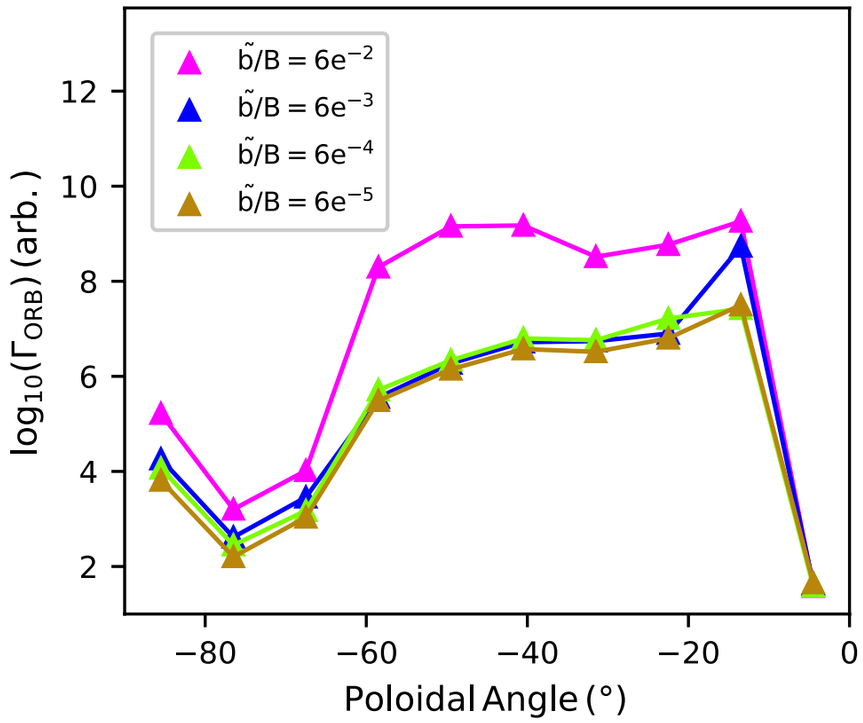

Orbit Transitions: Initial → Final

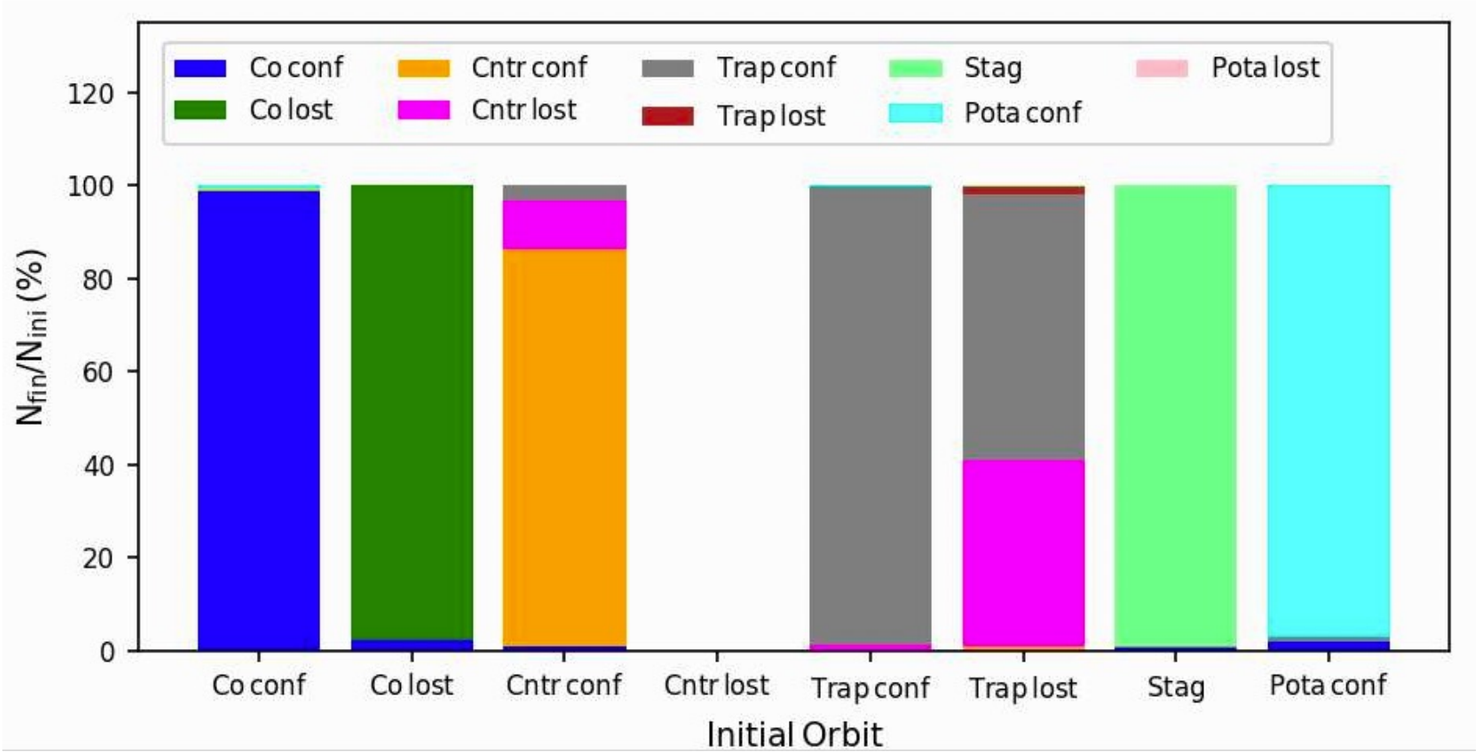

ORBIT is Being Converted to Integrate Particle Motion Backward from the Detector

- No biasing needed! All orbits should be collected by the FILD
- ORBIT-kicks work both forward and backward in time
- Employ similiar weighting scheme from TRANSP EP dist.
- ORBIT highlights:
  1. Functionality in the vacuum region
  2. Finite-Larmour radius position computed

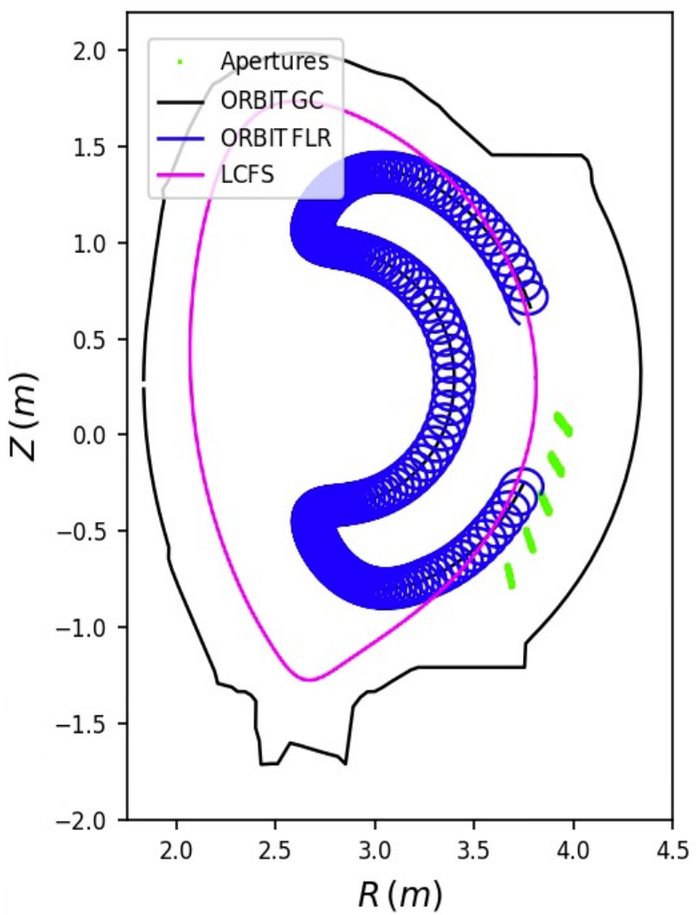

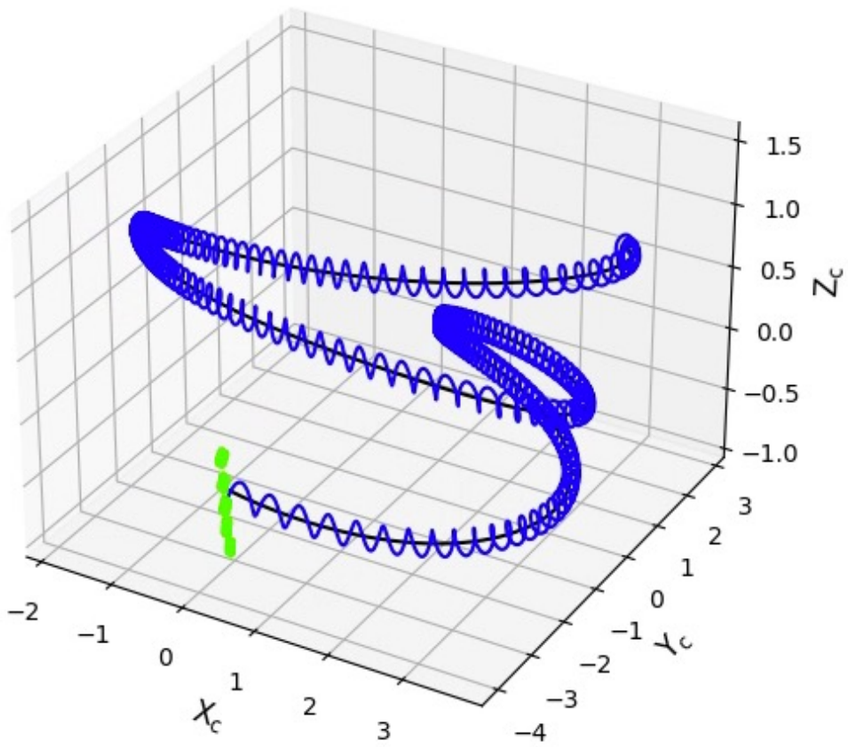

Foil Stacks are Susceptible to Capacitive Plasma Pickup

- The front foil is plasma facing and couples to MHD activity[a]. The foils can then capacitively couple to one another allowing noise pickup to traverse the stack
- Impossible to distinguish real fast ion losses from MHD activity (kinks, NTMs, AEs, etc.) vs. pickup noise
- Best way to eliminate this is through hardware changes

NBI only Discharge

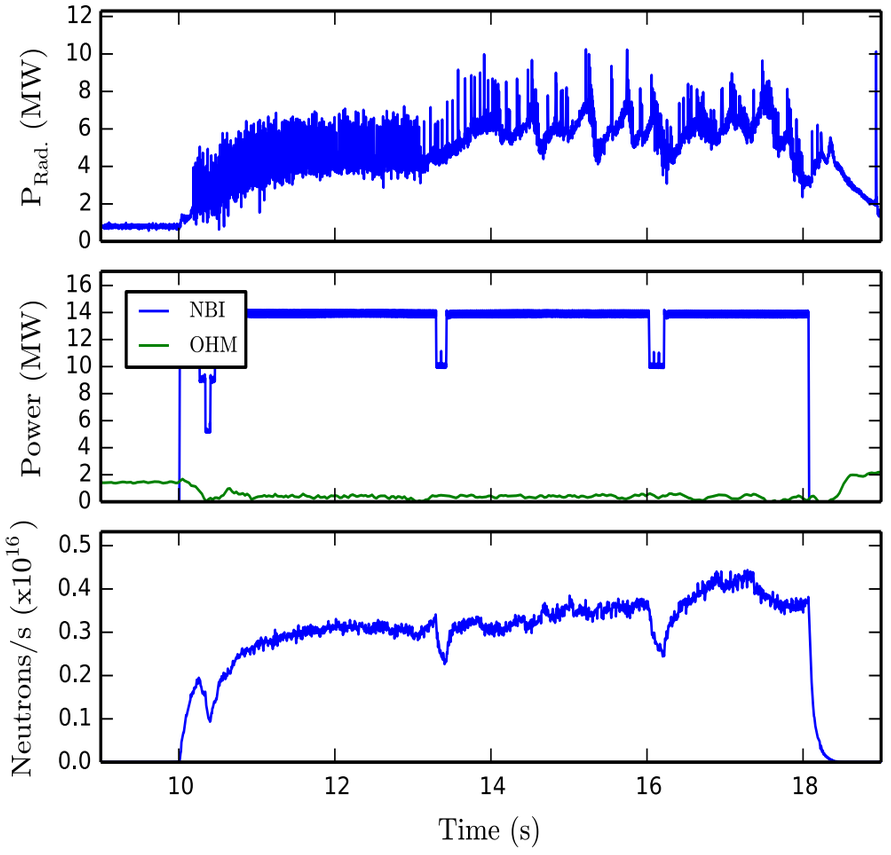

Spectrograms

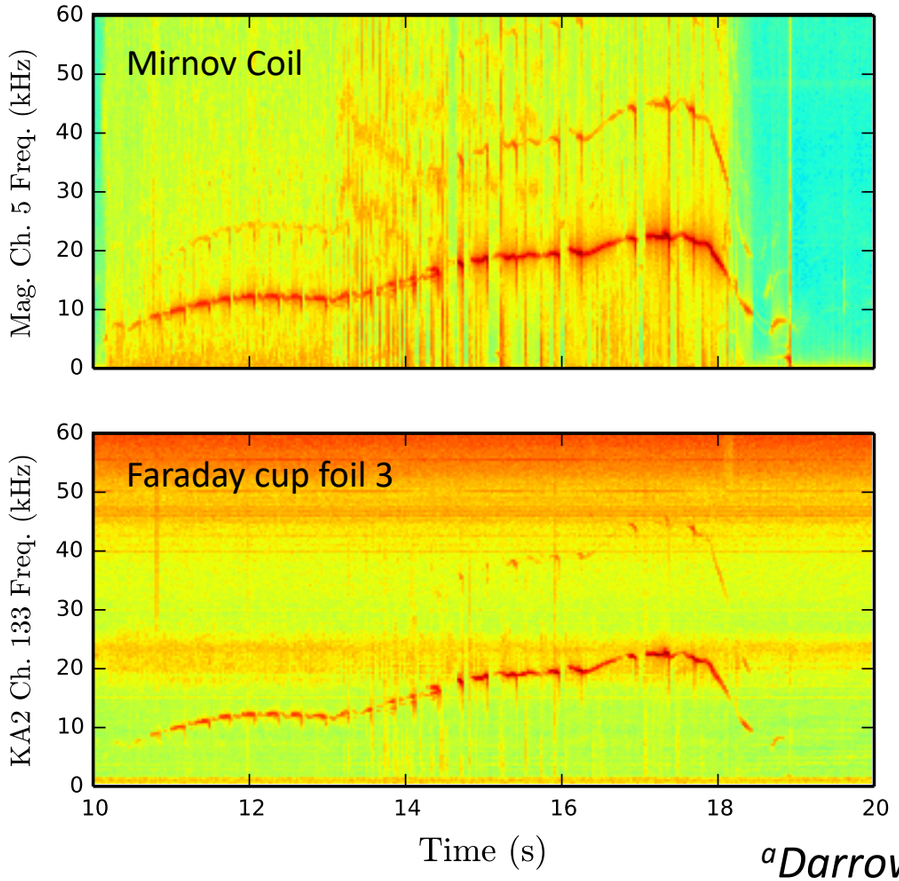

Insufficient population of MeV ions!

1.35-1.6 MeV deuts
1.48-1.76 MeV trits

[a]*Darrow RSI 2010, Cecil 2010 RSI*

Recent Hardware Upgrades[a] have been Performed to Remediate Past Issues

Detector Limitations

1. Large amount of foil-to-foil and foil-to-machine shorts
2. High freq. noise pickup from ambient surroundings
3. Amplifier noise and breaking
4. Limited analysis -> 5 kHz sampling rate

Recent Upgrades

1. Installed thicker foils in a 4-stack design to prevent foil-to-foil shorts
2. Installed superscreen cabling to hinder ambient noise pickup

3.–4. New 200 kHz ADC and amplifiers

Old Acquisition

- 16-bit, bipolar linear amps
- $\pm$ 200 μA range
- 5 kHz sampling rate ADC

New Acquisition

- 16-bit, bipolar linear amps
- $\pm$ 2000 μA range
- 200 kHz sampling rate ADC
- Each channel is fully controllable via software

[a] *Bonofiglo RSI 2020*

Energy Resolution is Determined by the Foil Stack Configuration

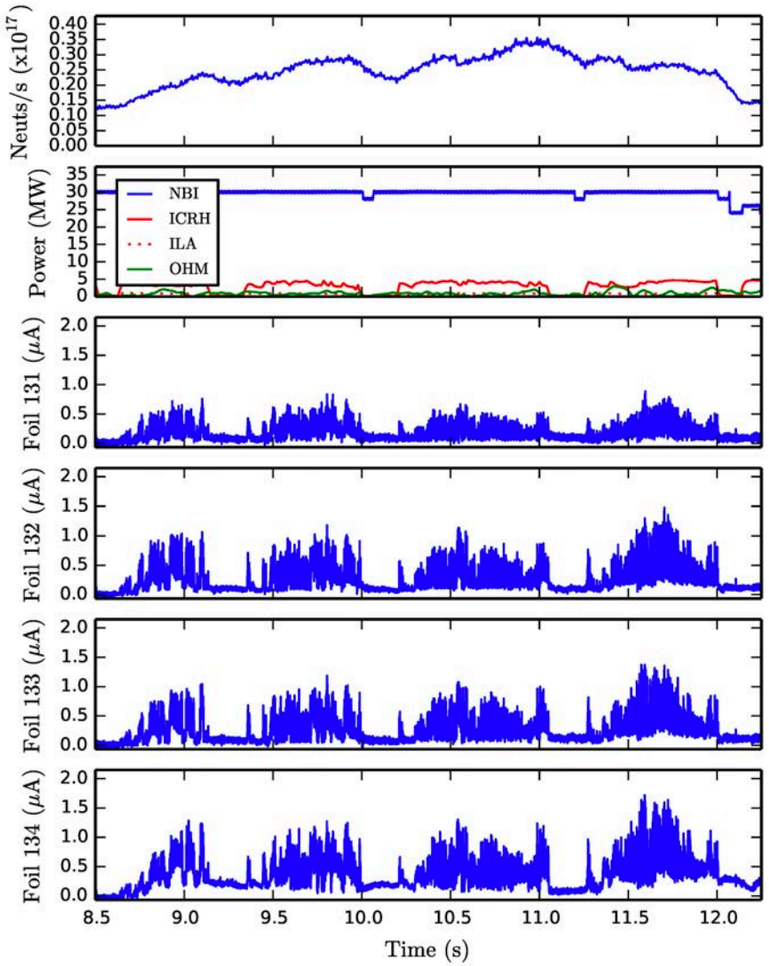

- Resolution determined by foil and insulator choice, thicknesses, ion species
- MeV scale ICRH heated deuterium NBI ions act as a proxy for fusion born DT alpha particles in deuterium plasmas
- The Faraday cup signals (left) are correlated with modulated ICRH input power indicative of heated deuteron losses

Energy Range per Foil†

Depth (μm)	Proton Energy Range (Mev)	Deuteron Energy Range (Mev)	Triton Energy Range (Mev)	He3 Energy Range (Mev)	Alpha Energy Range (Mev)
0.0 – 2.5	0.0 – 0.49	0.0 – 0.49	0.0 – 0.50	0.0 – 1.55	0.0 – 1.54
5.0 – 7.5	0.68 – 0.96	0.79 – 1.10	0.84 – 1.20	2.30 – 3.35	2.48 – 3.55
10.0 – 12.5	1.10 – 1.32	1.35 – 1.60	1.48 – 1.76	3.90 – 4.70	4.17 – 5.09
15.0 – 17.5	1.45 – 1.65	1.78 – 2.00	2.00 – 2.25	5.20 – 5.80	5.60 – 6.35

$\Delta E/E = 10 - 35\%$

†*Found via SRIM code*

More FILD Loss Measurements

- Deuterium plasmas with MeV scale ICRH heated deuterium NBI ions which act as a proxy for fusion born DT alpha particles
- Fusion products: D+D → H^3(1.01 MeV)+p(3.02 MeV) and D+He^3 → He^4(3.54 MeV)

Fusion Product Losses

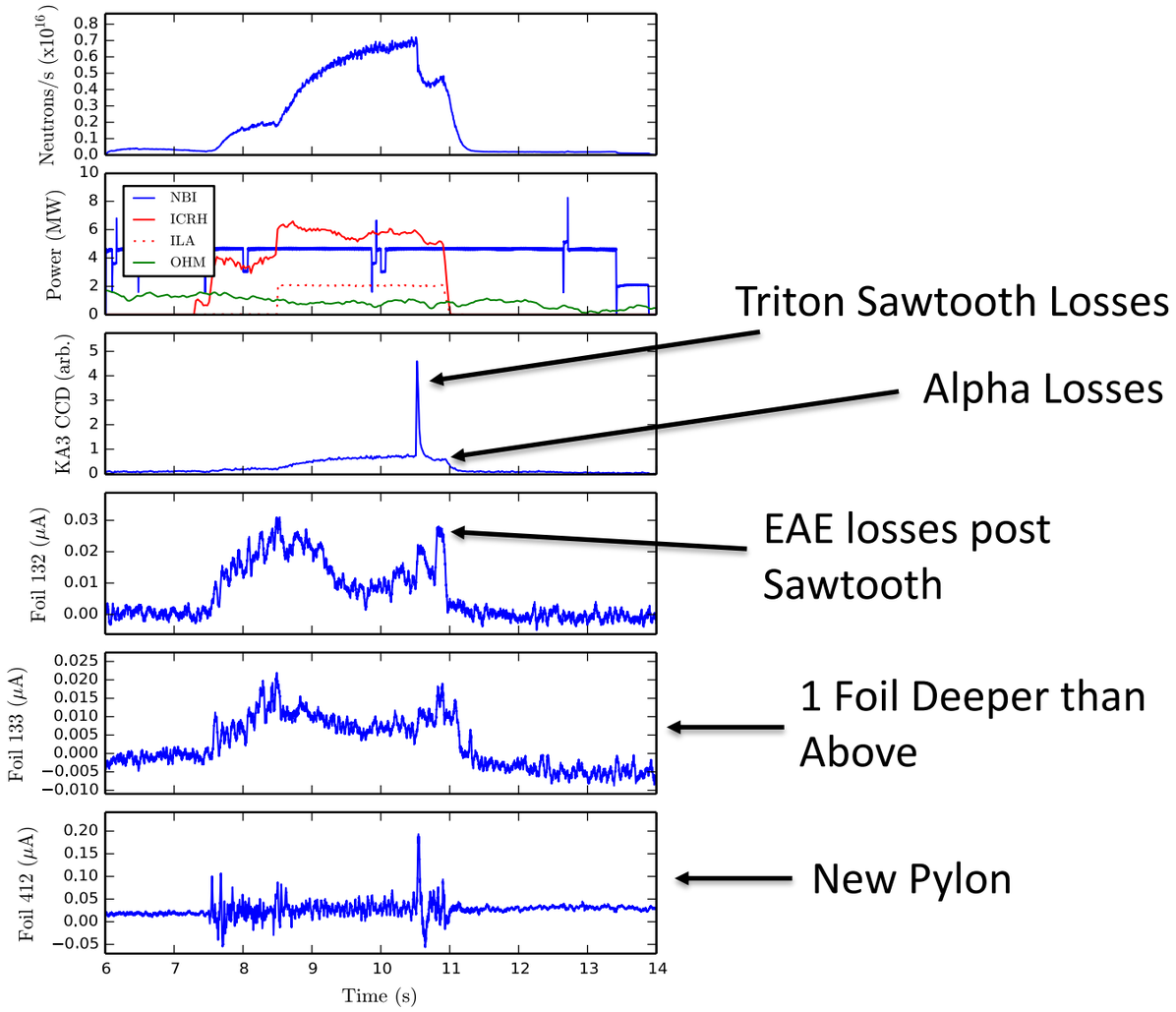

TAE Losses

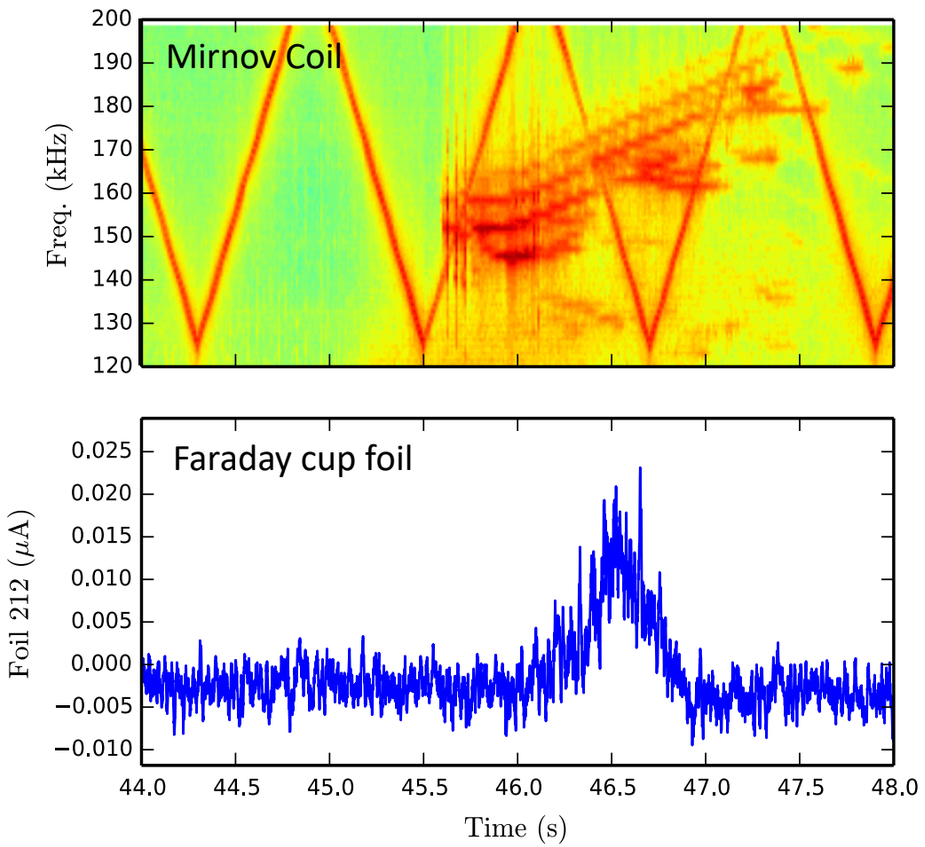

Strong Kink Modes and Sawteeth are Present for Fast Ion Transport

- Presence of phase inversion near the magnetic axis confirms kink activity in conjunction with sawteeth

Magnetic Spectrogram

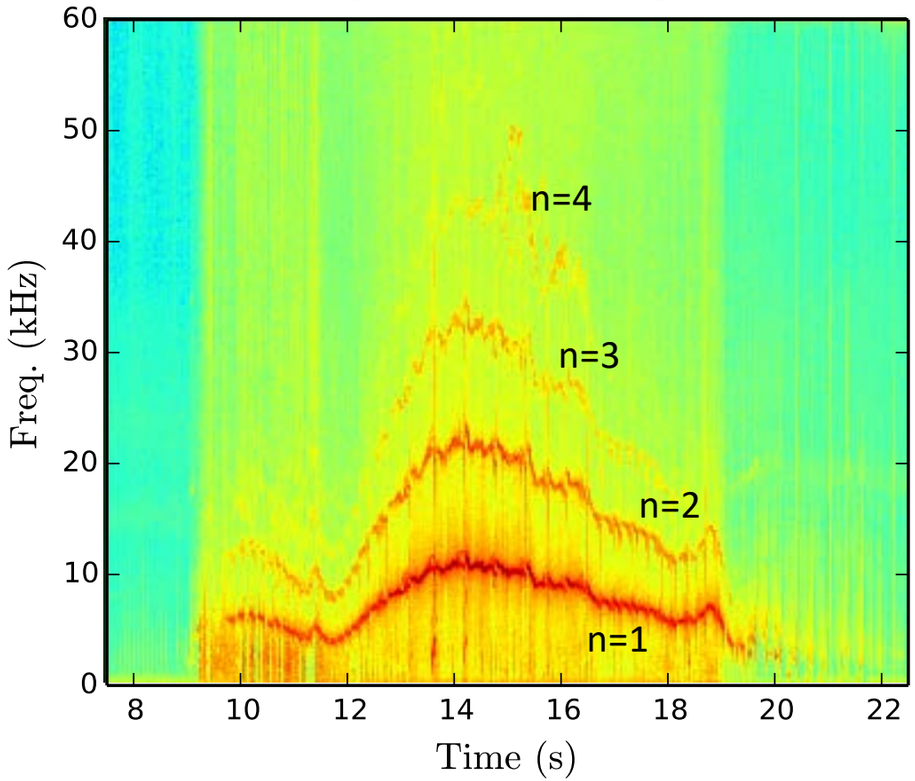

ST-Crashes in Neutrons and Te

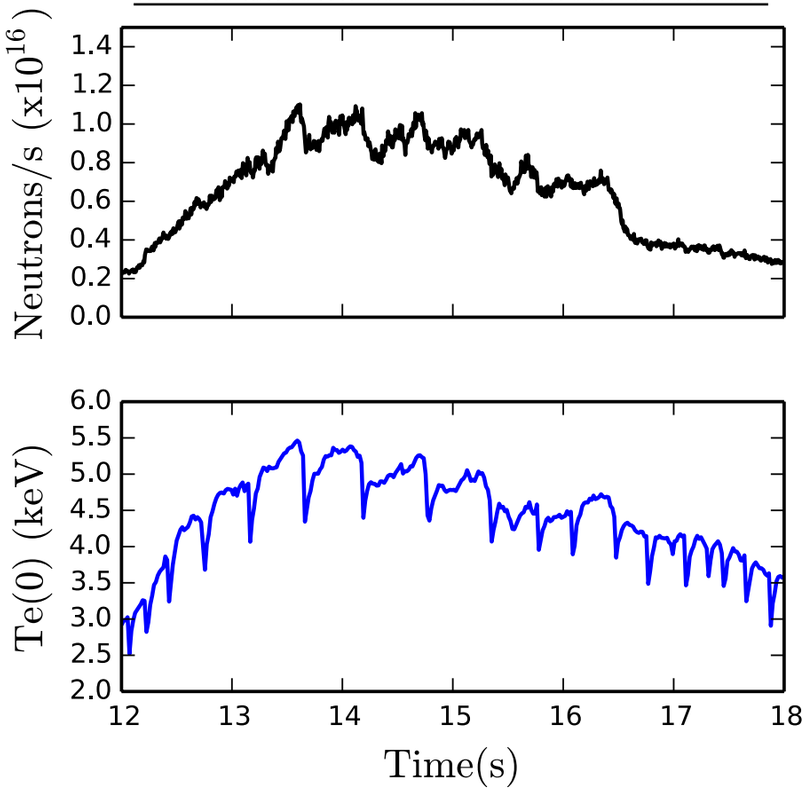

Scintillator FILD Measures Losses for a Similar Discharge

- Scintillator FILD[a] timing was incorrect for shot 96133, but was corrected for the repeated shot 97493

FILD Scintillator Probe

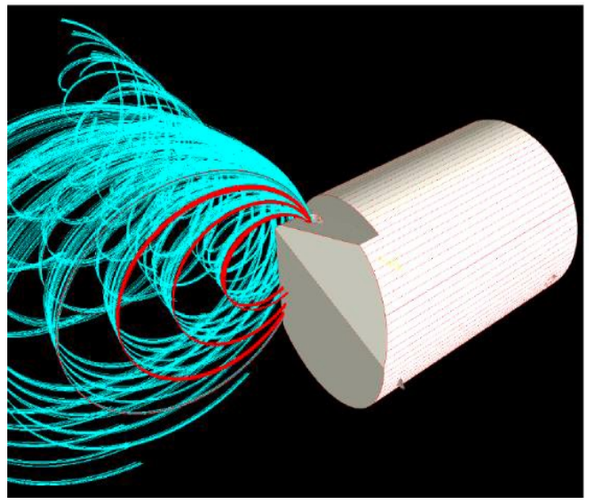

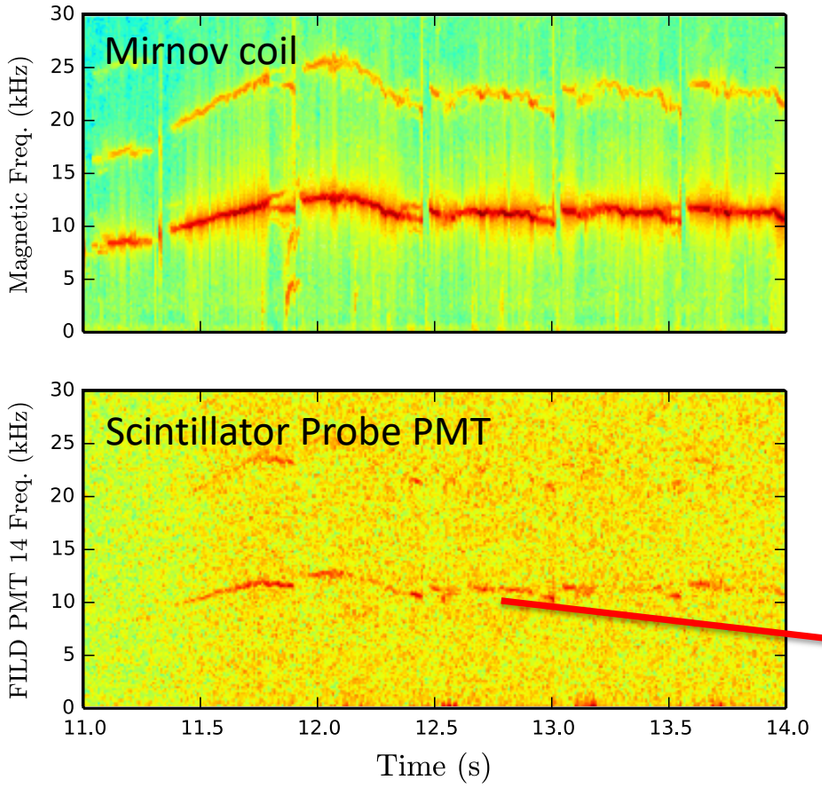

Scintillator CCD Image

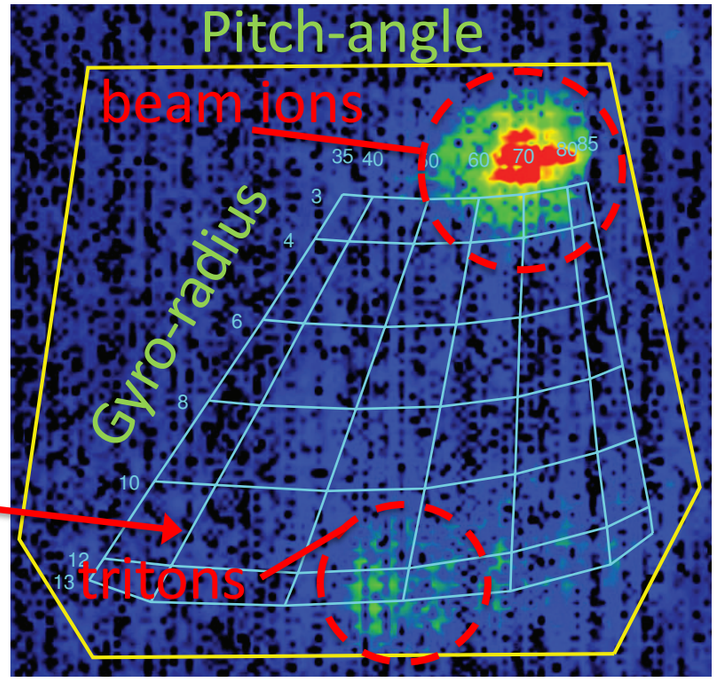

[a] *Baumel RSI 2004*

The Reverse Integrated Distribution is not Directly Comparable to that of TRANSP/NUBEAM

0.95 MeV Deuteron Lost Dist. - FBM

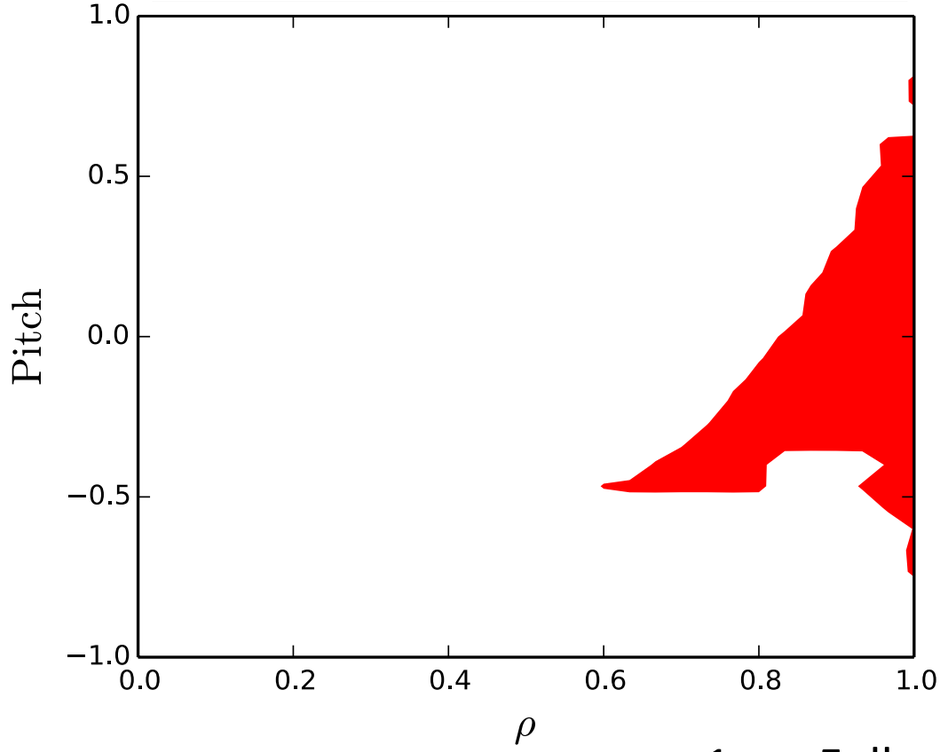

0.95 MeV Deuteron Lost Dist. - CoM

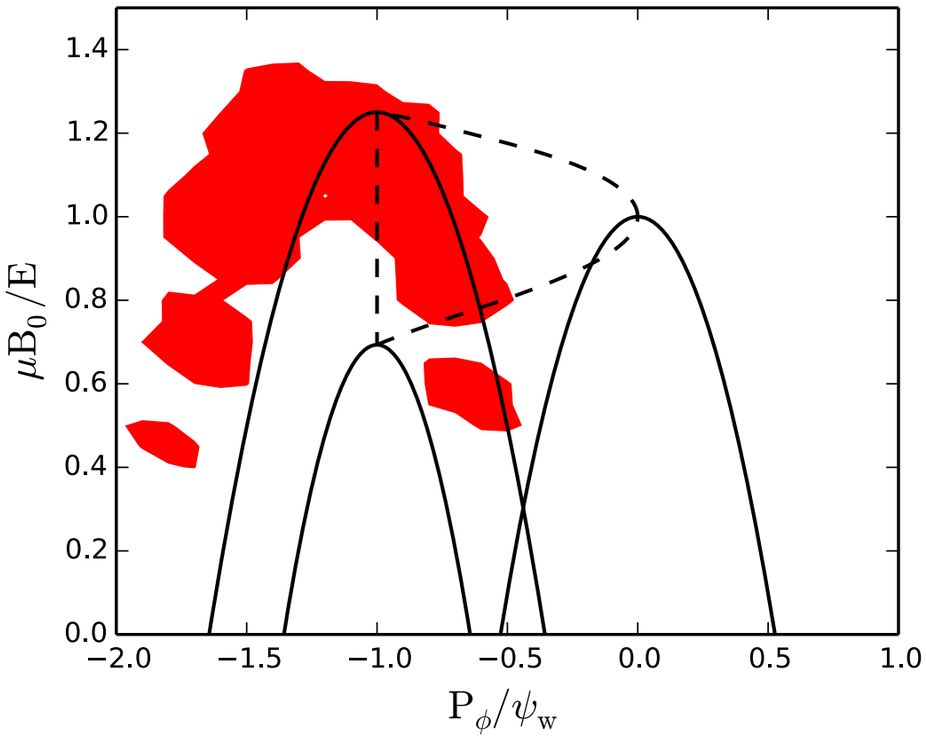

Caveats

1. Full orbit
2. Dist. is naturally in the lost region outside of the scope of NUBEAM
3. No perturbations

The q=1 Surface was Better Constrained from ECE Measurements

- Original equilibrium was magnetics+pressure EFIT (MSE was not active during this discharge)
- q=1 inversion surface was found from sawtooth effects in ECE and SXR (not shown)
- An initial q(0) is provided to TRANSP to seed the predictive PT-SOLVER[a] and give the q=1 location

ECE Channel during ST-Crash

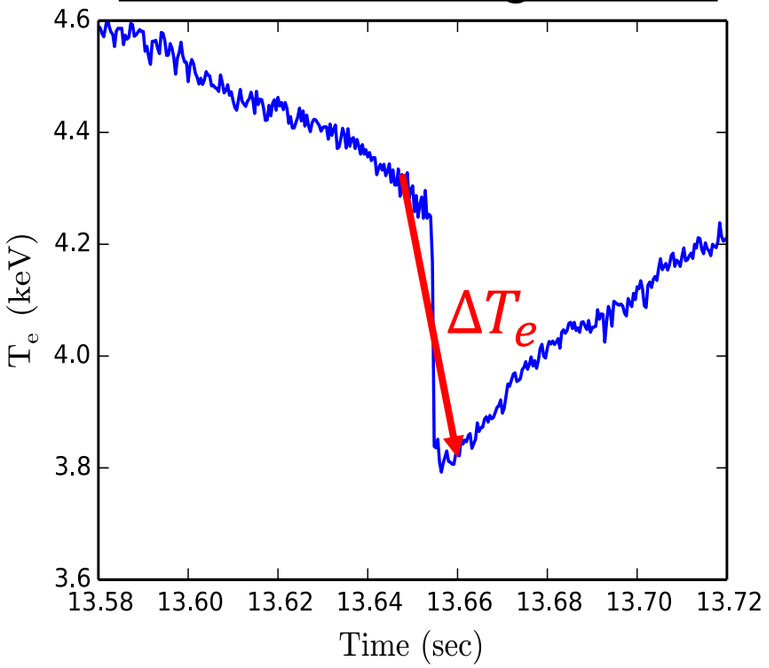

Radial Change in ΔT_e

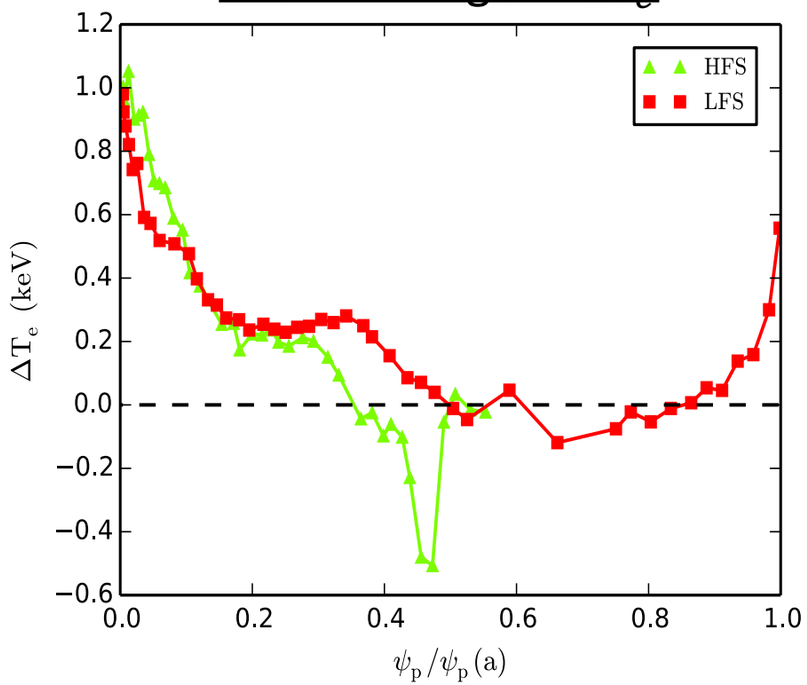

Constrained q-Profile Comparison

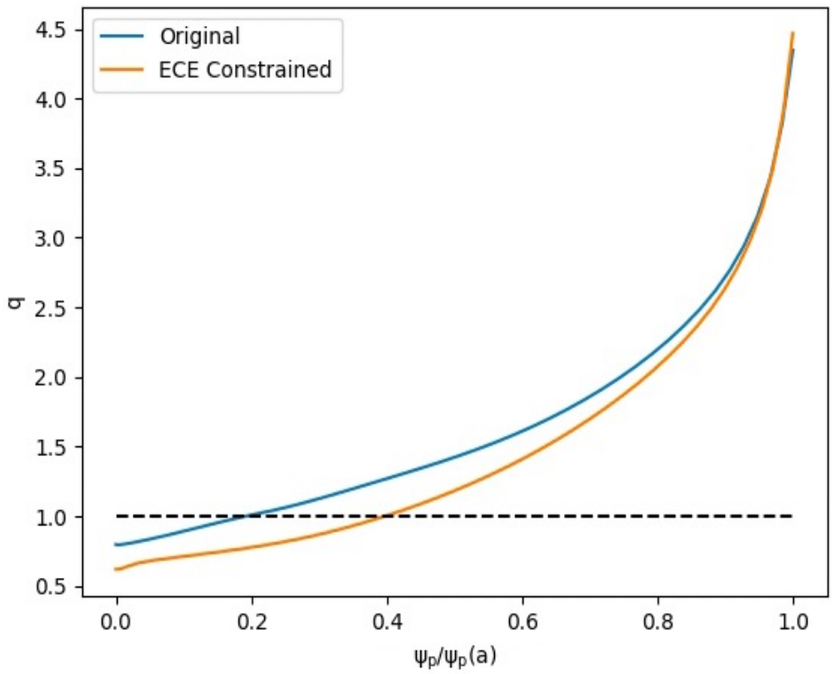

[a]*Yuan APS-DPP 2012, 2013*